

A Dissertation Work Phase-II on

**DESIGN AND DEVELOPMENT OF SERIES RESONANT
CONVERTER FOR UPS BATTERY CHARGING APPLICATION**

A Dissertation work submitted to Bangalore University for the Partial Fulfilment for
the award of the degree of

Master of Technology

In

POWER ELECTRONICS

By

SHUBHAM SUBHAS BORKAR

Register No.: - 20GAEL3011

Under the guidance of

Dr. GURUSWAMY K P

Associate Professor



**DEPARTMENT OF ELECTRICAL ENGINEERING
UNIVERSITY VISVESVARAYA COLLEGE OF ENGINEERING
K. R. Circle, Bengaluru- 560001**

January - 2023

DEPARTMENT OF ELECTRICAL ENGINEERING
UNIVERSITY VISVESVARAYA COLLEGE OF ENGINEERING
K. R. CIRCLE, BENGALURU- 560001



CERTIFICATE

This is to certify that the Dissertation Work entitled "**DESIGN AND DEVELOPMENT OF SERIES RESONANT CONVERTER FOR UPS BATTERY CHARGING APPLICATION**" successfully completed by "**SHUBHAM SUBHAS BORKAR**" bearing Register No.: - **20GAEL3011** in partial fulfilment for the award of degree in Master Of Technology in "**POWER ELECTRONICS**" in Department of Electrical Engineering as prescribed by BANGALORE UNIVERSITY in UNIVERSITY VISVESVARAYA COLLEGE OF ENGINEERING, K. R. CIRCLE, BENGALURU- 560001 during the academic year 2021-22.

Signature of the Guide

Dr. GURUSWAMY K P
Associate Professor
Department of Electrical Engineering
UVCE, K. R. Circle
Bengaluru- 560001

Signature of the Chairman

Dr. T S PRASANNA
Professor and Chairman
Department of Electrical Engineering
UVCE, K. R. Circle
Bengaluru- 560001

Signature of the Examiner(s)

DECLARATION

This is to declare that the entire work embodied in this report has been carried out by me at University Visvesvaraya College of Engineering under the supervision of Dr. Guruswamy K P, Associate Professor. This report has been submitted in partial fulfilment for the award of Master of Technology in Power Electronics.

This is also to declare that this report is written by me. No part of this report has been plagiarized from other sources. All the information included from other sources have been duly acknowledged. If any part of the report is found to have been plagiarized, I shall take the complete responsibility of it.

Place: Bengaluru
Date:

SHUBHAM SUBHAS BORKAR
Register No.: - 20GAEL3011

ABSTRACT

The different design phases for a resonant DC-DC converter with a Half-Bridge Inductor-Capacitor (LC) topology are shown in this work. It can be suggested that this converter be used for battery charging applications in UPS. The suggested DC-DC converter is built to deliver the most power possible from the DC Link's input voltage to the battery. Averaging Current Mode Controller is used to regulate the output voltage. According to the suggested design strategy, variable input voltages between 35V and 40V are used to regulate the output DC voltage at a constant 12V DC.

The design of resonant tank is done for line regulation, load regulation, and efficiency. Detailed design and selection of Mosfet, Inductor, Capacitor, Transformer, Rectifier circuit, Filter circuit and Load design is done. The mathematical modeling for the resonant converter is carried out by First Harmonic Approximation (FHA) and Small signal modeling for series resonant converter.

The simulation is run on the MATLAB/Simulink platform using the designed parameters, and the simulation results validate the resonant converter's performance in terms of overall high efficiency.

ACKNOWLEDGEMENT

The success of any project largely depends on the encouragement and guidelines of many others. I wish to convey my sincere thanks and gratitude to the people who have been instrumental in this achievement.

I would like to express my sincere thanks to my guide **Dr. GURUSWAMY K P**, Associate Professor, Department of Electrical Engineering, UVCE, Bengaluru for his constant support, guidance and encouragement throughout the course of the work.

I thank **Dr. T S PRASANNA**, Head of Department of Electrical Engineering, UVCE, Bengaluru for encouragement during this project.

I would like to express my profound gratitude to **Dr. RAMESH H N**, Principal, the management and the non-teaching staff of UVCE, Bengaluru for their immense support.

I also express our indebt thanks to our teaching and non-teaching staff of ELECTRICAL AND ELECTRONICS DEPARTMENT, UVCE.

Last but not the least, I wish to thank my parents, family and friends for their blessings and support.

SHUBHAM SUBHAS BORKAR
Register No.: - 20GAEL3011

CONTENTS

	Page No.
Abstract	i
Acknowledgement	ii
Contents	iii
List of Figures	viii
List of Tables	xi
List of Abbreviations	xii
List of Symbols	xiii
 CHAPTER - 1: INTRODUCTION.....	01-10
1.1 Introduction to PV System.....	02
1.2 Derivation of Nonlinear Equations Applied to Numerical Solution.....	03
1.3 Introduction to Series Resonant Converter.....	07
 CHAPTER – 2: LITERATURE SURVEY.....	11-19
2.1 Introduction.....	12
2.2 Problem Statement.....	17
2.3 Objective.....	17
2.4 Methodology.....	17
2.5 Conclusion.....	18
 CHAPTER - 3: ANALYSIS OF THE SERIES RESONANT CONVERTER FOR UPS BATTERY CHARGING.....	20-34
3.1 Introduction.....	21
3.2 Different Modes of Operation.....	22
3.2.1 Discontinuous Mode ($0 < f < 0.5f_n$).....	22
3.2.2 Continuous Mode ($f_s > f_n$ or Above Resonant Mode).....	26

3.2.3	Continuous Mode ($0.5f_n < f < f_n$ or Below resonant Mode)	29
3.3	Resonant Frequencies in an SRC.....	30
3.3.1	f_{CO} , f_O and f_P in an LC Circui.....	31
3.4	Operation at, Below and Above f_O	32
3.4.1	Operation at Resonance f_O	32
3.4.2	Operation Below Resonance f_O	33
3.4.3	Operation Above Resonance f_O	33
3.5	Conclusion.....	34

CHAPTER – 4: DESIGN OF THE SERIES RESONANT CONVERTER FOR UPS BATTERY CHARGING.....35-49

4.1	Introduction.....	36
4.2	Basic Design Conditions.....	36
4.2.1	Line Requirement.....	37
4.2.2	Load Regulation.....	39
4.2.2.1	Normal Load Operation.....	39
4.2.2.2	Overload Current.....	40
4.2.2.3	Load Short Circuit.....	40
4.3	Selecting Design Parameters f_{sw} , n , L_n and Q_e	41
4.3.1	Selecting the Switching Frequency.....	41
4.3.2	The Transformer Turns (n).....	42
4.3.3	Choosing Q_e and L_n	42
4.4	Design Example.....	42
4.4.1	Design Steps.....	43
4.4.2	Establish M_{g_max} and M_{g_min}	44
4.4.3	Calculate the Equivalent Load Resistance (R_e).....	45
4.4.4	Parameter Design for Resonant Circuits.....	45
4.4.5	Analyse the Resonant-Circuit Design.....	46
4.4.6	Determine the Primary-Side Currents.....	47
4.4.7	Calculate the Secondary-Side Currents.....	47

4.4.8	Select the Rectifier Diodes.....	48
4.4.9	Choose the Output Filter Type and Include the Capacitors.....	49
4.5	Conclusion.....	49

CHAPTER – 5: MATHEMATICAL MODELLING OF THE SERIES RESONANT CONVERTER FOR UPS BATTERY CHARGING.....50-75

5.1	Introduction.....	51
5.2	Mathematical Modelling of First Harmonic Approximation for Series Resonant Converter.....	51
5.2.1	Electrical Variable Relationships.....	52
5.2.2	Voltage-Gain Function.....	54
5.2.3	Normalized Volatge-Gain Function Format.....	55
5.2.4	Voltage-Gain Function Behavior.....	56
5.3	Mathematical Modelling of Small Signal Modelling of Series Resonant Converter.....	59
5.3.1	Small Signal Steady State Relationship for Resonant Converters.....	61
5.3.2	Equivalent Circuit Model of Small Signal.....	63
5.3.2.1	The Small Signal State Equations are Derived.....	65
5.3.2.2	Circuit Models for Lumped Parameters.....	67
5.4	Conclusion.....	74

CHAPTER – 6: DESIGN OF CONTROLLER FOR THE SERIES RESONANT76-92

6.1	Introduction.....	77
6.2	Need for the Controller.....	77
6.3	Introduction to Average Current Mode Control.....	77
6.4	Average Current-Mode Control.....	80
6.4.1	Principles and Implementation of Average Current-Mode Control.....	81
6.4.2	Dynamics of Average Current-Mode Control in Small Signals.....	82
6.5	Average Current-Mode Control Design.....	83

6.5.1	Design for Current Feedback Compensation.....	83
6.5.2	Design for Voltage Feedback Compensation.....	84
6.5.2.1	Modulator Gain.....	84
6.5.2.2	Sampling Gain.....	86
6.5.2.3	Feedback and Feed-Forward Gain.....	87
6.6	Transfer Function Characteristics.....	88
6.6.1	Current Loop Gain.....	89
6.6.2	Control-to-Output Voltage.....	89
6.6.3	Audio Susceptibility.....	89
6.6.4	Output Impedance.....	90
6.6.5	Stability.....	91
6.6.6	Output Voltage to Duty cycle Transfer Function.....	92
6.7	Conclusion.....	92

**CHAPTER – 7: SIMULATION OF THE SERIES RESONANT
CONVERTER FOR UPS BATTERY
CHARGING.....93-118**

7.1	Introduction.....	94
7.2	PV Source for Series Resonant Converter.....	94
7.3	Simulation of PV System with LC Resonant Converter under Open Loop..	100
7.4	Simulation of PV System with LC Resonant Converter for UPS Battery Charging under Open Loop.....	103
7.5	Closed Loop Matlab Programming for Average Current Mode Control of Series Resonant Converter.....	108
7.6	Conclusion	118

CHAPTER – 8: CONCLUSION AND FUTURE SCOPE....119-121

LIST OF PUBLICATIONS FROM THE DISSERTATION	
WORK PHASE – II.....	121
BIBLIOGRAPHY.....	122

LIST OF FIGURES

Fig. 1.1 Equivalent Circuit for a PV Cell's Double-Diode Model.....	03
Fig. 1.2 Circuit Diagram of Series Resonant Converter.....	07
Fig. 3.1 Circuit of a Half Bridge LC Resonant Converter.....	21
Fig. 3.2 Equivalent Circuit for Half Bridge LC Resonant Converter.....	22
Fig. 3.3 Waveform of Discontinuous Mode of Series Resonant Converter.....	22
Fig. 3.4 Discontinuous Mode Equivalent Circuit Diagram of Series Resonant Converter.....	23
Fig. 3.5 Continuous Mode Equivalent Circuit Mode of Series Resonant Converter Above Resonance.....	26
Fig. 3.6 Waveform of Continuous Mode of Series Resonant Converter Above Resonance.....	26
Fig. 3.7 Continuous Mode of Series Resonant Converter Below Resonance.....	29
Fig. 3.8 Waveform of Continuous Mode for Below Resonance of Series Resonant Converter.....	29
Fig. 4.1 Recommended Design Area.....	37
Fig. 4.2 Operation Boundary set by a_1 through a_4	39
Fig. 4.3 Flowchart of Resonant-Network Design.....	43
Fig. 5.1 Voltage-Gain Function (Mg) Plots with Various L_n Values.....	57
Fig. 5.2 Voltage-Gain Function (Mg) Plots with Various L_n Values.....	58
Fig. 5.3 Equivalent Circuit for the Series Resistor Converter's Y-Parameter Model using Lumped Parameters.....	70
Fig. 6.1 A Proposed Average Current Mode Control is Used in an Experimental LC Converter.....	79
Fig. 6.2 Block Diagram of ACMC for Resonant Converters.....	80
Fig. 6.3 Functional Circuit Diagram of Average Current-Mode Control Scheme....	81
Fig. 6.4 Experimental Waveforms of Feedback Circuits.....	81
Fig. 7.1 Matlab Simulation for Photovoltaic System.....	95
Fig. 7.2 Parameter of PV Array.....	96
Fig. 7.3 Plot for Voltage, Current and Power of PV Array.....	98

Fig. 7.4 Matlab Simulation Model of LC Resonant Converter.....	98
Fig. 7.5 Output Voltage of LC Resonant Converter.....	99
Fig. 7.6 Output Current of LC Resonant Converter.....	99
Fig. 7.7 Mosfet Current of LC Resonant Converter.....	99
Fig. 7.8 Mosfet Voltage of LC Resonant Converter.....	100
Fig. 7.9 Inductor Current of LC Resonant Converter.....	100
Fig. 7.10 Matlab Simulation for Open Loop LC Resonant Converter.....	100
Fig. 7.11 Output Voltage for Open Loop LC Resonant Converter.....	101
Fig. 7.12 Output Current for Open Loop LC Resonant Converter.....	101
Fig. 7.13 Mosfet Current for Open Loop LC Resonant Converter.....	101
Fig. 7.14 Mosfet Voltage for Open Loop LC Resonant Converter.....	102
Fig. 7.15 Inductor Current for Open Loop LC Resonant Converter.....	102
Fig. 7.16 Input Current for Open Loop LC Resonant Converter.....	102
Fig. 7.17 Diode Voltage for Open Loop LC Resonant Converter.....	103
Fig. 7.18 Input Voltage for Open Loop LC Resonant Converter.....	103
Fig. 7.19 Matlab Simulation for Open Loop LC Resonant Converter for Battery Charging Application.....	104
Fig. 7.20 Nominal Current Discharge Characteristics of the Battery.....	105
Fig. 7.21 Voltage vs Time Characteristics of Lithium-Ion Battery.....	105
Fig. 7.22 Output Voltage of Series Resonant Converter for Battery Charging under Open Loop.....	105
Fig. 7.23 Output Current of Series Resonant Converter for Battery Charging under Open Loop.....	106
Fig. 7.24 Mosfet Current of Series Resonant Converter for Battery Charging under Open Loop.....	106
Fig. 7.25 Mosfet Voltage of Series Resonant Converter for Battery Charging under Open Loop.....	106
Fig. 7.26 Inductor Current of Series Resonant Converter for Battery Charging under Open Loop.....	107
Fig. 7.27 Input Current of Series Resonant Converter for Battery Charging under Open Loop.....	107
Fig. 7.28 Diode Voltage of Series Resonant Converter for Battery Charging	

under Open Loop.....	108
Fig. 7.29 Input Voltage of Series Resonant Converter for Battery Charging under Open Loop.....	108
Fig. 7.30 Bode Plot of Current-Loop-Gain for Closed Loop LC Resonant Converter.....	115
Fig. 7.31 Bode Plot of Outer Loop-Gain for Closed Loop LC Resonant Converter.....	116
Fig. 7.32 Bode Plot for LC Converter Frequency to Output Voltage Transfer Function For Closed Loop.....	117

LIST OF TABLES

Table 2.1 Comparison Table for Different Converters.....	12
Table 2.2 Comparison Table for Different Control Technique.....	13
Table 2.3 Comparison Table for Different MPPT Techniques.....	14
Table 2.4 Comparison Table for Different Resonant converters.....	15
Table 2.5 Comparison Table for Series Resonant Converters.....	16
Table 7.1 Voltage and Current Measurements for change in Temperature.....	95
Table 7.2 Module Data.....	97
Table 7.3 Model Parameters.....	97
Table 7.4 Lithium-Ion Battery Parameters.....	104

LIST OF ABBREVIATIONS

SRC	Series Resonant Converter
PV	Photovoltaic
RC	Resonant Converter
ZCS	Zero Current Switching
UPS	Uninterruptible Power Supply
MPP	Maximum power point
FHA	First Harmonic Approximation
ACMC	Average Current Mode Control
PCMC	Peak Current Mode Control
PWM	Pulse Width Modulation
ZVS	Zero Voltage Switching
PCB	printed circuit board
RHP	Right Half Plane
AC	Alternating current
DC	Direct Current
MOSFET	Metal-Oxide Semiconductor Field-Effect Transistor
PF	Power Factor
UPF	Unity Power Factor
CCM	Continuous Current Mode
DCM	Discontinuous Current Mode
KCL	Kirchhoff's Current Law
KVL	Kirchhoff's Voltage Law
RMS	Root Mean Square
ESR	Equivalent Series Resistance
MATLAB	Matrix Laboratory

LIST OF SYMBOLS

C_r	Resonant capacitor
L_r	Resonant inductor
f_x	Normalized switching frequency
f_r	Resonant frequency (series)
f_p	Resonant frequency (Parallel)
Q	Quality factor
R_{ac}	Reflected load resistance
m	Inductance ratio
f_s	Switching frequency
N_p, N_s	Primary and Secondary turns
R_o	Load Resistance
P_{in}	Input power
P_o	Output power
V_{inmax}	Maximum input voltage
V_{inmin}	Minimum input voltage
M_{min}	Minimum gain of LC
M_{max}	Maximum gain of LC
n	Turns ratio
f_{min}	Minimum frequency
V_d	DC link voltage
D	Duty ratio
L_1	Primary inductor of converter
C_d	dc- link capacitor
Ω	Normalized frequency
M_f	Forward gain of LC
M_b	Backward gain of LC
t	Instantaneous time
ω	Angular frequency
R	Load resistance
C	Load capacitance

α	Duty cycle of the MOSFETs in ωt axis
β	Turn-on delay in ωt axis
V_o	Output voltage of a circuit
v_L	Voltage across an inductor
i_s	Supply current drawn by a converter
i_L	Current flowing through an inductor
i_c	Current flowing through a capacitor
I_o	Output current of a converter
V_{dc}	Voltage of the DC source
f	Supply frequency
L_c	Critical inductance
L_{rf}, C_{rf}	Passive components of the active front-end rectifier
L_{lpf}, C_{lpf}	Passive components of the low-pass filter
L_{reg}, C_{reg}	Passive components of the DC-DC converter
t_0, t_1, t_2	Time instants
T	Time period of a signal
P_L	Power loss occurring due to internal resistance of inductance
P_C	Power loss occurring due to ESR of capacitance
P_{con}	Conduction loss in power semiconductor devices
P_{sw}	Switching loss in power semiconductor devices
t_{dn}, t_{df}	Turn-on delay, turn-off delay in switching characteristic of power semiconductor switches
t_r, t_f	Rise time, fall time in switching characteristics of power semiconductor devices
$R_{D\ on}$	Resistance of the power semiconductor device when in on-state
M_p	Peak overshoot of the power converter
t_s	Settling time of the power converter
e_{ss}	Steady-state error in the output waveform of the power converter

CHAPTER - 1

INTRODUCTION

1 INTRODUCTION

1.1 Introduction to PV system

It is essential to create suitable models in order to simulate and predict how photovoltaic (PV) cells as well as modules will behave. This is valid for the design, production, and evaluation of PV systems. The two most prevalent models of photovoltaic cells & modules within literature are the single-diode models and double models. The accuracy and number of variables employed by these models to calculate the properties of PV current-voltage varies. It has been shown that, especially at low irradiance levels, the double-diode model more correctly predicts solar panel performance than the single-diode model. Prior to modelling and assessing PV systems, one must select the model's input parameters. It may be challenging to solve the implicit and nonlinear resulting equations for the estimation of the parameters of a PV model analytically, which makes the challenge of parameter identification for such models challenging. Additionally, as stated in [1], appropriate starting values are required for numerical solutions to converge.

A PV double-diode model's parameters can be obtained in one of two methods. The first method depends on some experimental data being matched with theoretical I-V curves. A few crucial elements from experimental data from the other approach are used to choose the parameters. This approach is interesting for industrial applications since it is rapid and only needs a small amount of information from I-V curves, which are usually accessible in PV vendor catalogues, according to [2],[3]. In order to solve the resulting nonlinear equations using this approach, it is required to select an adequate beginning point to guarantee that the numeric iterations will converge. For the parameters of the double-diode model, precise analytic solutions were determined. However, the slopes of a I-V curves at the open-circuit point, which are frequently required by these approaches but not provided either by

photovoltaic manufacturers.

The only information required to obtain innovative numerical model for such characteristics of such a five-parameter dual model of Photovoltaic cells and modules in this work has been the open-circuit, short-circuit, as well as maximum power point coordinates (MPP). In Newton-Raphson numeric iterations, these analytical solutions are successfully used to obtain convergence and generate more precise findings. The retrieved numerical and analytical solutions using the suggested method in this work can be used as a solid starting point for other approaches relying on curve-fitting methods, as illustrated in [1], [3].

1.2 Derivation of nonlinear equations applied to numerical solutions

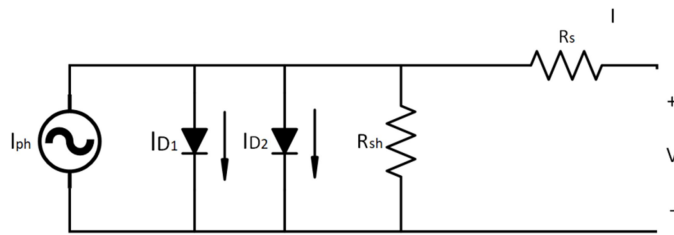


Fig 1.1: Equivalent circuit for a PV cell's double-diode model.

In Fig. 1.1, a PV cell's double-diode equivalent circuit is depicted. It should be noted as PV modules are made by stringing together PV series cells to provide high voltage and power levels. PV modules also have a small number of bypass diodes to avoid hot spots as well as avalanche breakdown under partial shadowing. A series of cells on the inside of a module are typically assumed to have almost identical qualities. As per [4], a PV module concept is therefore conceptualised as a single cell with a number of multiplies built within it that rely on the quantity of series-connected cells with in module. The equivalent circuit depicted in Fig. 1.1 provides the following current-voltage relationship for PV panels at a certain light intensity and temperature.

The PV cell's double-diode equivalent circuit is shown in Fig. It is important to keep in mind that PV modules are created by connecting Photovoltaic series cells to produce high power and voltage levels. PV modules also have a small number of bypass diodes to avoid hot spots as well as avalanche breakdown under partial shadowing. According to [5,] the properties of several cells inside a module are often believed to be roughly identical. Therefore, a PV module is modelled as an individual cells with such a range of multipliers embedded into to the cell model that vary depending on how many series-connected cells are in the module. The general PV panel current-voltage relationship under a certain light and temperature is shown by the corresponding circuit in Fig 1.1.

$$I = I_{ph} - I_{s1} \left[\exp \left(\frac{V + R_s I}{n_1 N_s V_t} \right) - 1 \right] - I_{s2} \left[\exp \left(\frac{V + R_s I}{n_2 N_s V_t} \right) - 1 \right] - \frac{V + R_s I}{R_{sh}} \quad (1.1)$$

I_{s1} & I_{s2} are indeed the saturation currents coming from the diffusion process and carrier combination with in the space-charge area, respectively. From (1.1) I & V are also the terminals current and voltage of the PV panel. The ideality coefficients for diffusion current as well as generation-recombination current in diodes are n_1 and n_2 , respectively. N_s is indeed the number of PV cells with in PV panel that are linked in series; R_s and R_{sh} are the series and shunt resistances; and V_t has always been the heat capacity of a cell.

$$V_t = \frac{kT}{q} \quad (1.2)$$

where q is an elementary charge (1.68×10^{-19} C), T stands for Boltzmann's constant (1.38×10^{-23} J/K), and k is the temperature of a p-n junctions in Kelvin. The ideality factors' numbers are often calculated as $n_1 = 1$ & $n_2 = 2$ with acceptable precision based on Shockley's theory

of diffusion to make computations easier in practical situations. Despite the fact it is frequently used in the literature, this assumption might not always be accurate. As a result, (1.2) may become into

$$I = I_{ph} - I_{s1} \left[\exp \left(\frac{V + R_s I}{N_s V_t} \right) - 1 \right] - I_{s2} \left[\exp \left(\frac{V + R_s I}{2N_s V_t} \right) - 1 \right] - \frac{V + R_s I}{R_{sh}} \quad (1.3)$$

Equation (1.3) is assessed as follows for such open circuit (0, V_{oc}), short circuit (0, I_{sc}), as well as MPP (I_m , V_m) places on the I-V curve of the PV module:

$$0 = I_{ph} - I_{s1} \left[\exp \left(\frac{V_{oc}}{N_s V_t} \right) - 1 \right] - I_{s2} \left[\exp \left(\frac{V_{oc}}{2N_s V_t} \right) - 1 \right] - \frac{V_{oc}}{R_{sh}} \quad (1.4)$$

$$I_{sc} = I_{ph} - I_{s1} \left[\exp \left(\frac{R_s I_{sc}}{N_s V_t} \right) - 1 \right] - I_{s2} \left[\exp \left(\frac{R_s I_{sc}}{2N_s V_t} \right) - 1 \right] - \frac{R_s I_{sc}}{R_{sh}} \quad (1.5)$$

$$I_m = I_{ph} - I_{s1} \left[\exp \left(\frac{V_m + R_s I_m}{N_s V_t} \right) - 1 \right] - I_{s2} \left[\exp \left(\frac{V_m + R_s I_m}{2N_s V_t} \right) - 1 \right] - \frac{V_m + R_s I_m}{R_{sh}} \quad (1.6)$$

The pv panel I-V curve's I-V expression for the power transferred at each location is

$$P = VI \quad (1.7)$$

The power word in (1.7) then is differentiated with respect to V as follows:

$$\frac{dP}{dV} = \left(\frac{dI}{dV} \right) V + I \quad (1.8)$$

The power's voltage-relative derivative is 0 at the MPP. Thus,

$$\frac{dI}{dV} = -\frac{I_m}{V_m} \quad (1.9)$$

Thus, the variations of (1.9) with regards to V are taken to get the formula dI/dV :

$$\frac{dI}{dV} = -\frac{I_{s1}}{N_s V_t} \left(1 + R_s \frac{dI}{dV} \right) \exp \left(\frac{V + R_s I}{N_s V_t} \right) - \frac{I_{s2}}{2N_s V_t} \left(1 + R_s \frac{dI}{dV} \right) \exp \left(\frac{V + R_s I}{2N_s V_t} \right) - \frac{1}{R_{sh}} \left(1 + R_s \frac{dI}{dV} \right) \quad (1.10)$$

Making the following change to (1.10) results in (1.9).

$$\frac{I_m}{V_m} = \frac{I_{s1}}{N_s V_t} \left(1 - R_s \frac{I_m}{V_m} \right) \exp \left(\frac{V_m + R_s I_m}{N_s V_t} \right) + \frac{I_{s2}}{2N_s V_t} \left(1 - R_s \frac{I_m}{V_m} \right) \exp \left(\frac{V_m + R_s I_m}{2N_s V_t} \right) + \frac{1}{R_{sh}} \left(1 - R_s \frac{I_m}{V_m} \right) \quad (1.11)$$

Using (1.4), one can write

$$I_{ph} = \frac{V_{oc}}{R_{sh}} + I_{s1} \left[\exp \left(\frac{V_{oc}}{N_s V_t} \right) - 1 \right] \quad (1.12)$$

Inputting (1.12) into (1.5) and (1.6) results in

$$I_{sc} = I_{s1} \left[\exp \left(\frac{V_{oc}}{N_s V_t} \right) - \exp \left(\frac{R_s I_{sc}}{N_s V_t} \right) \right] + I_{s2} \left[\exp \left(\frac{V_{oc}}{2N_s V_t} \right) - \exp \left(\frac{R_s I_{sc}}{2N_s V_t} \right) \right] + \frac{V_{oc} - R_s I_{sc}}{R_{sh}} \quad (1.13)$$

$$I_m \left(1 + \frac{R_s}{R_{sh}} \right) = I_{s1} \left[\exp \left(\frac{V_{oc}}{N_s V_t} \right) - \exp \left(\frac{V_m + R_s I_{sc}}{N_s V_t} \right) \right] + I_{s2} \left[\exp \left(\frac{V_{oc}}{2N_s V_t} \right) - \exp \left(\frac{V_m + R_s I_{sc}}{2N_s V_t} \right) \right] + \frac{V_{oc} - V_m}{R_{sh}} \quad (1.14)$$

1.3 Introduction to series resonant converter

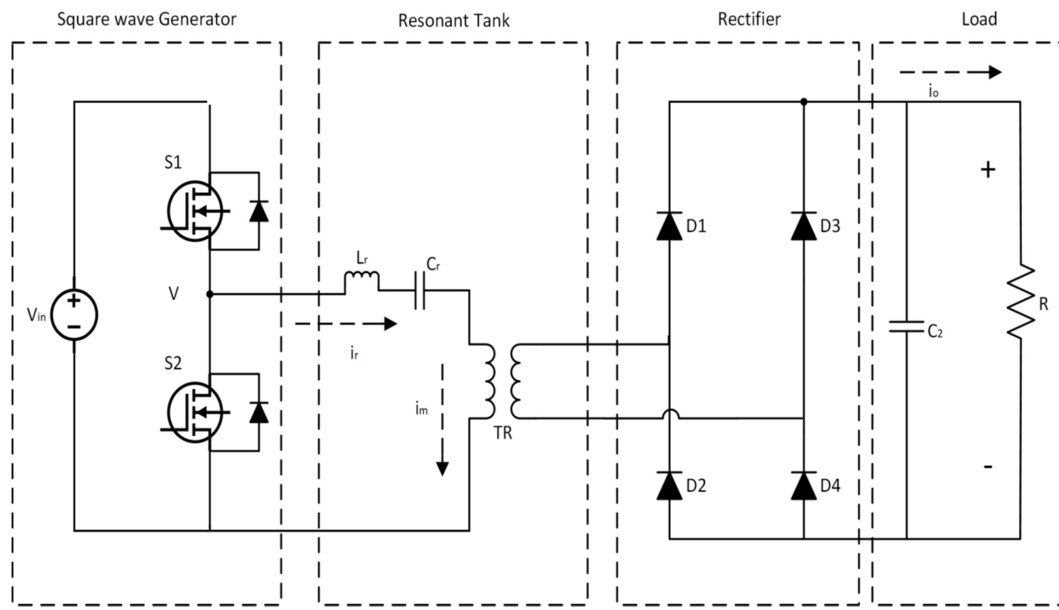


Fig 1.2: Circuit diagram of Series Resonant Converter

Figure 1.2 depicts the circuit design for such a series resonant converter. Due to a significant advancement in semiconductor power switching devices such as MOSFETs, IGBTs, and ESBTs and also high-frequency passive circuit components, High frequency resonant pulses inverters from switching type DC-DC energy conversion systems and circuits were being developed with a focus on hvdc power applications. Variable switching loss and decreased dependability plague "hard-switching" dc-dc converters. Size restrictions on the isolation transformer and reactive components have even been applied to power densities that are rising. Device switching losses seem to be proportional to the switching frequency that can be achieved in a given circuit, but as switching frequency increases, element sizes tend to decrease. High frequencies are essential for achieving the various benefits of high density & robust transient response. By utilising soft-switching approaches, switching loss issues may be resolved as well as the converters switching frequency can be significantly raised. The suggested architecture also has decreased EMI, large power density,

enhanced power factor, and device stress. Pulse width modulation (PWM) conversions experience switching losses, which are largely eliminated by resonance converters (RCs). The active device's terminals are switched with either zero current (ZCS) or zero voltage (ZVS). Any dc/dc converter's specification will include requirements for stability, reaction time, line control, and load regulation. The controller should be built to behave appropriately in every working condition of a converter since the supply voltage but also load regulation typically vary widely. Classical control techniques are frequently used in the construction of controllers for resonant converters. Changes to the linear model should also be taken into account if the operating point is susceptible to significant change. Studying the controller's design for the worst case scenarios is one technique to ensure that all requirements are met [32]. The easiest and most often used type of resonant converters are those in the LC series, where rectifier load network is linked in series with the LC resonant network. However, since LLC resonant converter was first developed in the 1990s, a great deal of research has been done on it. LLC resonant converters offer a variety of benefits above traditional LC series resonant converters' constrained frequency variation over a large range of loads, despite the absence of such a load, input variation, or voltage switching. Switched mode power supplies based on resonant operating converter topologies are growing in popularity nowadays for all power levels. When switching losses must be decreased to allow for higher frequencies during downsizing, resonant topologies are often used. A transformer may transmit high frequency electricity while operating in resonance. A LLC Series-Resonant half-bridge conversion has growing in favour as a high efficiency dc-dc converter. M. Emsermann studied the half bridge parallel resonant converters working on constant output voltage control and operating above resonance (1991). (1991). Control of such a resonant fixed frequency series' secondary side A converter that uses dual-edge PWM was introduced

by Praveen K. Jain and Darryl J. Tschirhart. (2010). H. N. and Krishnaswami Mohan described the three-port fixed frequency Series Resonant DC-DC Conversion (2008). (2008). Henry W. Koertzen and colleagues presented "Induction Cooking," for which the Series Resonant Half-Bridge Converter was designed (1995). The effectiveness of mechanically commutated, half-bridge, series resonant converters for induction cooking was examined in this study. The conventional SRC is indeed a converter having frequency regulation. To tune to the resonant frequency as an illustration of a changeable switching frequency disadvantage, the switching frequency fluctuates in line with to acquire the proper voltage gain. This study focuses on the Phase Modulation technique Series Resonant Converter (PM-SRC), a duty ratio-regulated SRC that runs at a fixed switching frequency. A steady state analysis of the PM-SRC operating over resonance frequency is conducted. Design relations are obtained, and chosen operating modes are defined. The outcomes of the investigation are verified using numerical simulation. The design process is supported by experimental findings on a lab prototype. SRC's two modified techniques are demonstrated in order to improve PM-performance. In the first, the converter's Zero Voltage Switching (ZVS) region is extended by utilising an external inductive circuit, and in the second, inherent short circuit safety is provided by using a resonant capacitor clamping strategy. The SRC consists of a half-bridge converter, a resonant frequency networks, an isolation transformer, as well as a rectifier. A body diode, parasitic capacitors, two switches, and a half-bridge inverter make up the device. The capacitor C_r and resonant inductor L_r are parts of the resonant circuit. The reactive elements L_r and C_r are coupled in series with the transformer winding in a series resonant converter. The load connected just at rectifier's output is in series with the resonant tank circuit. In this case, the load and tank circuit serve as voltage dividers. The impedance of a resonant tank may be changed by changing the

frequency of such a driving voltage, V . The load and impedance of the resonant tank share the input voltage. A voltage divider network is the SRC. The frequency of a driving voltage, V , can be altered to alter the impedance of the resonant tank. The input voltage is shared by the resonant tank's load and impedance. The SRC is a voltage divider circuit. As a result, the DC gain for SRC is never greater than 1. The impedance of the tank circuit is low at the resonant frequency. As a result, the resonant converter's output voltage is equal to its input voltage. As a result, resonance is when the SRC's voltage gain is maximum [32].

CHAPTER - 2

LITERATURE SURVEY

2.1 LITERATURE SURVEY

2.1. Introduction

Resonant circuits are electrical systems that vibrate with response to an external energy input. Resonant vibrations are utilised in a variety of electric circuits. The fundamental parts of such a resonant circuit consist of a coil (L) as well as a capacitor (C). Resonant circuits may be categorised into two groups based on their architecture: series and parallel resonant circuits. Parallel resonant circuits essentially have infinite impedance whereas series resonant circuits offer zero impedance somewhere at resonance frequency.

Table 2.1: Comparison Table for Different Converters

Proposed Converter	Controller	Efficiency	No. of Diodes	No. of Switches	Applications	Source	Software	Advantages	Disadvantages
Buck [6]	PI Controller	95%	1	5	Dual mode or Standalone application	PV	Matlab	Stable fixed frequency.	Error amplifier compensation.
Boost [7]	PI Controller	99%	3	6	3 phase inverter	PV	Matlab	Reduced ripple voltage	Higher core losses.
Sepic [8]	Voltage mode control	99.43%	1	2	Used in both resistive and battery loads	PV	Matlab	Fast tracking, less complexity	Drift problem occurs
Cuk [9]	PI Controller	98.9%	1	2	Generate error signals	PV	Matlab	Feasibility and improved functionality	nonlinearity nature of PV

Table 2.2: Comparison Table for Different Control Technique.

Proposed Converter	Controller	Efficiency	No. of Diodes	No. of Switches	Applications	Source	Software	Advantages	Disadvantages
Fuzzy logic control [10]	Boost	---	1	2	Mobile, transportation,	PV	Matlab	Improved reliability, better economics	high fabrication cost, low conversion efficiency
Sliding mode control [11]	Boost	High	1	2	satellite systems.	PV	Matlab	Better voltage regulation.	No limits on control cost
Predictive control [12]	Boost	High	2	3	voltage regulator module	PV	Matlab	High switching frequency	P&O is relatively slow
Current mode control [13]	Buck	90%	1	3	Li-ion battery, battery charging	PV	Matlab	High speed ADC	This method does not employ true MPP detection
Voltage mode control [14]	Boost	High	1	2	Low power application	PV	Matlab	High dynamic and static efficiencies	Required loop compensation
PI control	Boost	99.98%	2	3	High speed MPPT module	PV	Matlab	High accuracy, high efficiency	Drift problem occurs.

The energy loss of such a resonant circuit is represented by a statistic called a quality factor (Q factor). A higher Q factor resonator performs better because energy is lost more slowly. Care should be given, though, as resonant circuits with such a high Q factor may not achieve resonance or take a very long time to stabilise if their frequencies deviates even slightly from the resonant frequency, depending on their applications. In the situation of resonant inverters, the Q factor of such a resonant circuit changes dramatically with the load

impedance. Since it is expressed as ratio of the load impedance to the LC impedance, load impedance has an effect on the Q factor of such a resonant converters. The ideal topology of the resonant converters is influenced by the load impedance.

The name of such power converters is derived from resonance. Whenever the reactance of a capacitor and inductor cancel one another, an LC resonant network experiences this. Utilizing a resonant power conversion minimizes switching losses. The devices are switched on and off whenever there is no voltage applied across them or current flowing through switches. As a result, switching happens at either zero voltage as well as zero current.

Table 2.3: Comparison Table for Different MPPT Techniques.

MPPT Technique	Proposed Converter	Controller	Efficiency	No. Of Diodes	No. Of Switches	Applications	Source	Software	Advantages	Disadvantages
Perturbation and Observation [15]	Boost	PI Controller	96%	4	5	Fuel cell stack, battery	PV	---	High voltage gain	Increased complexity
Incremental Conductance [16]	Boost	Predictive Control	High	1	2	Generating the error signal	PV	Matlab	Very quickly MPP	Heavy oscillations problems
Proposed MPPT [17]	Boost	---	Medium	1	2	Residential	PV	Matlab	Low maintenance cost	Slow to respond
Ripple Correlation [18]	Buck	PI Controller	99.30%	---	2	Mobile application	PV	Matlab	---	reduced tracking efficiency

Table 2.4: Comparison Table for Different Resonant converters.

Proposed Converter	Controller	Efficiency	No. of Diodes	No. of Switches	Applications	Source	Software	Advantages	Disadvantages
Series resonant converter [19]	Average Geometric Control	95%	4	8	battery packs, hybrid automobiles and photovoltaic systems	PV	Matlab	AGC controller has ability to prevent voltage overshoot following disturbances	Limited frequency and high switching losses
LLC resonant converter [20]	Adaptive Voltage Control	High	2	4	off-line applications where hold-up time is normally required	PV	Matlab	Reduced ripple voltage	Difficulty in achieving consistent dynamic performance
LCC resonant converter [21]	Current mode control	---	2	6	Integrated circuits	PV	Matlab	Able to achieve wide operation together with high efficiency	Carry higher peak current values

The voltage between it and the current flowing through the switch determine the switching losses. With low loss switching, a particular parameter either its voltage across and the current through switch remains quite near to zero when switching. This results in practically 0% switching losses for the product. Power conversion improves as a result, and higher switching frequencies are also feasible. Another benefit is the smaller size of the transformer, inductor, and capacitor. By reducing the converter's overall weight and volume, this makes it more compact. Due to their smaller dv/dt , di/dt , and sinusoidal-like voltage and current shapes, these converters have less of an influence on EMI.

Design and Development of Series Resonant Converter for UPS Battery Charging Application

Table 2.5: Comparison Table for Series Resonant Converters.

Proposed Converter	Controller	Efficiency	No. of Diodes	No. of Switches	Applications	Source	Software	Advantages	Disadvantages
[22]	Hybrid Controller	Higher	8	12	Industrial magnetron, renewable energy, LED driver.	DC supply	PSIM	Higher power density, lower electromagnetic interference.	Complex circuit and high cost.
[23]	Linear PI Controller	---	4	8	power factor corrector systems	DC supply	PSIM	prevent voltage overshoot following disturbances	large transients
[24]	PI controller	Higher	8	8	bidirectional power flow applications	DC supply	PSIM	greater efficiency for light loads	Switching frequency is not constant
[25]	---	95.6%	6	10	battery charging and constant power motor drive	DC supply	Matlab	the switches are soft commutated	high component count, increased cost and complexity
[26]	voltage/ current stabilization controller	96.15%	8	16	high-voltage low-current applications	DC supply	PSIM	high power density, high efficiency and soft switching	high circulation current at light load
[27]	PI controller	96%	6	10	3 – phase inverter	DC supply	Matlab	Stable fixed frequency.	Error amplifier compensation
[28]	Fuzzy logic controller	97%	4	6	Used in both resistive and battery loads	DC supply	PSIM	Fast tracking, less complexity	Drift problem occurs.
[29]	Sliding mode control	---	8	8	Satellite systems.	DC supply	PSIM	Better voltage regulation.	No limits on control cost
[30]	Voltage mode control	---	6	10	Low power application	DC supply	Matlab	High dynamic and static efficiencies	Required loop compensation
[31]	PI controller	Higher	8	12	Fuel cell stack, battery	DC supply	PSIM	High voltage gain	Increased complexity

2.2. PROBLEM STATEMENT

Non-isolated dc-dc converters cannot work at high switching frequencies due to their lower switching frequency. The complexity, weight, and size of a converter are all enhanced in LLC as well as LCC resonant converters. The inability of an SRC converter to operate in the lack of such a load is one of its drawbacks. SRC is not appropriate for low-voltage, high-current applications.

2.3. OBJECTIVES

This dissertation's goal is to examine how well the Series Resonant Converter operates at various frequencies and how it performs in both open loop as well as closed loop systems. to comprehend the modelling of the series resonant converter's tiny signal and first harmonic approximation. to create a series resonant converter for the purpose of charging UPS batteries. Understanding about series resonant converter and performing simulation to confirm the theoretical design

2.4. METHODOLOGY

The step-wise procedure followed for the completion of this dissertation work is explained briefly in this section.

1. The topic of the dissertation work selected was based on its serviceability in the society.
2. The problem statement will be defined by obtaining information by referring to various literatures related to the studies done on resonant converters for battery charging systems- converter topology and control techniques.
3. The analysis will be done on the series resonant converters and its different modes of

operation.

4. The components for the resonant converter and resonant tank is designed for the battery charging application.
5. The simulations of the converters will be done under open-loop by manually entering the values of the control variables, also closed loop system is done and the respective simulation results will be analysed.
6. The appropriate controller will is selected
7. Software Simulation for the closed-loop charging system will be performed using MATLAB for Resonant converter, and the simulation results will be analysed

2.5. CONCLUSION

The motivation of this dissertation work was discussed initially. A study was done on works related to battery charging, where various converter topologies, converter techniques and the charging structures were explained briefly. The Half-Bridge LC resonant conversion is initially built and simulated under a range of frequencies, including those at, above, and below the resonance frequency. This series resonant converter has been shown to work better when used close to the resonance frequency. PV system is used to provide supply to the LC resonant converter, it is designed to provide 35V, 40V and 45V under temperature of 45C, 25C and 15C. The analysis of LC resonant converter is done for Continuous and Discontinuous mode of operations. The supply of 35V, 40V and 45V is bucked to 12V which is used for battery charging. The design of resonant tank is done for line regulation, load regulation, and efficiency. Detailed design and selection of Mosfet, Inductor, Capacitor, Transformer, Rectifier circuit, Filter circuit and Load design is done. First Harmonic

Approximation (FHA) & small signal modeling are used in the mathematical modeling of the resonant converter for series applications. For a closed loop analysis the controller used here is Average Current Mode Controller (ACMC) which is a combination of voltage and current mode controller and it is found that ACMC has various advantages over them.

The operation of each converter is thoroughly explained in the next chapter. The next chapters will provide details on the converter's design, mathematical modelling, control scheme, and simulation results.

CHAPTER – 3

ANALYSIS OF THE SERIES RESONANT

CONVERTER FOR UPS BATTERY CHARGING

3 ANALYSIS OF SERIES RESONANT CONVERTER

3.1. Introduction

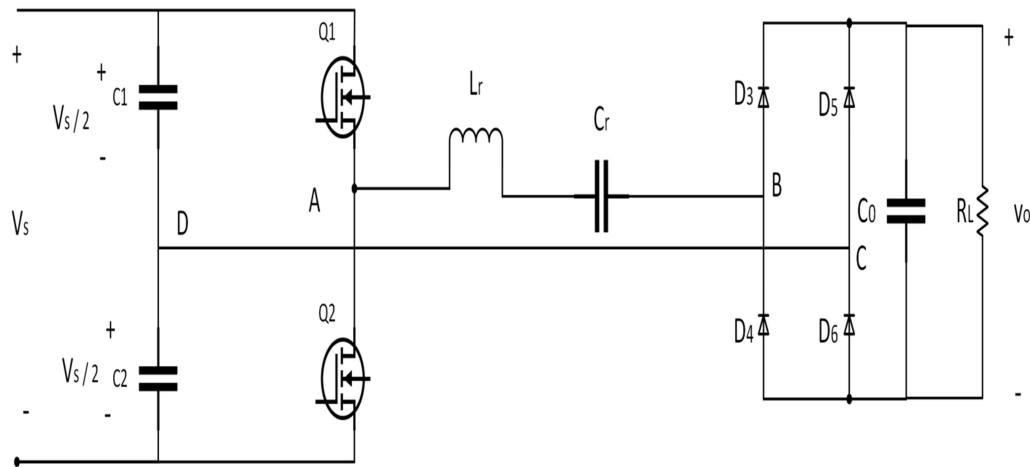


Fig 3.1: Circuit of a half bridge LC resonant converter

Figure 3.1 depicts the circuit design for a half-bridge series-loaded resonating converter of this type. In a full-wave rectification network, as the name suggests, the output load is linked in series with a resonant inductor L_r and a resonant capacitor C_r . Due to the lack of an output inductor, the series-loaded resonating converter construction has a significant advantage over the parallel-loaded kind in high-voltage applications. You may consider the rectification circuit and the load as a steady supply of V_o for a large output filter capacitor. The switching transistors Q_1 and Q_2 conduct less often than every half - cycles of a switching period inside the stable symmetrical operation. Similar behaviour is seen by the D and D_2 antiparallel diodes for a portion of each switching time half cycle. Therefore, it suffices to merely look at the first half of this resonant converter's operation. The two fixed input capacitance that act as input sources for each half of a switching period are split evenly

between the input voltage V_s . As a result, the one-half circuit diagram may be displayed as illustrated in Figure 3.1 by eliminating all parasitic resistances as stated in [33].

Essentially, this circuit is a natural frequencies series-resonant circuit. The half-bridge series-loaded conversion architecture may operate in both the discontinuous mode as well as the continuous mode in steady state. There appear to be two continuous operating modes, and based on the switching frequency, they are different.

3.2. Different Modes Of Operation

3.2.1 Discontinuous Mode ($0 < f < 0.5f_n$)

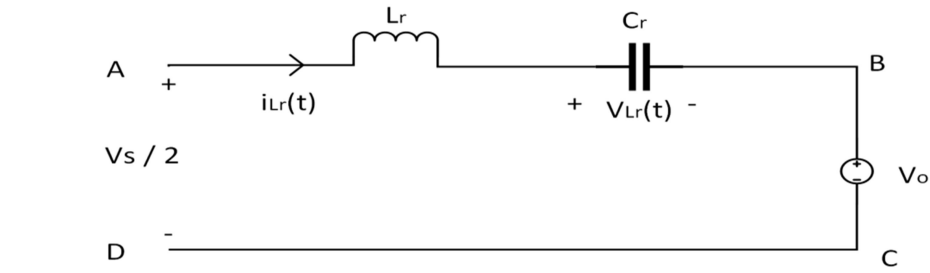


Fig 3.2: Equivalent circuit for half bridge LC resonant converter.

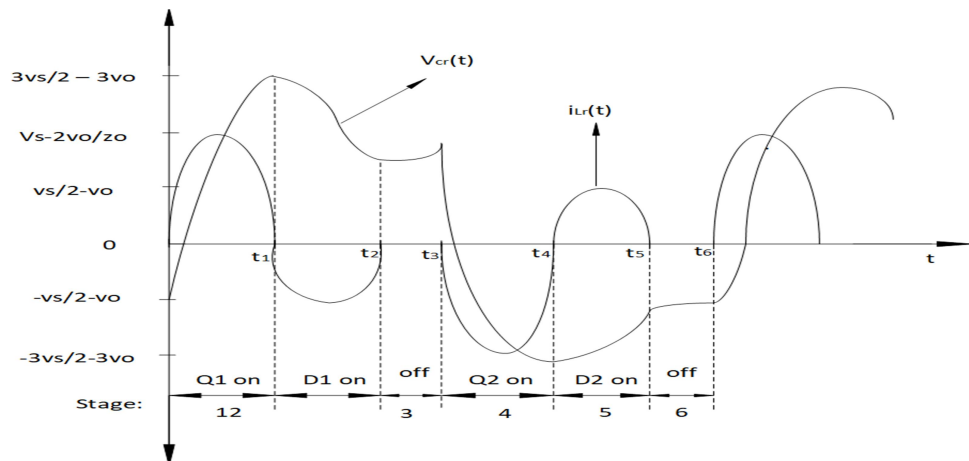


Fig 3.3: waveform of discontinuous mode of series resonant converter

A second switching transistor is activated in the second phase of a switching cycle within discontinuous operation mode even before energy within resonant inductor is used up. A switching cycle consists of six phases. Consider the case described in [33] where voltage all across resonant capacitor V_c (0) is charged to $(V_o - 0.5 V_s)$ Furthermore, before a switching cycle starts, the current through the resonant inductor, $i_L(0)$, is zero.

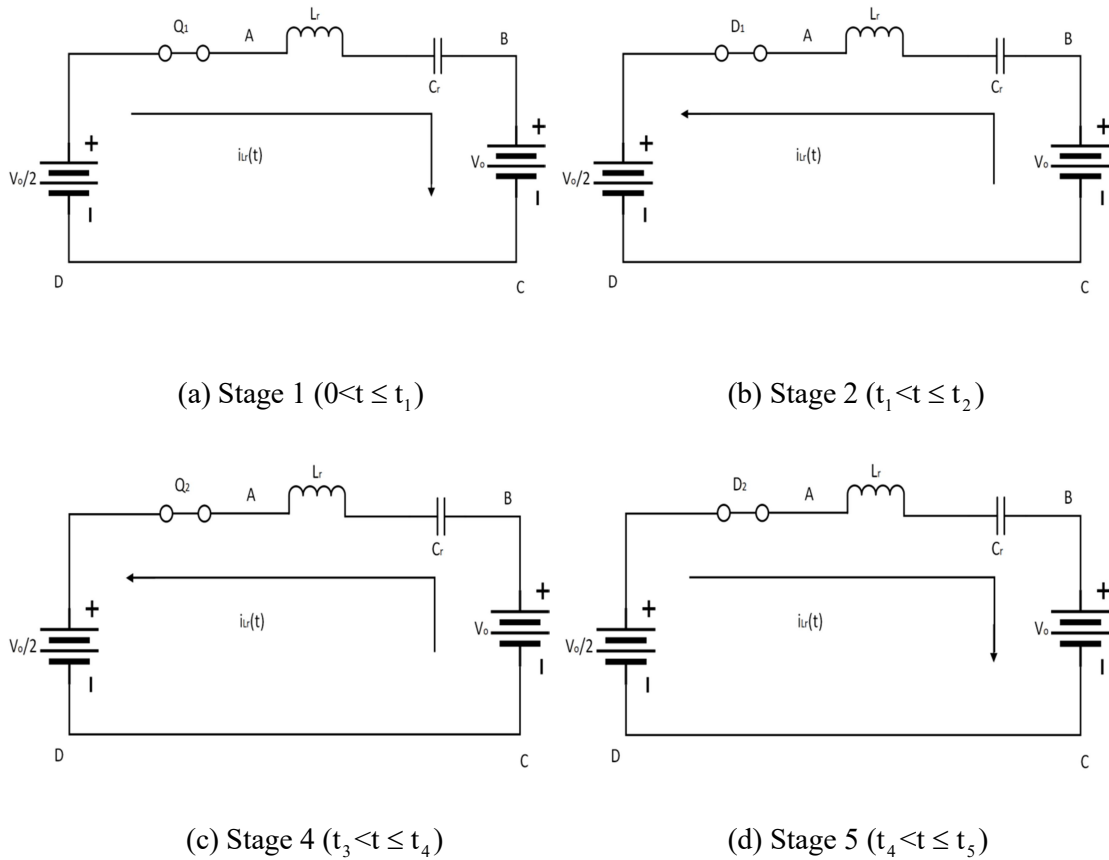


Fig 3.4: Discontinuous mode equivalent circuit diagram of series resonant converter

When the resonant inductor current changes direction as well as the antiparallel diode, D_1 , is forward biassed at time t , stage 2 starts. As the resonant capacitor transfers its stored energy to the larger input source, the voltage from across antiparallel diode $D1$ decreases. In Figure 3.4, the comparable circuit is displayed (b). Due to the current passing through

rectifiers D₄ and D₅, the voltage between terminal B and C (i.e., VBC) is shifted to the other polarity.

Applying KVL in the circuit ABCD we get,

$$\frac{V_s}{2} - L_r \frac{di}{dt} - \frac{1}{C_r} \int i_{Lr} dt - V_o = 0 \quad (3.1)$$

Taking Laplace transform to (3.1)

$$\frac{V_s}{2S} - L_r S I(S) - \frac{1}{C_r S} I(S) - \frac{V_o}{S} = 0 \quad (3.2)$$

$$\frac{V_s}{2S} = L_r S I(S) + \frac{1}{C_r S} I(S) + \frac{V_o}{S} \quad (3.3)$$

$$\frac{V_s}{2S} - \frac{V_o}{S} = I(S) \left[L_r S + \frac{1}{C_r S} \right] \quad (3.4)$$

$$\frac{V_s - 2V_o}{2S} = I(S) \left[\frac{L_r S C_r S + 1}{C_r S} \right] \quad (3.5)$$

$$I(S) = \frac{(V_s - 2V_o)C_r}{2(L_r S^2 C_r + 1)} \quad (3.6)$$

Dividing by L_r and multiplying by $\frac{1}{\sqrt{L_r C_r}}$

$$I(S) = \frac{\left(\frac{V_s - 2V_o}{L_r} \right) * \frac{1}{\sqrt{L_r C_r}}}{\left(S^2 + \frac{1}{L_r C_r} \right) * \frac{1}{\sqrt{L_r C_r}}} \quad (3.7)$$

w.k.t $\frac{a}{s^2+a^2} = \sin at$

$$I(S) = \left(\frac{V_s - 2V_o}{L_r} \right) \sin \left(\frac{1}{\sqrt{L_r C_r}} * t \right) * \sqrt{L_r C_r} \quad (3.8)$$

$$I(S) = \left(\frac{V_s - 2V_o}{\sqrt{L_r C_r}} \right) \sin \left(\frac{1}{\sqrt{L_r C_r}} * t \right) \quad (3.9)$$

$$i_{L_r}(t) = \left(\frac{V_s - 2V_o}{Z_o} \right) \sin(\omega_n t) \quad (3.10)$$

$\omega_n = \frac{1}{\sqrt{L_r C_r}}$
 $Z_o = \sqrt{\frac{L_r}{C_r}}$

Solving for $V_{cr}(t)$

$$\frac{d V_{cr}(t)}{d t} = \frac{\frac{V_s - 2V_o}{Z_o} \sin(\omega_n t)}{\sqrt{\frac{L_r}{C_r}}} \quad (3.11)$$

Integrating the above equation (3.11) we get

$$V_{cr}(t) = \int \frac{\frac{V_s - 2V_o}{Z_o} \sin(\omega_n t)}{\sqrt{\frac{L_r}{C_r}}} dt \quad (3.12)$$

$$V_{cr}(t) = \frac{V_s - 2V_o}{\sqrt{L_r C_r}} \sqrt{L_r C_r} \int \sin(u) du \quad (3.13) \quad u = \frac{t}{\sqrt{L_r C_r}}$$

$$V_{cr}(t) = \frac{V_s - 2V_o}{\sqrt{L_r C_r}} \sqrt{L_r C_r} \left(-\cos\left(\frac{t}{\sqrt{L_r C_r}}\right) \right) \quad (3.14)$$

$$V_{cr}(t) = \frac{V_s - 2V_o}{2} - \cos\left(\frac{t}{\sqrt{L_r C_r}}\right) (V_s - 2V_o) \quad (3.15)$$

$$V_{cr}(t) = \frac{V_s}{2} - V_o - (V_s - 2V_o) \cos(\omega_n t) \quad (3.16)$$

$\omega_n = \frac{1}{\sqrt{L_r C_r}}$
 $Z_o = \sqrt{\frac{L_r}{C_r}}$

3.2.2 Continuous Mode ($f_s > f_n$ Or Above Resonant Mode)

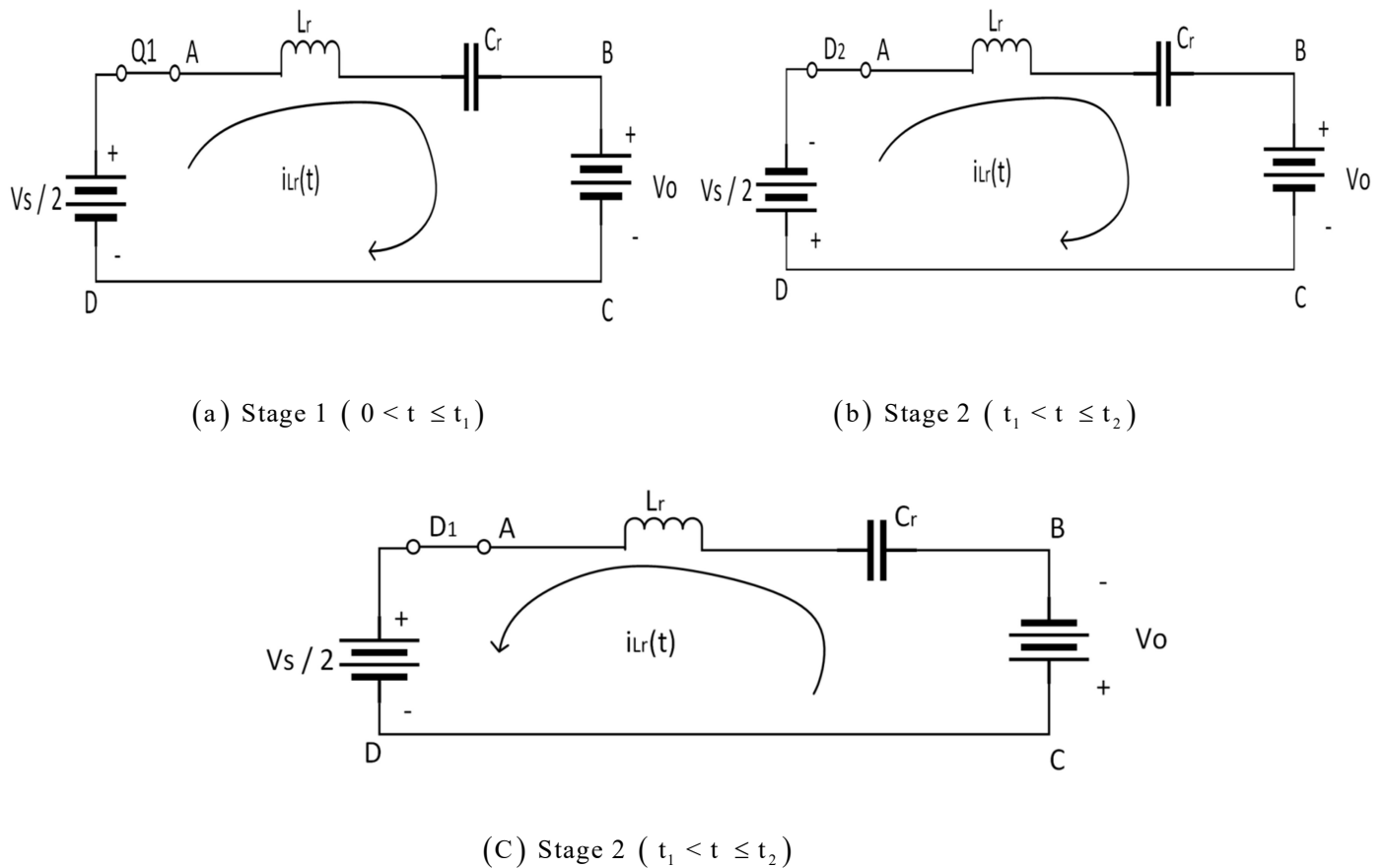


Fig 3.5: Continuous mode equivalent circuit mode of series resonant converter above resonance.

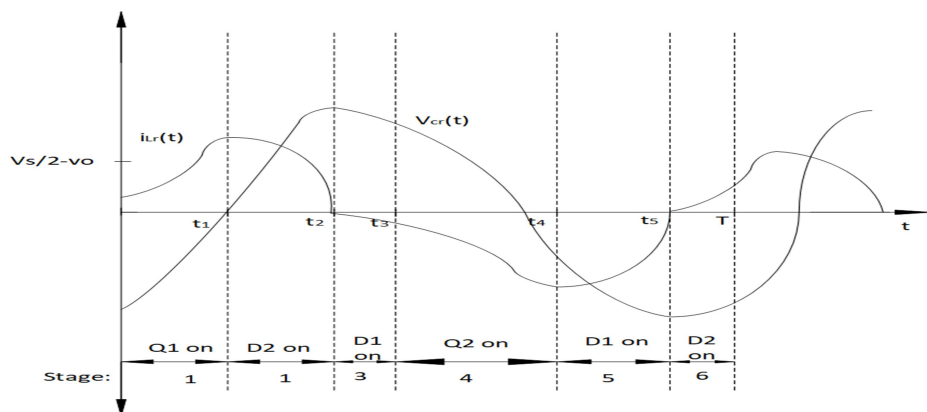


Fig 3.6: waveform of continuous mode of series resonant converter above resonance

The above-resonant continuous operating mode is composed of six stages. According to [33], Figure 3.5 depicts the first three phases of a cycle's first half. Assume that the voltage across the resonant capacitor is at a certain negative value before a switching cycle starts. It should be noted that the resonant capacitor voltage must be equal to for the resonant inductor current to peak ($0.5 V_s - V_o$). When the switching transistor Q_1 is set to turn off, stage 2 begins at time t_1 . The resonant inductor current cannot be halted, thus as soon as the forward-biased antiparallel diode D_2 begins to work, it travels through the channel through D_2 , the bottom input source $0.5 V_2$, and D_2 . A resonant capacitor voltage rises in accordance with the equation.

Applying KVL in the circuit

$$V_s = L_r \frac{di}{dt} + \frac{1}{C_r} \int i_{Lr} dt + V_o \quad (3.17)$$

Taking laplace transform (3.17) we get

$$\frac{V_s}{2S} = L_r S I(S) - I(O^-) + \frac{I(S)}{C_r S} + \frac{V_o}{S} + V_c(O^-) \quad (3.18)$$

$$I(S) = \frac{\left(\frac{V_s}{2S} - \frac{V_o}{S} \right) + I(O^-) - V_c(O^-)}{\left[L_r S + \frac{1}{C_r S} \right]} \quad (3.19)$$

$$I(S) = \frac{\left(\frac{V_s - 2V_o}{2S} \right)}{\left[L_r S + \frac{1}{C_r S} \right]} + \frac{+I(O^-)}{\left[L_r S + \frac{1}{C_r S} \right]} - \frac{V_c(O^-)}{\left[L_r S + \frac{1}{C_r S} \right]} \quad (3.20)$$

$$I(S) = \sqrt{\frac{C_r}{L_r}} \frac{(V_s - 2V_o)}{2} \sin \frac{t}{\sqrt{L_r C_r}} + \sqrt{\frac{C_r}{L_r}} \left(I(O^-) \left(\cos \left(\frac{t}{\sqrt{L_r C_r}} \right) \frac{1}{\sqrt{L_r C_r}} \right) \right) - \sqrt{\frac{C_r}{L_r}} \left(V_c(O^-) \left(\cos \left(\frac{t}{\sqrt{L_r C_r}} \right) \frac{1}{\sqrt{L_r C_r}} \right) \right) \quad (3.21)$$

$$I(S) = \frac{(V_s - 2V_o) \frac{1}{\sqrt{L_r C_r}}}{\frac{2L}{\sqrt{L_r C_r}} \left[(S^2) + \left(\frac{1}{\sqrt{LC}} \right)^2 \right]} + \frac{+I(O^-)S \frac{1}{\sqrt{L_r C_r}}}{\frac{L}{\sqrt{L_r C_r}} \left[(S^2) + \left(\frac{1}{\sqrt{LC}} \right)^2 \right]} - \frac{V_c(O^-)S \frac{1}{\sqrt{L_r C_r}}}{\frac{L}{\sqrt{L_r C_r}} \left[(S^2) + \left(\frac{1}{\sqrt{LC}} \right)^2 \right]} \quad (3.22)$$

$$i_{Lr}(t) = \frac{((V_s - 2V_o - V_{Cr}(0))}{Z_n} \sin(\omega_n t) + i_{Lr}(0) \cos(\omega_n t) \quad (3.23)$$

$$i_{Lr}(t) = \frac{-(V_s - 2V_o - V_{Cr}(t_1))}{Z_n} \sin(\omega_n t) + i_{Lr}(t_1) \cos(\omega_n t) \quad (3.24)$$

Solving for $V_{cr}(t)$

$$\frac{dV_{cr}(t)}{dt} = \frac{i_{Lr}(t)}{C_r} \quad (3.25)$$

$$\frac{dV_{cr}(t)}{dt} = \frac{\sqrt{\frac{C_r}{L_r}} \left(\frac{V_s - 2V_o}{2} \right) \sin \frac{t}{\sqrt{L_r C_r}} + \sqrt{\frac{C_r}{L_r}} \left(I(O^-) \left(\cos \left(\frac{t}{\sqrt{L_r C_r}} \right) \frac{1}{\sqrt{L_r C_r}} \right) \right) - \sqrt{\frac{C_r}{L_r}} \left(V_c(O^-) \left(\cos \left(\frac{t}{\sqrt{L_r C_r}} \right) \frac{1}{\sqrt{L_r C_r}} \right) \right)}{C_r} \quad (3.26)$$

Integrating the above equation we get

$$V_{cr}(t) = \int \frac{\sqrt{\frac{C_r}{L_r}} \left(\frac{V_s - 2V_o}{2} \right) \sin \frac{t}{\sqrt{L_r C_r}} + \sqrt{\frac{C_r}{L_r}} \left(I(O^-) \left(\cos \left(\frac{t}{\sqrt{L_r C_r}} \right) \frac{1}{\sqrt{L_r C_r}} \right) \right) - \sqrt{\frac{C_r}{L_r}} \left(V_c(O^-) \left(\cos \left(\frac{t}{\sqrt{L_r C_r}} \right) \frac{1}{\sqrt{L_r C_r}} \right) \right)}{C_r} dt \quad (3.27)$$

$$V_{cr}(t) = \left(\frac{V_s}{2} - V_o \right) - \left(\frac{V_s}{2} - V_o - V_{cr}(0) \cos(\omega_n t) \right) + i_{Lr}(0) Z_o \sin(\omega_n t) \quad (3.28)$$

$$V_{cr}(t) = \left(\frac{V_s}{2} + V_o \right) + \left(\frac{V_s}{2} + V_o + V_{cr}(t_2) \cos(\omega_n t) \right) + i_{Lr}(t_1) Z_o \sin(\omega_n t) \quad (3.29)$$

3.2.3 Continuous Mode ($0.5f_n < f < f_n$ or Below resonant Mode)

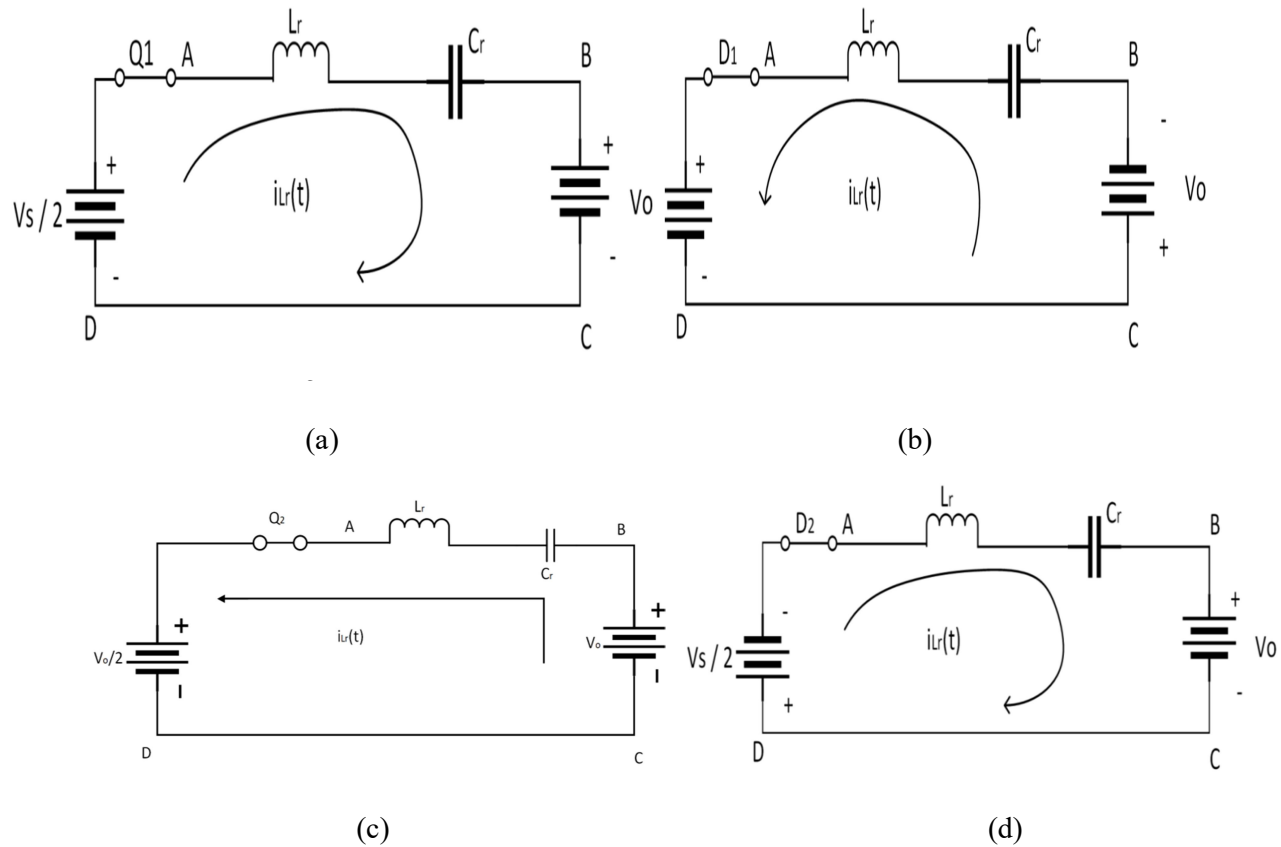


Fig 3.7: Continuous mode of series resonant converter below resonance

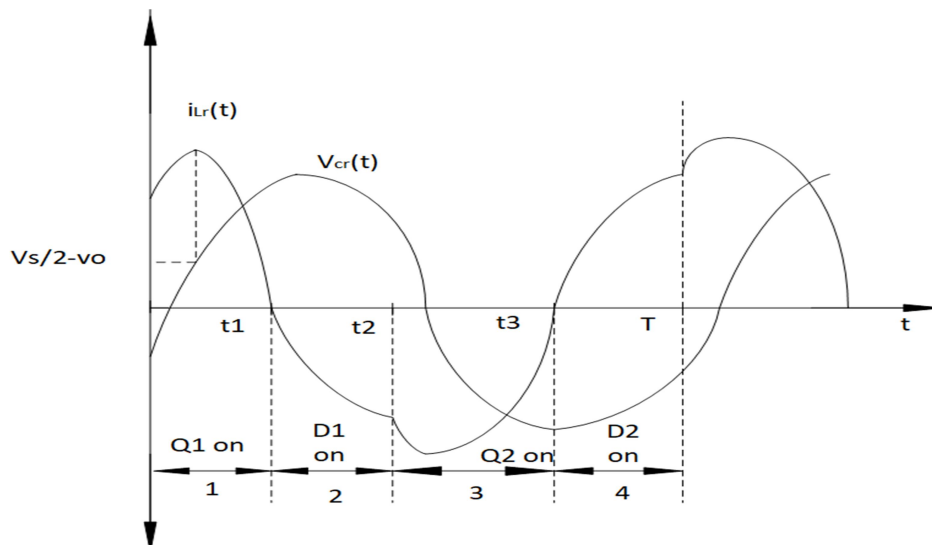


Fig 3.8: waveform of continuous mode for below resonance of series resonant converter [2]

In a single switching cycle, the below-resonant continuous state travels through four stages. Assume that before a switching cycle begins, the inductor current is still positive and the voltage across the resonant capacitor is minimal. Figures 3.7 and 3.8, respectively, illustrate the switching waveforms as well as analogous circuits. When switching transistor Q_1 engages at time $t = 0$, stage 1 begins. When the resonant capacitor voltage reaches a certain level, the resonant inductor current rises and achieves its maximum amplitude ($0.5V_s - V_o$). Therefore, the switching transistor automatically switches off when the resonant inductor current drops to zero. It's now running till then. Stage 2 starts as the antiparallel diode, D_1 , activates. The series-loaded resonant converter's steady-state normalised output current I_o vs f_s / f_n characteristics are displayed in Figure 3.8. The discontinuous mode requires a wider variation in switching frequency when the load current fluctuates in order to maintain the output voltage, V_o , as indicated. Therefore, with a significant load swing, the discontinuous operating mode should be avoided. In both of the continuous modes of operation, the output voltage is mostly constant. To increase the output voltage or current, switching frequency should be reduced in the resonant mode and increased in the below-resonant mode. According to [33], the frequency range required to regulate the output voltage is decreased.

3.3. Resonant Frequencies in an SRC

Fundamentally, the resonant circuit of an SRC displays a negligibly low resistance to a sinusoidal current only at resonant frequency, irrespective of the frequency of a square-wave voltage supplied at the input. This is commonly referred to as the selective aspect of the resonant circuit. The circuit exhibits increasing impedance values when it is not in resonance. The value of the resonant circuit's impedance at a specific frequency for a specific load

impedance determines the amount of current, or related energy, that will be delivered to the load. According to [34], a resonant circuit's impedance fluctuates with the square-wave generator's frequency to regulate how much energy is sent to the load.

The series resonant frequency, which is referred to as an SRC's single resonance, is

$$f_o = \frac{1}{2\pi\sqrt{L_r C_r}} \quad (3.30)$$

A circuit's greatest resonance frequency, f_{co} , is always equal to f_o . As a result (3.30) an SRC requires a significant frequency fluctuation to take input and output variations into account.

3.3.1. f_{co} , f_o and f_p in an LC Circuit

The LC circuit, however, would be unique. The frequency at peak resonance (f_{c0}) of the LC circuit, which shifts within the range of f_p , f_{co} and f_o as the load changes, becomes a function of load if a second inductance (L_m) is introduced. Additionally, f_o is still described, although the definition of the pole frequencies is.

$$f_p = \frac{1}{2\pi\sqrt{(L_r + L_m)C_r}} \quad (3.31)$$

Without a load, F_o is equivalent to F_p . As the load rises, F_{co} travels in the same direction as f_o . From (3.31) a load shorts out anytime $f_{co} = f_o$ happens. As a result, unlike SRC, where $f_{co} = f_o$ is defined by a single curve, LLC impedance modification follows a family of curves with f_p f_{co} f_o . This aids in lowering the frequency range needed for such an LLC resonant converter, but complicates circuit analysis.

It is obvious that f_o , as described by Equation (3.30), stays true regardless of the load,

but f_p , as expressed by Equation (3.31), only does so when the load is zero. The fact that such an LLC converter is often designed to operate close to f_0 will be shown later. For these and other undisclosed reasons, F_o is crucial for the converter's functionality and design.

3.4. Operation at, Below and Above f_o

The relationship between switching frequency, given by the acronym f_{sw} , and the series frequency describes how an LLC resonant converter operates at resonance level (f_o). An LLC resonant converter's waveform is shown in Figure with the switching frequency either at, below, or above the series resonance frequency. The graphs display the resonant circuit's magnetising current (I_m), secondary-side diode current (I_r), switch-node voltage (V_{sq}), Q_1 gate ($V_g Q_1$), and Q_2 gate ($V_g Q_2$) (I_s). The magnetising current only flows in the main side of the source, hence it has no impact on the power output of the primary-side source. However, the magnetising current and secondary-side current are combined to create the primary-side current.

3.4.1. Operation at Resonance

In this mode, the series resonant frequency and the switching frequency are the same. Once switch Q_1 is closed, there is no longer any power transfer to the secondary side since the resonant current equals the magnetising current. By delaying the moment at which switch Q_2 turns on, the circuit accomplishes primary-side ZVS and gets a mild commutation of the rectifier diodes on the secondary side. The specifications for attaining ZVS will be covered later. But it is obvious that operation at series resonance only leads to one point of operation. To take into account changes to input and output, the switching frequency must be adjusted

away from resonance.

3.4.2. Operation Below Resonance

In this scenario, the driving pulse width terminated before the resonant current reached the magnetising current's value, therefore the power transfer stops even while the magnetising current continues. It is still possible to operate below the series resonant frequency and yet achieve primary ZVS and secondary soft commutation of a rectifier diodes. To deliver the same amount of energy to the load, the secondary-side diodes must operate in discontinuous current mode, which increases the amount of circulating current in the resonant circuit. Both on the main side and the secondary side, this larger current results in higher conduction losses. However, it should be remembered that if a switching frequency dipped too low, the primary ZVS ran the danger of being lost. This will lead to significant switching losses and a number of related problems. Later on, this will be further discussed.

3.4.3. Operation Above Resonance

A resonant circuit's primary side will show less current flowing while it is in this mode. Since the resonant circuit's current runs in the continuous-current mode, providing a lower RMS current for the precise amount of load, this lowers conduction loss. While operating above the resonance frequency, primary ZVS is still feasible despite reverse recovery losses and harsh commutation of the rectifier diodes. In low-load conditions, operation over the resonance frequency may result in considerable frequency increases. As was discussed before, the converter may be created by using either f_{sw} f_o or $f_{sw} f_o$, or by altering f_{sw} on either side of f_o .

3.5. Conclusion

In this chapter, the fundamental design and functioning of a Series loaded resonant converter was thoroughly explained. Along with graphs illustrating how the output voltages, power loss, and efficiency varied as the corresponding parameters varied, the derivation of the formula for these variables was described each of the converters. The study was then examined in relation to the various operating modes. Initial discontinuous mode explanation was followed by explanations of continuous mode, then discontinuous mode. In this chapter, the SRC's resonant frequencies were also discussed.

CHAPTER – 4

DESIGN OF THE SERIES RESONANT

CONVERTER FOR UPS BATTERY CHARGING

4 DESIGN OF THE SERIES RESONANT CONVERTER FOR UPS

BATTERY CHARGING

4.1. Introduction

The series loaded resonant converter's basic construction and operation utilising their corresponding equivalent circuits were addressed in the chapter before. Using the formulas for the various circuit components and efficiency, it is possible to compute the components of converters, including their efficiency. The primary subject of this chapter is the design of the circuit elements for each converter.

As was already said, f_n is the determining element in frequency modulation. As a result, M_g can alter its output voltage by adjusting f_n given by (4.1).

$$V_o = M_g (f_n, L_n, Q_e) \times \frac{1}{n} \times \frac{V_{in}}{2} \quad (4.1)$$

Even while this argument has so far determined that the design should operate near to the series resonance, or close to $f_n = 1$, the optimal design should be restricted to the area.

4.2. Basic Design Conditions

Three crucial requirements line management, load regulation, and efficiency are nearly often taken into account initially for such a typical converter design.

The biggest output-voltage shift brought on by such input voltage fluctuation across a specific range, while an output load current is present, is known as line regulation.

The maximum output-voltage fluctuation brought on by a change in load over a predefined range typically from no load to maximum is known as load regulation.

Gain control in an LC converter is carried out via frequency modulation. It is actually possible to regulate these two methods through voltage-gain modification. In the proposed working region shown in Fig. 4.1, the gain has a rather steep slope, which can limit the range of the frequency modulation. The gain must therefore be appropriately adjusted in a range that satisfies the necessary regulatory criteria.

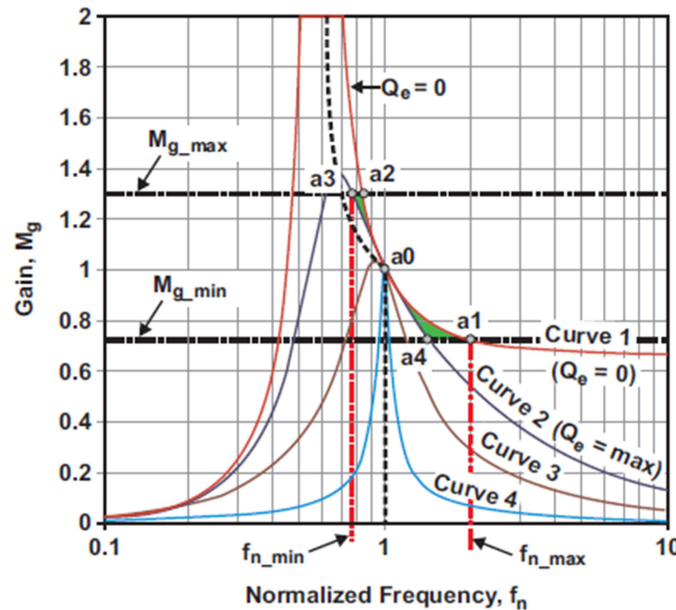


Fig 4.1: Recommended design area.

One of the main advantages of employing an LC converter is efficiency. By ensuring the primary side ZVS are maintained over the whole operating range, switching losses with the converter may be greatly decreased. ZVS cannot be achieved across the gain-plot region, as will be discussed, but ZVS will be guaranteed by maintaining the design inside the designated zone.

4.2.1.Line Requirement

Equation and the suggested design regions in Fig. 4.1 can both be used as a starting point

for developing line regulation in the creation of such a power-supply converter. It will be expected that there will be an output voltage, $V_{o\ min}$ as well as $V_{o\ max}$, with a minimum and maximum value. It is also considered that if any parasitic voltage drops, such as those generated by PCB traces, the $R_{ds\ on}$ of MOSFETs, a forward voltage of diodes, etc., have been converted or aggregated into a certain range of output voltage in order to simplify the issue. Furthermore, it is assumed that design is restricted to the switching frequency range between $f_{n\ min}$ and $f_{n\ max}$. In reality, line- and load-regulation requirements may call for modifying frequency limitations, or vice versa [34]. Given these prerequisites and assumptions, M_g should be constructed to meet Equation's requirements, which state that all feasible M_g values must have the amounts of $M_{g\ min}$ & $M_{g\ max}$ within the f_n boundaries. This makes line regulation possible (and load regulation, as explained later). For $I_o = 0$,

$$M_{g_min} = \frac{n \times V_{o_min}}{V_{in_max}/2} \quad (4.2)$$

$$M_{g_max} = \frac{n \times V_{o_max}}{V_{in_min}/2} \quad (4.3)$$

$$M_{g_∞} = \left| \frac{L_n}{L_n + 1} \right| \quad (4.4)$$

M_g shows the gain value for no load while f_n is almost at infinity from (4.2),(4.3) and (4.4)'. It is clear that the gain curve (M_g), which has its value determined by Equation at zero load, is moving closer to an asymptotic straight axis as f_n approaches infinity. $M_{g\ min}$ as well as $M_{g\ max}$ both form the horizontal line in Figure 4.1. In the no-load condition ($I_o = 0$), the quality factor (Q_e), shown in Fig. as Curve 1, is equal to zero. Since $Q_e = 0$ and L_n but also Q_e determine the gain curves, L_n is the only design element at this moment.

4.2.2. Load Regulation

4.2.2.1. Normal Load Operation

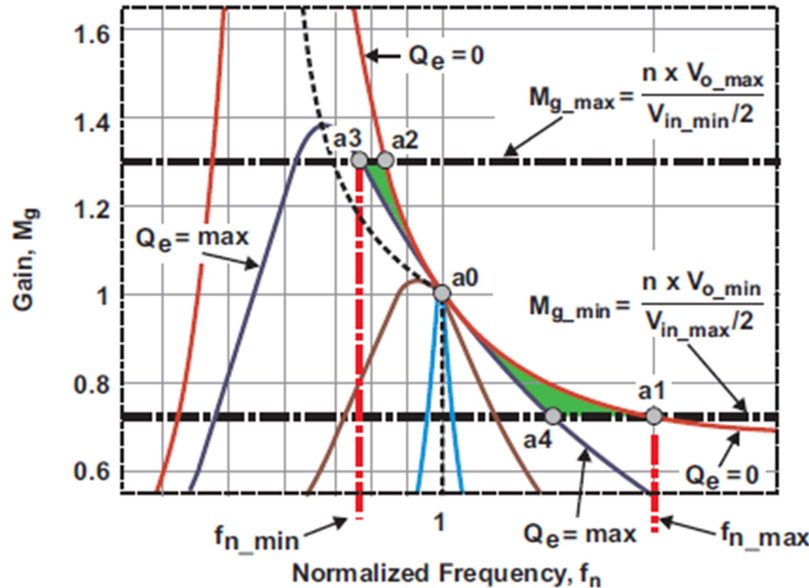


Fig 4.2: Operation boundary set by a_1 through a_4

The gain is shown as a series of curves in Fig. 4.2. Every value of Q_e results in a unique gain curve for a particular L_n . The gain curve slopes downward with a smaller peak as Q_e increases. As a result, the gain curve changes from its no-load form (Curve 1) to a smaller representation as load current increases. The peak load current ($Q_e = max$) is shown by Curve 2 in Fig. 4.2 for the same L_n and under the circumstances of Equation. As a result, the designated design area generates design points a_3 and a_4 . If the load is in fact increased, Curve 2 will start to resemble Curve 3 as well. Because of straight stripe M_{g_max} never cross over the gain curve, Equation's restrictions cannot be satisfied.

Thus, the control of the output voltage is lost. In this scenario, the gain curve will need to be rebuilt by design changes like changing L_n or possibly the switching frequency limitations. Since Q_e and load current are connected, it is acceptable to include both overload and short-circuit scenarios in this discussion.

4.2.2.2. Overload Current

The example's proposed design region in Fig. 4.2 has an overload since $Q_{e \text{ max}}$ was specified to have a quantity for it. As was already established, each further load increase causes Curve 2 to move toward Curve 3 or even beyond, extending the design's range and putting it at risk of short circuit.

4.2.2.3. Load Short Circuit

Examining the gain plot is essential to understanding what happened and learning how to regulate it in the event of a load short circuit, which might result in an excessive amount of current flowing through the converter circuit. When L_m is bypassed by such a loaded short circuit, as shown by Curve 4 in Figure, the associated gain plot is shown, identifying Curve 4 as the gain form with such a shorted output. Curve 4 explains the potential safeguards for LLC converter. Raising the switching frequency is one way to lower the gain. The gain will drop below 10% if the switching frequency is raised to a value greater than twice the series resonant frequency, as illustrated in Fig. 12. (f_o). The gain essentially zeroes out when the frequency is raised to 10 times the frequency f_o . Equation demonstrates that a loaded short circuit receives no input voltage when the gain is 0. The converter may be safeguarded against a loaded short circuit malfunction using this technique from [34].

It should be emphasised that the success of such a safety mechanism depends on how quickly the controller can receive the short-circuit alert to start increasing the frequency. The gain will unavoidably be shifted to the left of a resonant peak in the permissible design zone for some time before reaching Curve 4. The polarity of the feedback control might potentially alter as a result, among other serious problems. In light of this, an independent overcurrent

shutdown could be the best choice. If a frequency increase is still needed, two more possibilities are proposed. Add a separate high-speed control loop or reposition the suggested design area such that the minimum switching frequency ($f_{n \min}$) is always larger than the series resonant frequency (f_0), i.e., where $f_{n \min} > f_0$, to immediately begin the frequency shift.

4.3. Selecting Design Parameters f_{sw} , n , L_n and Q_e

It is now feasible to build the design after better understanding the gain behaviour. The basis of the discussion up to this point has been the consideration of the f_{sw} , n , L_n , with Q_e factors and their possible implications on circuit performance. But where should the designer begin if these aspects are not recognised while a design is being developed.

4.3.1. Selecting the Switching Frequency

Typically, the permitted switching frequency is established for a specific application. For instance, switching frequencies of 100 to 150 kHz are necessary for the majority of off-line AC/DC applications to operate well. Typically, this is due to the fact that conduction EMI testing begins at around 150 kHz. The application can pass the test by keeping the switching frequency just above the lower barrier of the EMI test. As a result, components for circuits that work in this frequency range are frequently more sophisticated, available, and affordable. There are a few factors to take into account if a special frequency range is needed for special applications. As everyone knows, switching losses and ZVS efficiency become less significant as switching frequency lowers, but converter bulk grows. A LLC converter becomes less desirable when conduction losses gain control. The advantages of the LLC converter over hard-switched converters are more evident at higher switching frequencies. If the switching frequency is actually very high, further considerations may need to be made,

such as component availability and pricing, additional board-layout issues, and additional switching losses beyond MOSFET ZVS, such as magnetic-core losses.

4.3.2. The Transformer Turns (n)

The increase magnitude in the suggested design zone might be greater or less than unity, according to Fig. 4.2. This gives the transformer turns ratio considerable flexibility. At the output voltage's initial setup, the gain can be set to unity ($M_g = 1$) at the output voltage's midpoint between $V_{o\ min}$ and $V_{o\ max}$. Even if it may not always be the case, it is possible to refer to the nominal value of the output voltage, $V_{o\ nom}$, as the halfway point. The nickname for the notional value of the input voltage is $V_{in\ nom}$, which has the same meaning. Equation (4.5) may be used to first construct the transformer turns ratio.

$$n = M_g \times \frac{V_{in}/2}{V_o} = \left. \frac{V_{in_nom}/2}{V_{o_nom}} \right|_{M_g=1} \quad (4.5)$$

4.3.3. Choosing Q_e and L_n

To execute line and load regulation over the operation range, keep in mind that the design must fulfill the requirements of Equations, which calls for two horizontal lines to pass over two gain curves between frequency boundaries. Designing circuit settings to select L_n as well as Q_e values that satisfy the equation will be covered in the next section.

4.4. Design Example

This section will guide you through utilizing the provided approach to create a LC

resonant half-bridge converter. The design is intended for small output voltage applications where energy efficiency is critical, such as the ATX12 power supply prevalent in servers and PCs.

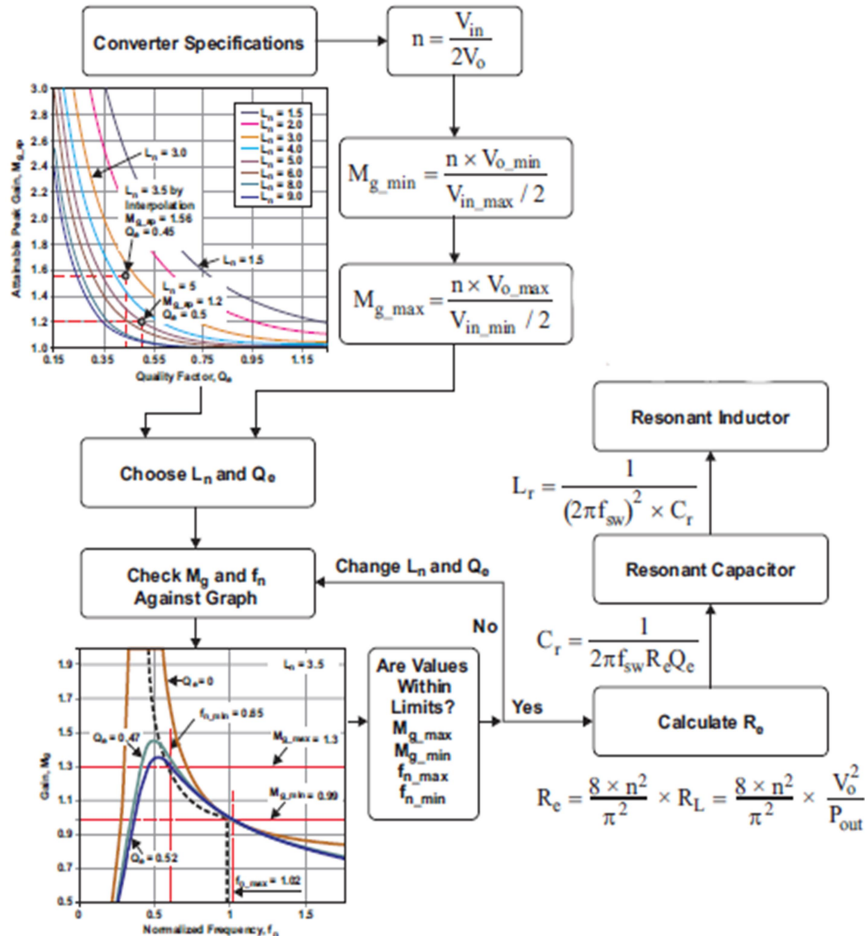


Fig 4.3: Flowchart of resonant-network design.

4.4.1. Design Steps

1. Calculate the transformer turns ratio (n)

The following equation yields the transformer turns ratio:

$$n = M_g \times \frac{V_{in}/2}{V_o} = \left. \frac{V_{in_nom}/2}{V_{o_nom}} \right|_{M_g=1} \quad (4.7)$$

$$\frac{35.20/2}{12} = 1.466 \approx 2$$

The nominal input and output voltages are 390 V and 12 V, respectively, according to (4.7) the specifications, so the turns ratio can be computed as follows:

4.4.2. Establish $M_{g\min}$ and $M_{g\max}$

Equations (4.8) and (4.9) can be used to determine $M_{g\min}$ and $M_{g\max}$.

$$M_{g\min} = \frac{n \times (V_{o\min} + V_F)}{V_{in\max}/2} \quad (4.8)$$

$$= \frac{2 \cdot (12 \cdot (1 - 1\%) + 0.7)}{40/2} = 1.27$$

$$M_{g\max} = \frac{n \times (V_{o\max} + V_F + V_{loss})}{V_{in\min}/2} \quad (4.9)$$

$$= \frac{2 \cdot (15 \cdot (1 - 1\%) + 0.7 + 1.05)}{35/2} = 1.914$$

In these calculations, 1% is added to both the load regulation and the power output from the line. It is assumed that $V_F = 0.7$ V represents with a forward voltage drop over the secondary-side diode. Power losses are thought to cause a voltage drop of $V_{loss} = 1.05$ V. If the effectiveness was expected to also be 92% ($> 90\%$ as required by the regulations), then power losses would account for 8% of a total power. An voltage output of would be produced

at 25 A with an 8% loss, which is increased to $M_{g \max}$ in order to maintain the voltage-load regulation.

4.4.3. Calculate the Equivalent Load Resistance (R_e)

$$R_e = \frac{8 \times n^2}{\pi^2} \times \frac{V_o}{I_0} \quad (4.10)$$

$$= \frac{8 \cdot (2)^2}{\pi^2} \cdot \frac{12}{12} = 3.2 \Omega$$

At 110% overload,

$$R_e = \frac{8 \times n^2}{\pi^2} \times \frac{V_o}{I_0} \quad (4.11)$$

$$= \frac{8 \cdot (2)^2}{\pi^2} \cdot \frac{12}{12 \cdot 110\%} = 2.945 \Omega$$

4.4.4. Parameter Design for Resonant Circuits

The resonant circuit's parameters are calculated using equations. A series resonant frequency may well be set to 130 kHz initially, and the resonant circuit's characteristics may then be established at full load:

$$C_r = \frac{1}{2\pi \times Q_e \times f_o \times R_e} \quad (4.12)$$

$$= \frac{1}{2\pi \times 0.5 \times 200 \times 10^3 \times 3.2} = 49.73 nF$$

$$L_r = \frac{1}{(2\pi \times f_o)^2 C_r} \quad (4.13)$$

$$= \frac{1}{(2\pi \times 200 \times 10^3)^2 \times 49.73 \times 10^{-9}} = 12.733 \mu H$$

4.4.5. Analyze the Resonant-Circuit Design.

The following describe the design criteria:

Resonant frequency in a series (4.14):

$$f_0 = \frac{1}{2\pi \sqrt{L_r \times C_r}} \quad (4.14)$$

$$= \frac{1}{2\pi \sqrt{12.733 \times 10^{-6} \times 49.73 \times 10^{-9}}} = 200.007 \text{ kHz}$$

Quality factor at full load (4.15):

$$Q_e = \frac{\sqrt{L_r / C_r}}{R_e} \quad (4.15)$$

$$= \frac{\sqrt{12.733 \times 10^{-6} \times 49.73 \times 10^{-9}}}{3.2} = 5.0004 \approx 5$$

Quality factor at 110% overload:

$$Q_e = \frac{\sqrt{L_r/C_r}}{R_e} \quad (4.16)$$

4.4.6. Determine the Primary-Side Currents

Equation gives the primary-side RMS load current (I_{oe}) with a 110% overload (4.17).

$$I_{oe} = \frac{\pi}{2\sqrt{2}} \times \frac{I_o}{n} \quad (4.17)$$

$$= \frac{\pi}{2\sqrt{2}} \times \frac{12 \times 110\%}{2} = 7.326A$$

4.4.7. Calculate the Secondary-Side Currents

The primary-side current (I_{oe}) that is referred to the secondary side is the entire secondary-side RMS load current (4.18):

$$I_{oe_s} = n \times I_{oe} \quad (4.18)$$

$$= 2 \times 7.326 = 14.652A$$

This current is equally split between the transformer's two transformer windings on the secondary side thanks to its center-tapped construction. The following formula is used to determine the current via each winding:

$$I_{sw} = \frac{\sqrt{2} \times I_{oe_s}}{2} \quad (4.18)$$

$$= \frac{\sqrt{2} \times 14.652}{2} = 10.36 \text{A}$$

Average half-wave current that corresponds to this is (4.19)

$$I_{\text{sav}} = \frac{\sqrt{2} \times I_{\text{oe_s}}}{2} \quad (4.19)$$

$$= \frac{\sqrt{2} \times 14.6}{\pi} = 6.595 \text{A}$$

4.4.8. Select the Rectifier Diodes

The voltage rating (4.20) of the diodes is calculated as

$$V_{\text{DB}} = \frac{V_{\text{in_max}}/2}{n} \times 2 \quad (4.20)$$

$$= \frac{40/2}{2} \times 2 = 20 \text{V}$$

The current rating of the diodes (4.21) is calculated as

$$I_{\text{sav}} = \frac{\sqrt{2} \times I_{\text{oe_s}}}{\pi} \quad (4.21)$$

$$= \frac{\sqrt{2} \times 14.652}{\pi} = 6.59 \text{A}$$

4.4.9. Choose the Output Filter Type and Include the Capacitors

Instead of the LC filter used in the majority of pulse-width modulated converters, an LC converter's output filter might just be capacitors, but a modest second-stage LC filter is also an option. If the filter just comprises capacitors, the capacitors should be selected such that rectifier current may flow through all AC components.

The full-wave output current (4.22) of the rectifier is written as

$$I_{\text{rect}} = I_{\text{sw}} = \frac{\pi}{2\sqrt{2}} \times I_o \quad (4.22)$$

4.5. Conclusion

According to the necessary loads, the ratings of a series resonant converter's components were established. Calculations were made to determine each power converter's efficiency. In this chapter, the ratings of the low-pass filter's filter parts were computed, and the effectiveness of a resonant converters was assessed.

In the chapter after, we'll go over the mathematical analysis of the series resonant converter applying First Harmonic Approximation as well as Small Signal.

CHAPTER – 5

MATHEMATICAL MODELLING OF THE

SERIES RESONANT CONVERTER

FOR UPS BATTERY CHARGING

5 MATHEMATICAL MODELLING OF SERIES RESONANT CONVERTER FOR UPS BATTERY CHARGING

5.1. Introduction

Depending on the particular issue that has been taken into consideration and the level of precision needed, there are several techniques to model the physical system. A mathematical modelling can also be obtained once the physical model for the system has been acquired. The mathematical models of the system define the mathematical model, which is the system's conceptual representation of the actual model. Depending on the choice of factors and the coordinate system, the physical model described might lead to several mathematical models. The method for determining basic mathematical modelling of resonant power converters utilising small-signal modelling and first harmonic approximation, as well as the transfer function of a power converters with the aid of the resonant converter ratings.

5.2. Mathematical Modelling of First Harmonic Approximation for Series Resonant Converter

When the LC converter was used, it was similar to series resonance. This suggests that the series resonance frequencies are at or close to where the primary circulating current of the resonant system is located. It may be concluded that circulating current is totally sinusoidal and mostly made up of a single frequency as a result. Even while this assumption isn't quite correct, it's close especially when the switching cycle of the square wave coincides with the series resonant frequency. What about the mistakes, though? Reality includes additional frequency components if the square wave departs from series resonance; However, an approximation using the squared wave's single fundamental harmonic may be made by

ignoring any higher-order harmonics and delaying any possible accuracy difficulties for the time being. The first harmonic approximation, a technique for creating resonant converters, is presented here (FHA). As demonstrated in [34], this method yields useful design outcomes as long as the converter runs at or near the series resonance. The gain—commonly referred to as the input-to-output voltage-transfer function can be created using the FHA approach. Following are the first steps in this process:

- 1) Treat the voltage and current of the primary-input unipolar square wave as its basic constituents, disregarding any higher-order harmonics.
- 2) Ignore the effects of the output capacitor and the transformer's secondary-side leakage inductance.
- 3) Transfer the variables you collected from the secondary side to the primary side.
- 4) Use just their fundamental components to represent the referred secondary current and the referred secondary voltage, which is the bipolar square-wave voltage (V_{so}), again excluding any higher-order harmonics.

This model is the FHA circuit model of the resonant converter. The design sample discussed in this article is built on top of it. The voltage-transfer function, commonly known as the voltage gain, may be derived using this model, as will be discussed in more detail in the next section. But first, the electrical characteristics and connections shown in Fig. 5.1 must be gathered.

5.2.1. Electrical Variable Relationships

The square-wave voltage's fundamental voltage (V_{sq}) is present on the input side as (5.1).

$$V_{ge}(t) = \frac{2}{\pi} * V_{DC} * \sin(2\pi f_{sw} t) \quad (5.1)$$

its RMS value is given in (5.2)

$$V_{ge} = \frac{\sqrt{2}}{\pi} * V_{DC} \quad (5.2)$$

Since V_{so} is roughly a square wave on the output side (5.3), the fundamental voltage is

$$V_{oe}(t) = \frac{4}{\pi} * n * V_o * \sin(2\pi f_{sw} t - \phi_v) \quad (5.3)$$

where (5.4) the RMS output voltage is and ϕ_v is the phase angle between V_{oe} and V_{ge}

$$V_{oe} = \frac{2\sqrt{2}}{\pi} * n * V_o \quad (5.4)$$

The primary current component that corresponds to V_{oe} and I_{oe} is given as (5.4)

$$i_{oe}(t) = \frac{\pi}{2} * \frac{1}{n} * I_o * \sin(2\pi f_{sw} t - \phi_i) \quad (5.4)$$

where the RMS output current is given in (5.5)

$$I_{oe} = \frac{\pi}{2\sqrt{2}} * \frac{1}{n} * I_o \quad (5.5)$$

Following that, the AC equivalent load resistance, R_e , may be computed as (5.6)

$$R_e = \frac{V_{oe}}{I_{oe}} = \frac{8*n^2}{\pi^2} * \frac{V_o}{I_o} = \frac{8*n^2}{\pi^2} * R_L \quad (5.6)$$

Similar calculations for other sinusoidal AC circuits can be used for this one (5.7). The angles occur with a frequency of

$$\omega_{sw} = 2\pi f_{sw} \quad (5.7)$$

$$\omega = \omega_{sw} = 2\pi f_{sw} \quad (5.8)$$

The respective capacitive and inductive reactances of C_r and L_r are

$$X_{C_r} = \frac{1}{\omega C_r} \quad X_{L_r} = \omega L_r$$

The connection can be explained by the ratio or gain between the input and output voltages as (5.9).

$$M_{g_min} = \frac{n * (V_{o_min} + V_F)}{V_{in_min}/2} \quad (5.9)$$

Switching mode conversion of the DC input voltage and output voltage

$$M_{g_max} = \frac{n * (V_{o_max} + V_F + V_{loss})}{V_{in_min}/2} \quad (5.10)$$

5.2.2. Voltage-Gain Function

Of course, the connection between the input and output voltages can be stated by their gain or proportion:

$$M_{g_DC} = \frac{n \times V_o}{\frac{V_{in}}{2}} = \frac{n \times V_o}{\frac{V_{DC}}{2}} \quad (5.11)$$

Once the DC input voltage and output voltage are switched into switching mode, equation (5.11) can be approximated as the proportion of the bipolar square-wave voltage (V_{so}) to the unipolar square-wave voltage (V_{sq}), as previously explained:

$$M_{g_DC} \approx M_{g_sw} = \frac{V_{so}}{V_{sq}} \quad (5.12)$$

The fundamental elements can be employed to estimate the AC voltage ratio (5.12), M_g AC, by changing V_{ge} with V_{oe} for V_{sq} and V_{so} , respectively.

To make the notation simpler, M_g will be used in place of M_g AC in this case. Fig. 5.1 illustrates how the link between V_{oe} and V_{ge} may be expressed using the electrical characteristics L_r , L_m , C_r , and R_e . the supply to output power comes next.

$$M_g = \frac{V_{oe}}{V_{ge}} = \left| \frac{jX_{Lm} PR_e}{(jX_{Lm} PR_e) + j(X_{Lr} - X_{Cr})} \right| \quad (5.13)$$

shows how the supply voltage (V_{in}) and output voltage (V_o), that were defined in regard to a metal magnesium utilising LLC-circuit standards, may be connected. Although this expression is only roughly accurate, it is nevertheless quite close to the region of series resonance. By assuming that the approximation is accurate, the equation may be stated as (5.13):

$$V_o = M_g \times \frac{1}{n} \times \frac{V_{in}}{2} \quad (5.13)$$

5.2.3. Normalized Voltage-Gain Function Format

The absolute value format is used to represent the voltage-gain function in the equation. It is hard to generalize about design challenges with such a framework. Things would be better to describe it in a conventional way. To accomplish this, the series frequency response can be used as the normalization basis (f_o). The following is then used to indicate the normalised frequency as (5.14):

$$f_n = \frac{f_{sw}}{f_o} \quad (5.14)$$

The series resonant circuit's quality factor is described as (5.15)

$$Q_e = \frac{\sqrt{L_r}}{R_e} \quad (5.15)$$

The voltage gain function can then be normalized and stated as a result of these definitions.

$$M_g = \left| \frac{L_n \times f_n^2}{[(L_n + 1) \times f_n^2 - 1] + j[(f_n^2 - 1) \times f_n \times Q_e \times L_n]} \right| \quad (5.16)$$

Additionally, the correlation between input and output voltages can be found in (5.16).

$$V_o = M_g \times \frac{1}{n} \times \frac{V_{in}}{2} = M_g (f_n, L_n, Q_e) \times \frac{1}{n} \times \frac{V_{DC}}{2} \quad (5.17)$$

5.2.4. Voltage-Gain Function Behavior

It is crucial to understand how M_g behaves in connection to the three factors f_n , L_n , and Q_e since the design strategy in this section is dependent on voltage-gain function indicated by Equation (5.17) as well as the circuit design in Fig. 5.1. The gain function's controlling parameter is frequency, abbreviated f_n . Since their physical features have already been determined, L_n and Q_e are dummy variables. Following the completion of a design, F_n changes M_g . The behavior of a gain function may therefore be illuminated by showing M_g with regard to f_n under specific conditions from a variety of L_n and Q_e parameter values.

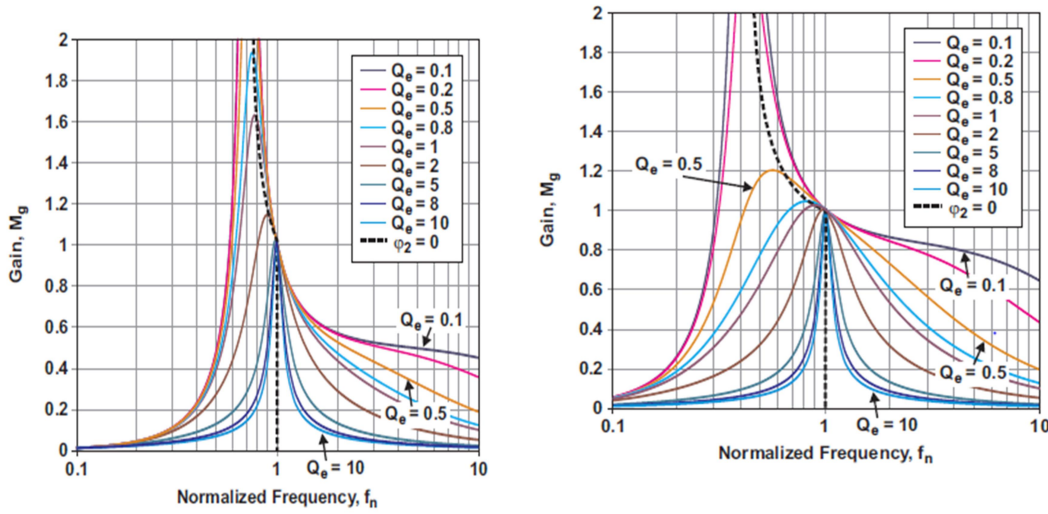
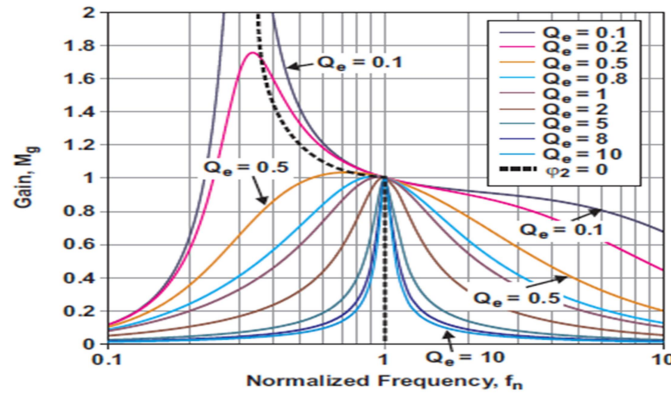


Fig 5.1: Voltage-gain function (M_g) plots with various L_n values.

The value of M_g cannot be negative. This is clear from the fact that M_g comes from the modulus operation, which symbolizes a complex expression containing real and fictional numbers. These values indicate both magnitude as well as the phase angle, however only the magnitude seems significant in this case. Within a certain L_n and Q_e , M_g displays a convex curve form in the vicinity of a circuit's resonant frequency. This is an illustration of a curve that shows a resonant converter's gain. The normalized frequency (f_n , or $f_{sw} = f_{co}$) that correspond to the resonant peak for a given L_n is changing in proportion to a variation in the load and, as a result, to a change in Q_e .



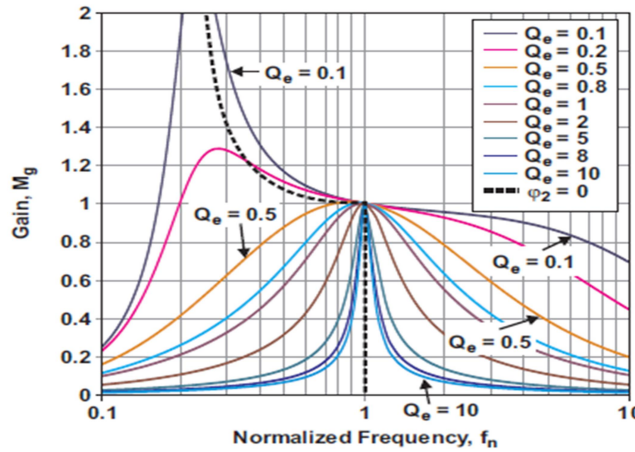


Fig 5.2. Voltage-gain function (M_g) plots with various L_n values.

Given that Q_e is the series resonant circuit's quality factor, it seems reasonable that increasing Q_e would result in a narrower curve for a set L_n . As a result, the frequency-control band would become smaller. Even as entire curve shifts downward, the amplitude of M_g likewise lowers, which causes the f_n related to that value to shift to the right as well as closer to $f_n = 1$. This frequency shift with increasing Q_e is due to the increased load. Examining equations indicates that while L_m and L_r are both constant, a rise in Q_e can be caused by a drop in RL . For the exact same series resonant frequency, C_r is fixed. Lowering RL will reduce the effect of L_m and bring f_{co} closer to f_o since RL and L_m operate in tandem. Let's examine two extremes to clearly highlight this point:

1. If RL is open, Equation states that $Q_e = 0$ & $f_{co} = f_p$. The gain peak for f_{co} is exceedingly high and theoretically limitless and is located a long way left of f_o .
2. If RL is short circuited, $Q_e = 0$ and L_m are completely bypassed or shorted, which eliminates L_m 's impact on gain. When this occurs, f_{co} moves the all way to a right, overlapping f_o , and the peak gain value for the L_m effect is equal to zero. If RL grows through infinite into zero, infinite into unity, as well as the resonant peak gain stays infinite, the

appropriate frequency at maximum resonance (f_{co}) moves from f_p to a series resonant frequency (f_o).

For a given Q_e , a decrease in L_n leads the curve to tighten, which causes f_{co} to move in the opposite direction to f_o . As a result, the peak gain of a frequency control band is higher. There are two reasons for this. Due to the dip in L_m , the arcs from f_p to f_o are initially constricted as L_n declines. Second, a smaller L_n results in a bigger L_r , which increases Q_e . As previously mentioned, the curve shrinks as Q_e rises. At first look, it seems that any combination of L_n and Q_e would be suitable for a converter design and that f_n could operate on either side of $f_n = 1$. There are other additional issues, as is stated in the section that follows.

5.3. Mathematical Modelling of Small Signal Modelling of Series Resonant Converter

Every dc-to-dc converter must meet requirements for load control, line regulation, stability, and responsiveness. It is crucial to understand how a converter responds to changes in the control signal, input, and output. Small signal circuit models are frequently used as a design tool for conventional switched mode converters as a result of this issue. The small signal equivalent circuit model provides a flexible and accessible way to get data on converter dynamics. With a rigid state space matrix system specification or a set of solved transfer functions, it is impossible to get the level of physical grasp of converter behaviour that is provided by such a model. For different impedances and transfer functions, it is simply to solve.

Since a resonant converter is frequently a component of a closed-loop system regulator

system that also includes an output and input filter, a feedback/compensation system, and a modulator, circuit models are very helpful in this situation. The entire system may be examined using the well-known methods of linear circuit theory if the resonant converter energy phase is in fact treated as a circuit. With the use of such a model, it is simple to see how the regulator responds to modifications made to existing circuit components or the addition of new ones. For resonant converters, several equivalent circuit models have been described. The research was used to something akin to a series resonant converter inside CY control mechanism, where switching frequency is implicitly regulated by the diode conduction angle α , as a first step toward comparable circuit modelling for resonant converters. The output side of the tank circuit is detailed using a lumped transfer matrix at the investigation's completion. It is recommended that the series and parallel resonant converters have direct switching frequency control using comparable circuit modelling. This theory claims that the dynamic of series resonant converters is controlled by a single slow pole, which is mostly caused by the filter capacitor and load, whereas the dynamic of the former is controlled by a complex pair of quick poles, which are mainly caused by the resonant states. The switching and resonant frequencies are said to diverge at this time. Later, this idea is expanded to include the impact of the tank circuit's dc output impedance. This method utilises an approximation since it relies on an intuitive rather than a formal derivation, achieving a suitable compromise between accuracy and simplicity. For such a series resonant converter, a brand-new lumped model with precise definitions was proposed. The suggested models have both accurate (discrete time) and inaccurate (continuous time) variations, and experimental validation is provided.

The current thesis presents a systematic, all-inclusive, and user-friendly technique for modelling resonant converters that can be used to any resonant converter, independent of the

number of tank or filter components. Any operating mode and any operating point within that mode are properly predicted by the research. Similar to the modelling for pulse width modulated conversion filter states, the proposed precise model takes into account both the tank states as discrete data and the filter states as continuous time average states. As a result, it is feasible to discover new information on the differences between the filter storage states and resonant energy transfer states. After obtaining the accurate model, a low frequency estimate is generated to create an approximate model that offers a better understanding of the performance of resonant converters. The poles and zeros of the lumped parameters can be predicted using this approximation, and the relevant dc advantages of output impedance as well as the control the output transfer function can be found instantly.

5.3.1. Small Signal Steady State Relations for Resonant Converters

Finding an operating point for a stable state is the first step in the dynamic analysis of resonant converters. In particular, the steady state behavior of parallel and series resonant converters is covered in this section. There are solutions provided for various dc quantities, a quick review of terminology is given, and converter functioning is described.

A series resonant converter rectifies and filters this current to produce the dc output current I . For the parallel resonant converter described in [35], the piecewise sinusoidal tank capacitor is rectified and filtered to provide a dc output voltage V . The connection between switching frequency f_s as well as the resonant frequency f_o determines the size of the resonant current with in series resonant converter and, therefore, the output current. Similar to this, this connection regulates the output voltage by determining the size of a tank capacitor voltage with in parallel resonant converter.

For such a normalised switching frequency $F = F_s/F_o$ given by the series resonant

converter, the k th continuous conduction mode arises.

$$\frac{1}{(k+1)} < F < \frac{1}{k} \quad (5.18)$$

Fig. 5.2 shows the continuous conduction mode of a series resonant converter with resonance at $k = 1$ or lower. The other mode investigated in this thesis is the continuous conduction mode with $k = 0$, often known as above resonance. Similar investigations are made of the above resonance ($k = 0$) and below resonance ($k = 1$) modes of operation of the parallel resonant converter. Current and voltage waveforms of a parallel resonant converter in the mentioned resonance operation mode.

The analysis makes use of the following terminology: Capital letters are employed to represent dc steady state amounts, whereas lower case letters are employed to represent time-varying or small signal ac values. The sign M is used to indicate voltages, which are normalized in relation to a input voltage V_r . As an illustration, the normalised dc output voltage is represented by

$$M = \frac{V}{V_g} \quad (5.19)$$

Currents are represented by the letter J and normalised with respect to the base current V_g/R_o , where R_o is the tank's characteristic impedance.

$$J = \frac{1}{(V_g / R_o)} \quad (5.20)$$

A radian amount is additionally normalised for the dc switching period to complete the picture:

$$\Gamma = \frac{\pi}{F} \quad (5.21)$$

These rules apply to each and every part of this discussion. A series resonant converter's behaviour in steady state is well known. When output current J vs. output voltage M is depicted with on the normalised output plane, it has been found that the solutions for output voltage and current look to be an ellipse. The continuous conduction mode's output qualities, each ellipse representing a different operating frequency value. It is possible to acquire the parallel resonant converter's steady state analysis. The output characteristics, like the input characteristics, are elliptical curves for a specific switching frequency.

5.3.2. Equivalent Circuit Model of Small Signal

The general derivation of the parallel and series resonant converter small signal circuit types is covered in detail in this section. The results are a sample two-port model for such tank and switches, as well as an estimated model of a filter states. The parameters of the model are then described, and a continuous time network is constructed that used a low frequency approximation.

Prior to anything else, it is important to select the appropriate state variables, that is a difficult procedure in and of itself. The resonant converter is transformed into a sampled system by the modulator's action. However, the converter can exist in two categories of energy storage modes that are fundamentally different from one another: the filter states as well as the tank states, both natural frequencies are in the same range as the switching frequency whose natural frequencies differ greatly from one another. At frequencies close to the switching frequency, waveforms in the tank react to sampling. It is necessary to think of a

tank states as discrete data according to [36] in order to take sampling effects into consideration. The filter inductor and capacitor must be modelled differently, though. The output voltage variations have continuous temporal values that may be accurately quantified. The high frequency effects caused by the sampling have no influence on the filter's inductor current or capacitor voltage since the switching frequency is significantly lower than the intrinsic time constants of the output filter state. The precision of a filter capacitor voltage and inductor current response may also be averaged over a short time period compared to its intrinsic time constant. The output voltage state is considered as a continuous time power storage state as a consequence of averaging the dependant quantity V_2 or I of a tank states that is applied to the filter.

As a result, the suggested model treats the filter inductor current as well as capacitor voltage as continuous time quantities while treating the tank output and input current as averaged values. The input voltage is presumed constant throughout, the filter states were averaged across the switching period, and the tank states are sampled. We find that the tank states and the filter states are connected by the average values for the dependent tank variables, such like I for the series as well as V_2 for parallel resonant converter. These dependent values are recognized as tank outputs, whilst the independent terminal values either at tank circuit port are known to as tank inputs. Large signal state formulae for such inductor current and tank capacitor voltage are provided. Auxiliary expressions are found for a variety of intermediate quantities, including bridge switching time a . For the averaged filter states, it is also feasible to find big signal state equations. The big signal state equations including auxiliary equations were perturbed and linearized, and the coefficients of a small signal ac formulas is simplified by applying the dc relations. This approach results in a number of tiny signal equations, as well as the coefficients are provided a circuit meaning.

These two port models of a tank circuit and the model of a filter states are combined numerically to form the final model.

5.3.2.1. The Small Signal State Equations are Derived

The small signal derivation is based on the formulation of big signal difference equations again for energy storage components. These inductor current & tank capacitor voltage changes can be expressed in writing as follows:

$$\frac{\Delta V_c(t)}{\frac{T_s}{2}} = \frac{-V_c\left(\frac{t_s}{2}\right) - V_c(0)}{\frac{T_s}{2}} \quad (5.22)$$

$$\frac{\Delta i_L(t)}{\frac{T_s}{2}} = \frac{-i_L\left(\frac{t_s}{2}\right) - i_L(0)}{\frac{T_s}{2}} \quad (5.23)$$

Where numbers have such a negative sign at the conclusion of a half switching period due to the waveform's peculiar symmetry around $t/2$ during switching period t_s . The two sides of a difference equation are divided by the sampling time $T/2$ to convert the tiny signal coefficients into circuit values that can be measured. Large signal equations also are given for dependent numbers at the output and input ports of a resonant element of the converter. Currents make up both dependent variables in the series converter.

$$-i_2(nT_s) = \frac{q_{0n} + q_{1n}}{\frac{t_{sn}}{2}} \quad (5.24)$$

$$-i_2(nT_s) = \frac{q_{0n} - q_{1n}}{\frac{t_{sn}}{2}} \quad (5.25)$$

According to an examination of the flux on the output inductor, the dependent quantity at the output port of the parallel converter is a voltage:

$$V_2(nT_s) = \frac{f_{0n} - f_{1n}}{\frac{t_{sn}}{2}} \quad (5.26)$$

the final values of a states at time $t_s/2$ in relation to the initial values of a states & inputs for such a time period. This connection is found by solving the circuit topologies in the resonant sub-intervals between and after the bridge rectifier switches. For example, the circuit topology which emerges after bridge switches are solved to deliver the series converter's inductor current in the $k = 1$ mode during time $1/2$ is as follows:

$$i_L\left(\frac{t_s}{2}\right) = \frac{1}{R_o} (V_{c1} - V_c - V_g) \sin\left(\omega_o\left(\frac{t_s}{2} - t_a\right)\right) \quad (5.27)$$

Then equation (5.21) is substituted into equation to obtain the actual big signal equation (5.25). The series converter's tank inductor current is 0 when the bridge changes. The rectifier switching time = W_{of} & capacitor voltage V_c are obtained whenever the bridge switches are provided (already disturbed and linearized) in 5.26 and 5.27:

$$\hat{a} = \frac{R_o \cos(A) \hat{i}_L - \sin(A) (\hat{v}_c + \hat{v} - \hat{v}_g)}{-V_{AO}} \quad (5.28)$$

$$\hat{V}_{Cl} = \frac{R_o^2 I_{Lo} \hat{i}_L - V_{Lo} \hat{V}_C + (V_{Co} - V_{Cl})(\hat{V} - \hat{V}_g)}{-V_{AO}} \quad (5.29)$$

The proper equations for alpha & i_{L1} are, since the bridge switches in such a parallel converter whenever the capacitor voltage is zero. The big signal equations is perturbed, linearized, as well as the dependent quantities are removed using (5.27) to provide a set of small signal state equations that captures the dynamics of the converter at a certain steady-state operating point (5.29). The units of a coefficients correspond to the linear circuit components since the system has been linearized. The inputs and independent state variables are rigorously represented in terms of each state equation. The letters R, g, and K in the following analysis stand for resistance, conductance, and a gain with no dimensions, respectively. A series resonant converter contains two tank states, an equation for the input current, and an equation for the output current:

$$L \frac{\Delta \hat{i}_L}{T_s} = -K_{1c} \hat{V}_m - R_a \hat{i}_L + K_1 \hat{V}_g - K_1 \hat{V}_c - K_2 \hat{V} \quad (5.30)$$

$$-\hat{i}_2 = -g_{1c} \hat{V}_m + K_4 \hat{i}_L - g_1 \hat{V}_g + g_1 \hat{V}_c - \frac{1}{R_b} \hat{V} \quad (5.31)$$

$$\hat{i}_g = -g_{3c} \hat{V}_m - K_5 \hat{i}_L + \frac{1}{R_g} \hat{V}_g + g_4 \hat{V}_c + g_2 \hat{V} \quad (5.32)$$

5.3.2.2. Circuit Models for Lumped Parameters

The tiny signal state equations for the parallel and series resonant converters have the form of (5.18) - (5.20). Since understanding tank states only helps to the extent that they

impact the converter's output and input ports, the stated tank state variables could be eliminated.

\hat{i}_L	K_{1C}	$2M_{L0}$
	R_a	$R_o \left(1 + \frac{M_{LO}(M_{LO}-2)}{M_{AO}^2} - \frac{(-1)^k J_{LO}^2}{M_{AO}M_{A1}} \right)$
	K_1	$\frac{J_{LO}}{\Gamma M_{AO}} \left(\frac{(2-M_{LO})}{M_{AO}} + \frac{(-1)^k M_{LO}}{M_{A1}} \right)$

\hat{V}_c	g_{2c}	$\frac{-J_{LO}}{R_o}$
	K_5	$\frac{(-1)^k J_{LO}}{\Gamma M_{AO}} \left(\frac{(2-M_{LO})}{M_{A1}} + (-1)^k \frac{M_{LO}}{M_{AO}} \right)$
	$\frac{1}{R_c}$	$\frac{1}{\Gamma R_o} \left(1 - \left(\frac{J_{LO}}{M_{AO}} \right)^2 + (-1)^k \frac{M_{LO}(2-M_{LO})}{M_{AO}M_{A1}} \right)$
	g_2	$\frac{(-1)^k}{\Gamma R_o} \left(-1 + \left(\frac{J_{LO}}{M_{AO}} \right)^2 - (-1)^k \frac{(2M_{AO}-M_{LO})(2-M_{LO})}{M_{AO}M_{A1}} \right)$

	g_3	$\frac{1}{\Gamma R_o} \left(1 + \left(\frac{J_{L0}}{M_{A0}} \right)^2 + (-1)^k \frac{(M_{L0}-2)M_{L0}}{M_{A0}M_{A1}} \right)$
--	-------	---

\hat{i}_g	g_{3c}	$\frac{(J + (-1)^k MJ)}{R_o}$
	$\frac{1}{R_g}$	g_3
	g_4	$-g_3$

A lumped parameter models the effect of such an independent quality on a dependent variable at the port of interest. A y parameter model is the most suitable one since the currents I_s and I_2 as well as the voltages v_g and v represent independent and dependent variables, respectively, for series resonant converter. For the parallel resonant converter, the voltage v_g and the current I_2 are independent variables, while the voltage v_2 and the current I_e are dependent variables. A hybrid mode is therefore the suitable model. For instance, a series resonant converter model's y parameter, y_{21} , is given by

$$\omega_{sw} = 2\pi f_{sw} \quad (5.33)$$

And k_{21} is given by

$$K_{21} = \frac{\hat{v}_2}{\hat{v}_g} \Big|_{\hat{v}_m=0, \hat{i}_2=0} \quad (5.34)$$

An independent source is added to each port in both models to explain the influence of the control variable f , and the effect of the control variable is represented by a lumped parameter with the subscript c . The tiny signal filter model is connected with the lumped parameter model of the tank circuit to complete the overall equivalent circuit [37]. The series resonant converter's filter state equation is

$$C_F \frac{d\hat{v}}{dt} = - \left(\hat{i}_2 + \frac{\hat{v}}{R} \right) \quad (5.35)$$

$$C_F \frac{d\hat{v}}{dt} = - \left(\hat{i}_2 + \frac{\hat{v}}{R} \right) \quad (5.36)$$

$$L_F \frac{d\hat{i}_F}{dt} = \hat{v}_2 - \hat{v} \quad (5.37)$$

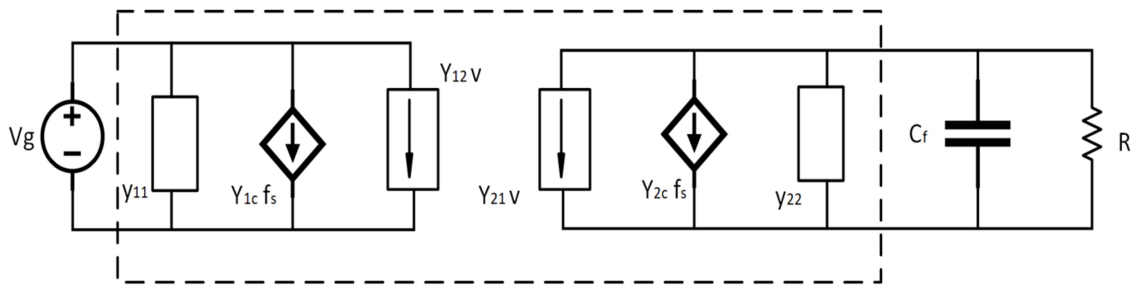


Fig 5.3: equivalent circuit for the series resistor converter's y-parameter model using lumped parameters

$$z = e^{j\omega T_s/2} = \cos\left(\omega \frac{T_s}{2}\right) + j \sin\left(\omega \frac{T_s}{2}\right) \quad (5.38)$$

For accuracy at high perturbation frequency $w = 2/T$, the discrete version of a y parameters given (5.38) must be used. However, an approximation may be employed to simplify the analysis at low perturbation frequencies:

$$e^{j\omega T_s/2} \approx 1 + j\omega \frac{T_s}{2} \quad (5.39)$$

The y parameters then take on the following form:

$$y_{mn} = A_\infty \frac{a_o + a_1 \left(\frac{s}{\omega_o} \right) + \left(\frac{s}{\omega_o} \right)^2}{b_o + b_1 \left(\frac{s}{\omega_o} \right) + \left(\frac{s}{\omega_o} \right)^2} \quad (5.40)$$

where the definition of ω_o in Eq (5.40). This equation can be rewritten in standard form and has a continuous time interpretation:

$$y_{mn} = A_o \frac{1 + \frac{1}{Q_z} \left(\frac{s}{\omega_z} \right) + \left(\frac{s}{\omega_z} \right)^2}{1 + \frac{1}{Q_p} \left(\frac{s}{\omega_p} \right) + \left(\frac{s}{\omega_p} \right)^2} \quad (5.41)$$

$$A_o = A_\infty \frac{a_o}{b_o} \quad (5.42)$$

$$\omega_z = \omega_o \sqrt{a_o} \quad (5.43)$$

$$Q_z = \frac{\sqrt{a_o}}{a_1} \quad (5.44)$$

$$\omega_p = \omega_o \sqrt{b_o} \quad (5.45)$$

$$Q_p = \frac{\sqrt{b_o}}{b_1} \quad (5.46)$$

The frequency domain is used to illustrate these associations. In this instance, A denotes the zero-frequency gain and A denotes the infinite frequency gain. Be mindful that the identical coefficients, b_o and b_1 , apply to all twelve lumped parameters.

$$b_o = \frac{R_a}{R_c} + K_1 K_5 \quad (5.47)$$

$$b_1 = \frac{R_o}{R_c} + \frac{R_a}{R_o} \quad (5.48)$$

Even though it is expected that the coefficients for the series and parallel converters have different values. An even simpler model may be created by using just the dc gain A of each of the lumped parameters [38]. This especially accurately approximates the parameters $y_{22}(0)$ and $k_{22}(0)$, which are constant up to frequencies close to the switching frequency. It is a decent low-frequency approximation for $y_s(s)$ and $y_o(s)$, but it differs from the real converter behaviour at higher perturbation frequencies because it ignores the high-frequency dynamics caused by sampling. The dc gain A. may be obtained directly by differentiating steady state formulations for the input current relations and output plane relations.

$$R_{22} = \frac{R_o \Gamma \left(J\Gamma/2 + (-1)^k \right)}{2M \tan^2(\Gamma/2)} \quad (5.49)$$

The other parameters' dc gains can be determined using implicit using the parameter R_{22} allows for differentiation and simplification. The dc gain of $y_{21}(s)$, for instance, is given by

$$G_{21} = \left(\frac{J}{R_o} + \frac{M}{R_{22}} \right) \quad (5.50)$$

For each of the parameters, this method offers a convenient way to evaluate the parameter a.

$$a_o = b_o \frac{A_o}{A_\infty} \quad (5.51)$$

The dc gain of the controller transfer function requires special consideration. An implicit derivative of a steady flow output equation for such series resonant converter must take the fluctuations in output voltage & output current into account:

$$\frac{\partial J}{\partial \Gamma} = \frac{1}{\Gamma} \left[-J + \frac{-2M \frac{\partial M}{\partial J} \frac{\partial J}{\partial \Gamma} \tan^2\left(\frac{\Gamma}{2}\right) + (1+M^2) \tan\left(\frac{\Gamma}{2}\right) \sec^2\left(\frac{\Gamma}{2}\right)}{\sqrt{1+(1-M^2)\tan^2\left(\frac{\Gamma}{2}\right)}} \right] \quad (5.52)$$

But from the output relation's normalization,

$$J=MQ$$

$$K_{2c} = \frac{\partial i_2}{\partial f_s} = \frac{V_g}{R_o f_s} \left[\frac{-J + (1-M^2) \tan\left(\frac{\Gamma}{2}\right) \sec^2\left(\frac{\Gamma}{2}\right)}{\frac{J\Gamma}{2} + (-1)^k + \frac{2M}{\Gamma Q} \tan^2\left(\frac{\Gamma}{2}\right)} \right] \quad (5.53)$$

The load resistance R, filter capacitor C, and control source current generator K are shown in parallel. Consequently, in this simplified model, the control to output transfer function is

$$\frac{\hat{v}}{f_s}(s) = -K_{2c} R \parallel R_{22} \frac{1}{1+sC_F R \parallel R_{22}} \quad (5.54)$$

Where K_2 and R/R_{22} stand for the transfer function's dc gain. It is also possible to determine the dc gain of such a transfer function by resolving the steady state equation for output current J for such normalised output voltage M. The resulting expression can then be identified in relation to f. Since the parameter R is, in fact, the slope of the ellipse in the output plane, using this approach is comparable to determining the slope of a M versus F characteristic. Consequently, the control curve's slope is likewise determined by

$$\frac{\partial v}{\partial f_s} = -K_{2c} R \parallel R_{22} \quad (5.55)$$

Similar claims can be made for the parallel resonant converter, however because the load resistor and ac resistor are connected in series, the control transfer function's dc gain is

$$\frac{\hat{v}}{\hat{f}_s}(0) = K_{2c} \frac{R}{R + R_{22}} \quad (5.56)$$

In conclusion, the initial stage in the development of small signal models with resonant converters is the building of large signal state equations for such independent tank states with large signal averaged equations for such dependent tank values, like tank input and output currents. These huge signal equations are perturbed, linearized, as well as the intermediate values were eliminated using auxiliary equations to produce the compact signal circuit equations. Then, using lumped parameters, the tank states are readily simulated. The lumped parameter tank equivalent circuit is merged with a small signal model of the averaged states to produce the model for the entire resonant converter. Several comparable circuit types are available. First, a specific model that considers the sampled nature of the tank is presented. After that, a lower frequencies assumption is used to continually simulate the tank and switches. This method results in each lumped parameter having two poles & two zeros. In the simplest model, the lumped components are eventually expressed by their dc gains. Differentiating the steady flow output expressions will reveal these advantages.

5.4. Conclusion

In this chapter, the mathematical modelling of the First Harmonic Approximation and Small Signal was done for Series Resonant Converter. The expression for the transfer

function of for the resonant converters were obtained, and the bode plots of these transfer functions were drawn. The time response specifications of both, the rectifier and the regulator were calculated in this chapter. The mathematical models so obtained in this chapter aid in designing the controller for the resonant converters. The design procedure of the control system employed for the resonant converters will be covered in the next chapter.

CHAPTER – 6

DESIGN OF CONTROLLER FOR

THE SERIES RESONANT CONVERTER

FOR UPS BATTERY CHARGING

6 DESIGN OF CONTROLLER FOR THE SERIES RESONANT CONVERTER FOR UPS BATTERY CHARGING

6.1. Introduction

Using the parameters provided in Chapter 4 and the mathematical modelling for the First Harmonic Approximation & Small Signal in the preceding chapter, their transfer function was determined. The controller for resonant converters may be developed using the transfer functions that were acquired. This chapter will first describe the requirement for a controller before going into great depth on how to create resonant converters.

6.2. Need for the Controller

The control system is a way to maintain any amount in any system, whether it a machine, mechanism, or piece of equipment, as well as to change how it performs. The controllers help with automated control of the system's output and increase the converter's steady-state performance and transient responsiveness. Open-loop controls and closed-loop controls are the two different types of controls. In most cases, closed-loop control is used. A closed-loop control for such resonant converter would be described in this chapter.

6.3. Introduction to Average Current Mode Control

The concept for average current mode control (ACMC) first put out in the latter part of the 1980s. Despite being widely used in power factor correction rectifier application using the Boost topology for continuous conduction mode, the ACMC has not yet been fully adopted in

low voltage DC-DC converters. The intricacy of the control mechanism may be a contributing factor in this.

Although small signal average models of varied complexity have been developed in the past, modelling is opposed to Peak Current Mode Control has received less attention in the literature (PCMC). The simplest model, which only considers the low frequency dominant pole, is offered to make control loop study and building simpler. A substantially more complicated model is developed [39] to examine the effect of a inductor current ripple just on precision of the loop increase estimation of ACAC DC-DC converters. Because of a lack of physical comprehension of the methodology and results, the model has not been adopted for design-oriented evaluation or practical application. After a detailed examination of the effect on inductor ripple current also on modulator gain, a corrective term is introduced to a PWM modulator gain. By transferring sampled data modelling, which was used in PCMC, to ACAC, a set of right half plane poles with such a frequency half of the switching frequency were added to a control to output voltage transfer function. The idea suggests that sub harmonic oscillations might still exist in ACAC. However, results from simulations and experiments imply that this may not be case. An ACAC model is proposed in light of this result and the well-established multi-loop analysis. The model does not account for the sampling impact or the ripple effect of a inductor current mostly on PWM modulator gain. The voltage feed forward as well as feedback is also incorporated into the prediction models from separate research [40], which is in good agreement with the experimental results. The model is quite succinctly given; however, it is difficult to modify for design-oriented study and practical designs. A unique model for such Buck converter is presented in a recent work, greatly simplifying the previous idea. The freshly constructed model offers useful insight on ACAC in contrast to older models, and all parameters of the model are given by parameters

of a Buck converter circuit. This work greatly extends the analytical method to extract additional equations for such Boost & Buck-Boost architectures in a cohesive way. The ACMC investigation in this publication is more extensive when compared to evaluations that include all duty cycle procedures. Experimental results are shown using a Boost converter as such an illustration, and measurements are used to confirm the precision of a new model prediction.

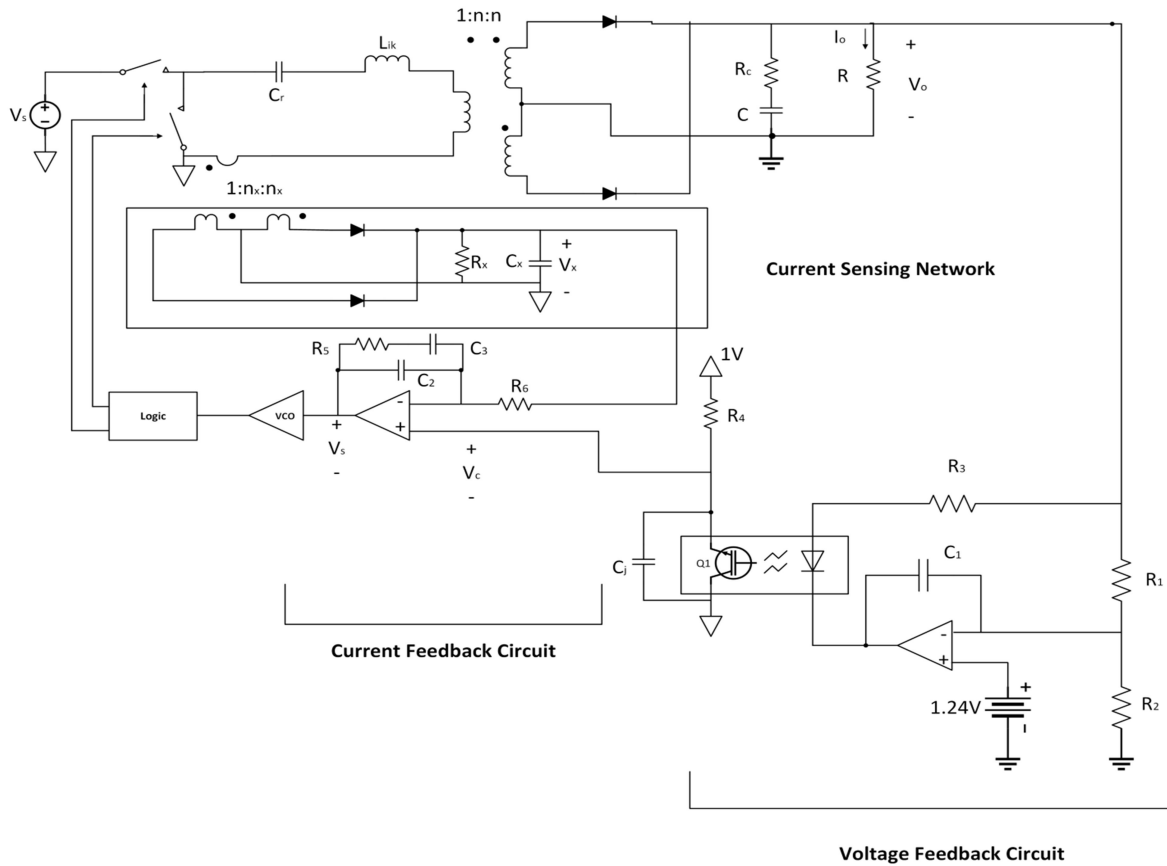


Fig 6.1: A proposed average current mode control is used in an experimental LC converter.

The operating modes, operational area, and four extreme working points of a LC series resonant converter are established for a wide variety of operating situations. The proposed average current-mode control is implemented in the circuit design of the experimental LC converter in Figure 6.1. As a conventional offline power supply, the

converter's input voltage may be changed from 340V to 390V while the load current could be modified from 1A to 6A. The center-tapped current transformer as well as a rectifier circuit make up the current sensing network, which is installed in the current loop after current feedback compensation.

6.4. AVERAGE CURRENT-MODE CONTROL

To overcome the shortcoming of the typical voltage mode control, a average current-mode control was modified for LC series resonant converters. Small-signal dynamics' core concepts, implementation, and analysis are discussed in relation to the proposed scheme.

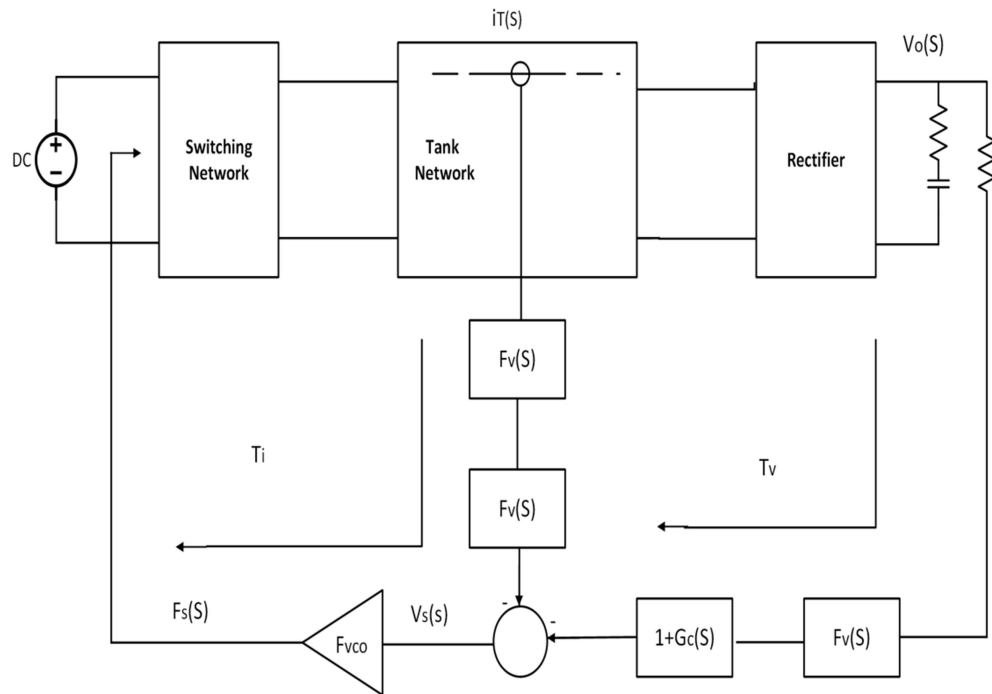


Fig 6.2: Block diagram of ACMC for Resonant Converters.

6.4.1. Principles and Implementation of Average Current-Mode Control

Figure 6.3 depicts the functional circuit design for a typical current-mode control that has been altered for use with an LLC series resonant dc-to-dc converter. Through active sensor network perceived, the resonant tank current employed in this control approach is detected. An error amplifier, two current feedback compensators, Z_{C1} & Z_{C2} , and an error feedback circuit are used to handle the measured current after it has been converted into a voltage signal, V_x . If the subsequent condition is met by the existing feedback compensation.

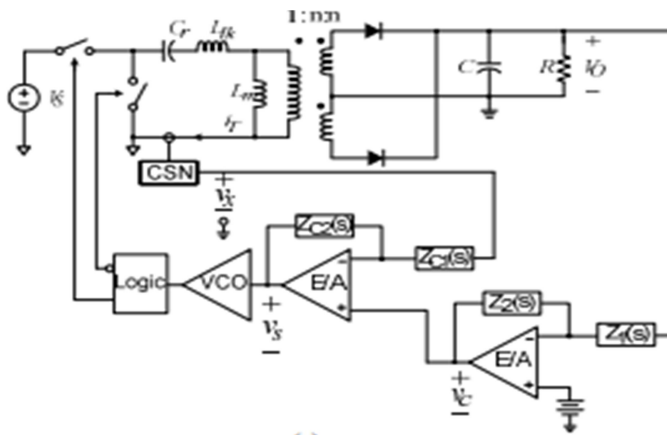


Fig 6.3: Functional circuit diagram of average current-mode control scheme.

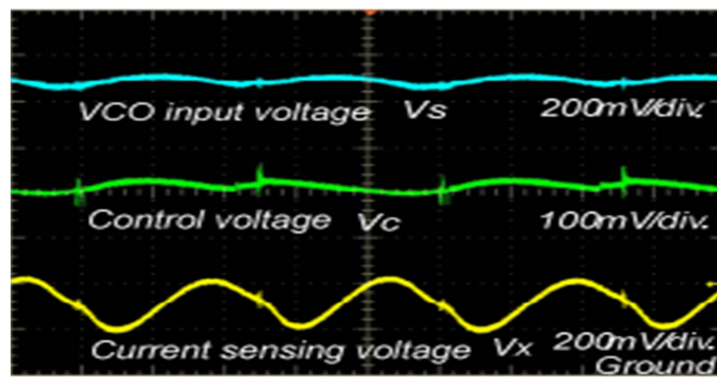


Fig 6.4: Experimental waveforms of feedback circuits

$$\lim_{\omega \rightarrow 0} \frac{|Z_{C2}(j\omega)|}{|Z_{C1}(j\omega)|} = \infty \quad (6.1)$$

The measured voltage signal V_x is compelled to closely resemble the control voltage V_c . In light of this, V_x only follows V_c with in average sense, that is, the scaled average of the resonant current will do so. The total voltage signal V_x , that is a scaled representation of a resonant tank current, likewise has a rectified sinusoidal waveform. In the average current mode control, a voltage copy of the resonant tank current x_v is produced using the center-tapped current transformer & rectifying circuits. It is then delivered to the current feedback compensation, that acts as a low-pass filter. As a result, the average current mode control's continuous current feedback signal V_s is resistant to the greater ripple components.

$$V_s = -\frac{Z_{C2}}{Z_{C1}} V_x(t) + \left(1 + \frac{Z_{C2}}{Z_{C1}}\right) V_c(t) \quad (6.2)$$

6.4.2. Dynamics of Average Current-Mode Control in Small Signals

Expressions for the average current-mode controlled LC conversion and a functioning small-signal block schematic. The feedback loops created either by voltage feedback & resonant current feedback, respectively, are represented by voltage loop gain T_v as well as the current loop gain T_i . A control-to-output transfer function $G_{vci}(S)$, which has been evaluated using resonant tank current feedback, may be determined.

$$G_{vci}(s) \equiv \left. \frac{V_o(s)}{V_c(s)} \right|_{H_i(s) \neq 0} = \frac{F_{vco} \frac{V_o(s)}{f_s(s)}}{1 + F_{vco} \frac{i_T(s)}{f_s(s)} G_c(s) H_i(s)} \quad (6.3)$$

$$G_{vci}(s) \equiv \frac{G_{vco}(s)}{F_{vco} \frac{i_T(s)}{f_s(s)} G_c(s) H_i(s)} \quad (6.4)$$

6.5. Average Current-Mode Control Design

Working to implement the suggested average current-mode control necessitates designing the present feedback and voltage feedback adjustment.

6.5.1. Design for Current Feedback Compensation

A average current mode control does have a special feature that affects the both current loop & loop gain for voltage. This feature is the current sensing network $H_i(s)$ as well as current $G_c(s)$.

- 1) Design of a Current Sensing Network High (S): A rectifier circuit's existence causes the current feedback circuit to have a first-order low-pass filter transfer function. The values used are $R_x = 50$, $x_n = 100$, and $C_x = 0.1$ F.
- 2) Design of a Current Feedback Compensation $G_c(S)$: A two-pole one-zero circuit is thoughtto be the current feedback compensation.

$$G_c(s) = \frac{K_C (1+s/\omega_{zc})}{s(1+(s/\omega_{pc}))} \quad (6.5)$$

By selecting one of the choices below, you may select the $G_c(s)$ parameter.

- 1) Place z_c at frequency below the power stage's double pole.
- 2) Lower PC to half its switching frequency to lessen switching ripple noise.

3) Modify K_c to make T_i 's crossover frequency high.

6.5.2. Design for Voltage Feedback Compensation

Finding a precise equation for the control-to-output transfer function $G_{vci}(S)$, assessed in the presence of a tank current feedback, may be essential in order to construct the voltage feedback circuit. However, given the intricate dynamics of the power stage, this undertaking will be too difficult. Based on the overall character of the Bode graphs, a third-order polynomial might be used as an alternate engineering method to approximate $G_{vci}(S)$.

$$G_{vci}(s) \approx G_{vci} \frac{\left(1 + \frac{s}{\omega_{esr}}\right)}{\left(1 + \frac{s}{\omega_{pl}}\right)\left(1 + \frac{s}{Q\omega_o} + \frac{s^2}{\omega_o^2}\right)} \quad (6.6)$$

$$F_v(s) = \frac{K_v \left(1 + \frac{s}{\omega_{zv}}\right)}{s \left(1 + \frac{s}{\omega_{pv}}\right)} \quad (6.7)$$

6.5.2.1. Modulator Gain

S-domain transfer function for the current compensator is

$$G_{ci}(s) = \frac{K_{ci} \cdot (1 + s / \omega_{zci})}{s} \quad (6.8)$$

Where $\omega_{zci} = \frac{1}{C_1 \cdot R_2}$ and $k_{ci} = \frac{1}{C_1 \cdot R_1}$

delay = $\tan^{-1}(2\pi f_s C_1 R_2) - 90^\circ$

where f_s stands for the incoming signal's frequency. The current compensator that output lags the input has a negative value. Due to the capacitor C_1 and resistor R_2 's ability to produce a zero just below power stage's resonance frequency, the first term is often near to 90° . Whenever the inverted supply is taken into account, the current compensator's output is equivalent to a inverted inductor current. The corrected output signal may be calculated to have falling slope of S_{nc} at the switch turn-on instant considering that input signal (the inductor current) has a rising slope of S_n .

The s-domain transfer function for the inductor current while the switch is turning on the output of the current compensator is represented by the equation below:

$$V_i(s) = -G_{ci}(s) \cdot I_L(s) = -S_n \cdot k_{ci} \left(\frac{1}{\omega_{zci} \cdot s^2} + \frac{1}{s^3} \right) \quad (6.9)$$

The result of the Laplace transformation can be expressed in the time domain.

$$V_i(t) = -S_n \cdot k_{ci} \cdot \left(\frac{t}{\omega_{zci}} + \frac{t^2}{2} \right) \quad (6.10)$$

S_{nc} is produced by taking the previous equation's derivative and evaluating it at time $t = DT_s$.

$$S_{nc} = -S_n \cdot k_{ci} (DT_s + 1/\omega_{zci}) \quad (6.11)$$

Because S_{nc} changes with duty ratio as well as the current loop compensator design, the total modulator gain changes with operating point. with the current compensator's output and the inductor current's slope. The variables V_i & $R_i \cdot I_L$, which are indicated by dashed lines, stand in for the cycle's average value. It is fair to presume that the delay produced by PI controller is 180° degrees because the estimated angle is often close to zero. As a result, it is satisfied during steady-state operation. Since its waveforms both for fast loop as well as the slow loop are changing over the course of a cycle, the absolute slope for modulation is linked

to the difference between both the slopes of the two current waveforms.

$$\langle V_i \rangle = \langle R_i \cdot I_L \rangle + \frac{1}{2} D T_s (S_n - S_{nc}) \quad (6.12)$$

Modulate the inductor current while holding the other parameters constant to determine the fast loop's modulator gain, F_{m1} .

$$F_{m1} = \frac{\hat{d}}{\langle R_i \cdot \hat{I}_L \rangle} = -\frac{2}{(S_n - S_{nc}) \cdot T_s} \quad (6.13)$$

The slow loop's modulator gain F_{m2} , can be determined using a similar process.

$$F_{m2} = \frac{\hat{d}}{\langle \hat{V}_i \rangle} = \frac{2}{(S_n - S_{nc}) \cdot T_s} \quad (6.14)$$

Whenever the duty ratio is close to or greater than 0.5, "sub harmonic oscillation," a frequent problem of multiple-loop control approaches like PCM and V₂ control, affects I₂ ACM control. If a steep ramp is necessary, the modulator gain could be decreased to use an artificial slope to stabilise the present loop.

$$F_m = \frac{\hat{d}}{\langle \hat{V}_i \rangle} = \frac{2}{(S_n - S_{nc} + S_e) \cdot T_s} \quad (6.15)$$

If slope compensation is added via a voltage divider, the current sense resistor of the fast loop, which differs from that of the slow loop, should also be subjected to the dividing ratio.

6.5.2.2. Sampling Gain

Similar to PCM, I² ACM control makes advantage of the inductor current ripple with in fast loop. The present PCM loop does not employ averaged state feedback, but sampling

instead. By using the same derivation method, it is discovered that the I² ACM control's fast loop has the same sampling gain.

$$H_e(s) \approx 1 + \frac{s}{\omega_n Q_z} + \frac{s^2}{\omega_n^2} \quad (6.16)$$

Where $Q_z = \frac{-2}{\pi}$ and $\omega_n = \frac{\pi}{T_s}$

A phenomenon known as "subharmonic oscillation" has two RHP zeros on half its switching frequency. It is to be noted that such a model is only precise to about half its switching frequency due to approximations. Remember that such an assumption is only reliable when used with a fixed frequency. On the other hand, variable frequency operation's sampling impact cannot be sufficiently described by constant on-time control. Due to the PI controller it contains, which allows the output to contain the average signal for inductor current, the slow loop provides real state feedback.

6.5.2.3. Feedback and Feed-Forward Gain

Based on a simplification of the common current cell used by all converters, the feed-forward gain from input voltage to an inductor current and the feedback gain from output voltage to an inductor current were fully created. The following is a list of the pertinent generated profits:

$$K'_{f_fl} = -\frac{DT_s R_i}{L} \left(1 - \frac{D}{2} \right) \quad (6.17)$$

$$K'_{f_fl} = \frac{D'^2 T_s R_i}{2L} \quad (6.18)$$

Since the fast loop within I² ACM control functions on the same PCM idea, the output and input voltages have an identical influence upon that inductor current through fast loop. Despite the presence of a current compensator with in slow loop, the inductor current ripple still arises at the output because a PI controller is used, which has so little damping than a type II compensator. The slow loop's feed-forward and feedback effects will change with the current compensator, as seen in

$$\begin{aligned} K'_{f_sl} &= K'_{f_fl} \cdot G_{ci} \\ K'_{r_sl} &= K'_{r_fl} \cdot G_{ci} \end{aligned} \quad (6.19) \text{ and } (6.20)$$

A PI controller offers a phase delay of about 180 degrees, as was discussed in the section on modulator gain, which is essentially comparable to an input signal which is inverted and amplified at the switching frequency.

$$\begin{aligned} K'_{f_sl} &= K'_{f_sl} \cdot |G_{ci}|_{f=f_s} \\ K'_{r_sl} &= K'_{r_fl} \cdot |G_{ci}|_{f=f_s} \end{aligned} \quad (6.21) \text{ and } (6.22)$$

6.6. Transfer Function Characteristics

The small-signal model that's been constructed in the preceding section provides a thorough explanation of the advantages of I² ACM control. To demonstrate the I² ACM control's rapid dynamics and accuracy, it is compared to traditional ACM control & PCM control. A buck converter was used to conduct this comparison. This output impedance, current loop, audio susceptibility, & control-to-output voltage all had their frequency responses checked. Stability analysis was also carried out. The circuit requirements for the converter prototype are obtained. The prototype used in this study is not a conventional commercial switch-mode power source and is not designed for any specific application;

instead, it is used to investigate the unique characteristics of I² ACM control.

6.6.1. Current Loop Gain

With the voltage loop open, the current loop gain is the transfer function and is expressed as follows for I² control:

$$T_{ii} = G_{id} \cdot F_m \cdot R_i (G_{ci} + H_e) \quad (6.23)$$

It is analogous to PCM and ACM's transfer functions. With voltage loop open at lower frequency, I² control & ACM serve as the optimum current sources. Contrarily, PCM has significantly lower frequency gain, which results in dc current accuracy. I² ACM control is shown to increase the phase angle as well as the current loop gain. I² controllers offer quicker tracking speeds and reduced overshoot as a consequence.

6.6.2. Control-to-Output Voltage

Mason's gain formula can be used to compute the transfer function from the voltage controller output to the output voltage for I² controllers when the voltage loop is closed.

$$G_{vc} = \frac{(1+G_{ci}) \cdot F_m \cdot G_{vd}}{1 + T_{ii} - K_r \cdot F_m \cdot G_{vd}} \quad (6.24)$$

As can be observed, I² control operates similarly to ACM at lower frequency and similarly to PCM at mid-range frequency. The spiking at half of a switching frequency indicates that a pair of the double poles must be damped by an artificial ramp.

6.6.3. Audio Susceptibility

For both closed current loops and an open voltage loop, the input-to-output voltage transfer function seems to equal the closed-loop audio susceptibility. Therefore, the influence

of a voltage loop compensators is disregarded in order to emphasise the impact of the loops since current loops of I² ACM control, PCM, and ACM have distinct frequency responses. A few formulae may be used to handle the audio susceptibility for I² ACM control.

$$\begin{aligned}\hat{V}_o &= \hat{V}_g G_{vg} + \hat{d} G_{vd} - \hat{I}_o Z_{out} \\ \hat{d} &= F_m \left[\hat{V}_g k_f + \hat{V}_o k_r - \hat{I}_L (H_e + G_{ci}) R_i \right] \\ \hat{I}_L &= \hat{V}_g G_{ig} + \hat{d} G_{id} + \hat{I}_o G_{il}\end{aligned}\quad (6.25), (6.26) \text{ and } (6.27)$$

The output current is taken to be constant for the purposes of deriving the audio-susceptibility transfer function. So, the small-signal variable I_o is equal to 0. The transfer function that results is

$$\frac{\hat{V}_o}{\hat{V}_g} = \frac{G_{vg} (1+T_{ii}) + F_m \cdot G_{vd} \left[K_f - G_{ig} (H_e + G_{ci}) R_i \right]}{1 + T_{ii} - K_r \cdot F_m \cdot G_{vd}} \quad (6.28)$$

the assessment of the impact of different control approaches on auditory susceptibilities. I² controls, that have the smallest magnitude inside the low frequency range, notably increase acoustic sensitivity, as is evident. Due to its higher amplitude at low frequencies, PCM provides the most sensitive control method in this scenario. The appropriate transfer function may be calculated, the voltage loop compensator, that is not addressed here, can be derived, and the duty ratio equation may be used to reflect the influence of the fluctuation from the voltage loop.

6.6.4. Output Impedance

$$\frac{\hat{V}_o}{-\hat{I}_o} = \frac{Z_{out} (1+T_{ii}) + G_{vd} F_m G_{il} (H_e + G_{ci}) R_i}{1 + T_{ii} - K_r \cdot F_m \cdot G_{vd}} \quad (6.29)$$

A output impedance for three control methods has virtually comparable values and a similar slope above half of a switching frequency. Given that the gain of the current loops is very low at high frequencies, the key determining factor will be the properties of a power stage's output impedance. I² ACM is a fantastic option for situations with frequent load changes because it has the minimum output impedance below half of a switching frequency. However, the voltage loop has always been closed in real-world situations. In this instance, the output impedance of I² controllers is changed by voltage loop compensator G_c.

$$Z_{out_cl} = \frac{Z_{out}(1+T_{ii}) + G_{vd}F_mG_{il}(H_e + G_{ci})R_i}{1+T_{ii}-F_mG_{vd}[K_r + G_c(1+G_{ci})]} \quad (6.30)$$

6.6.5. Stability

Knowing whether I² control is stable and whether slope adjustment is required is very important. The loop gain, bandwidth, and transient speed are all reduced when an external slope is added. Define a parameter first

$$m_c = \frac{S_e}{S_n} \quad (6.31)$$

The control-to-output power converter function's variable m_c. A rise in magnitude peak as well as phase at half of a switching frequency, which indicates a set of right half-plane poles, signifies that the system is unstable whenever m_c = 0. For I² ACM control, its duty ratio can be decreased to 0.4, but the control loop continues to oscillate without slope correction. the results following a 2 V reduction in the nominal output voltage. The second crossover, which happens often in PCM, is produced when the magnitude peak passes 0 dB and occurs at half its switching frequency. The same thing happens when m_c equals 1. This

peaking can also be lessened by adjusting the slope of the RHP poles more toward the left half plane.

6.6.6. Output Voltage to Duty cycle Transfer Function

When the load changes, the output impedance, that is also affected by the control method, displays a drop in output voltage. In order to highlight the unique characteristics of I² controls in this comparison, the output impedance generated here is approximated with current loops closed as well as the voltage loop open; the voltage compensator is therefore ignored here. Whenever the variable V_g is equal to 0, its output impedance is stated as follows.

$$\frac{\hat{V}_o}{\hat{d}} = \frac{\hat{V}_g G_{vg} + \hat{d}G_{vd} - \hat{I}_o Z_{out}}{F_m [\hat{V}_g k_f + \hat{V}_o k_r - \hat{I}_L (H_e + G_{ci}) R_i]} \quad (6.32)$$

6.7. Conclusion

In this chapter, the design of the Average Current Mode Control system for the series resonant converter was designed. The ACMC techniques employed in order to get the desired output voltage were discussed. The controllers employed for resonant converters are combination of current mode and voltage mode controller is employed. In the next chapter, the simulation results of the resonant converter, under open-loop and closed-loop will be described.

CHAPTER – 7

SIMULATION OF THE

SERIES RESONANT CONVERTER

FOR UPS BATTERY CHARGING

7 SIMULATION OF THE SERIES RESONANT CONVERTER FOR UPS BATTERY CHARGING

7.1. Introduction

Half bridge series resonant circuit analysis and in-depth discussions of its many modes of operation were covered in the preceding chapters. The efficiency of these converters was computed after the losses occurring in these circuits were identified and the ratings of the components employed in such power electronics converters were designed. The design of the power converter's control system and the mathematical modelling of both FHA & small signal were done after the design calculation. These power converters were modelled in MATLAB Simulink using both an open-loop and a closed-loop control strategy. The half bridge series resonant converter's simulation diagrams and results under open-loop and closed-loop control are explored in length in this chapter.

7.2. PV Source for Series Resonant Converter

Fig 7.1 shows the PV system which needs to be given as a supply to the resonant converter. Here the temperature varies during a period of time so the output side of the pv system also varies. The supply which needs to be given to resonant converter is around 35V to 40V. From the table below shows the variation of voltage and current with change in temperature at 1000w/ m^2 .

Design and Development of Series Resonant Converter for UPS Battery Charging Application

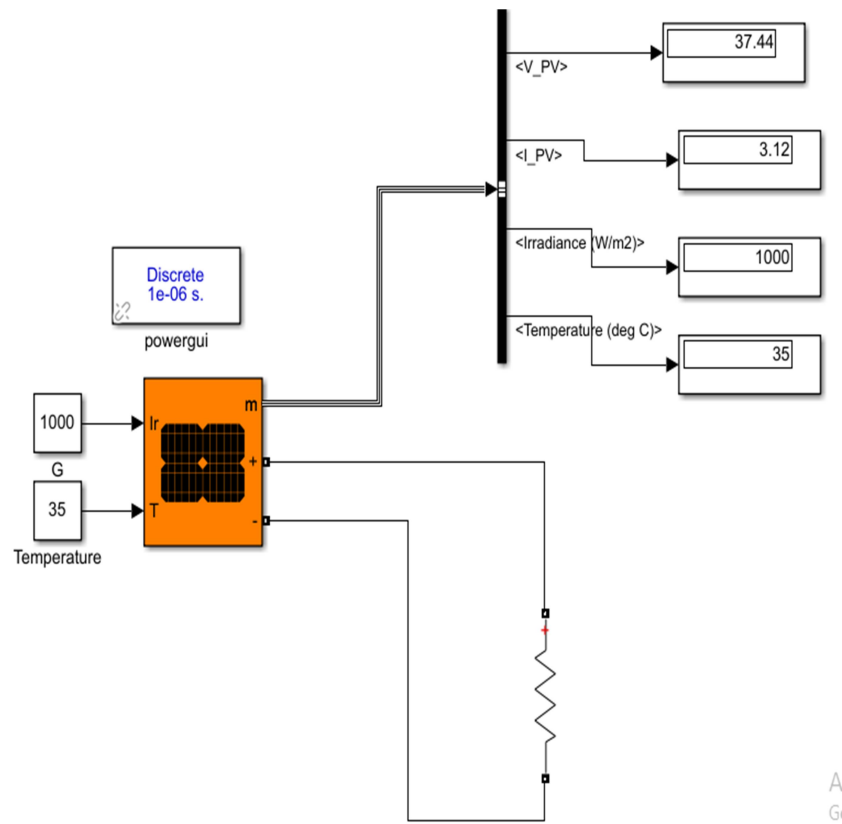


Fig 7.1: Matlab simulation for photovoltaic system

Table 7.1: Voltage and Current measurements for change in Temperature

Temperature (degrees)	Irradiance (W / m ²)	Voltage (V)	Current (I)
25	1000	39.31	3.27
30	1000	38.07	3.17
35	1000	37.44	3.12
40	1000	36.81	3.06
45	1000	36.18	3.01
50	1000	35.55	2.96

Design and Development of Series Resonant Converter for UPS Battery Charging Application

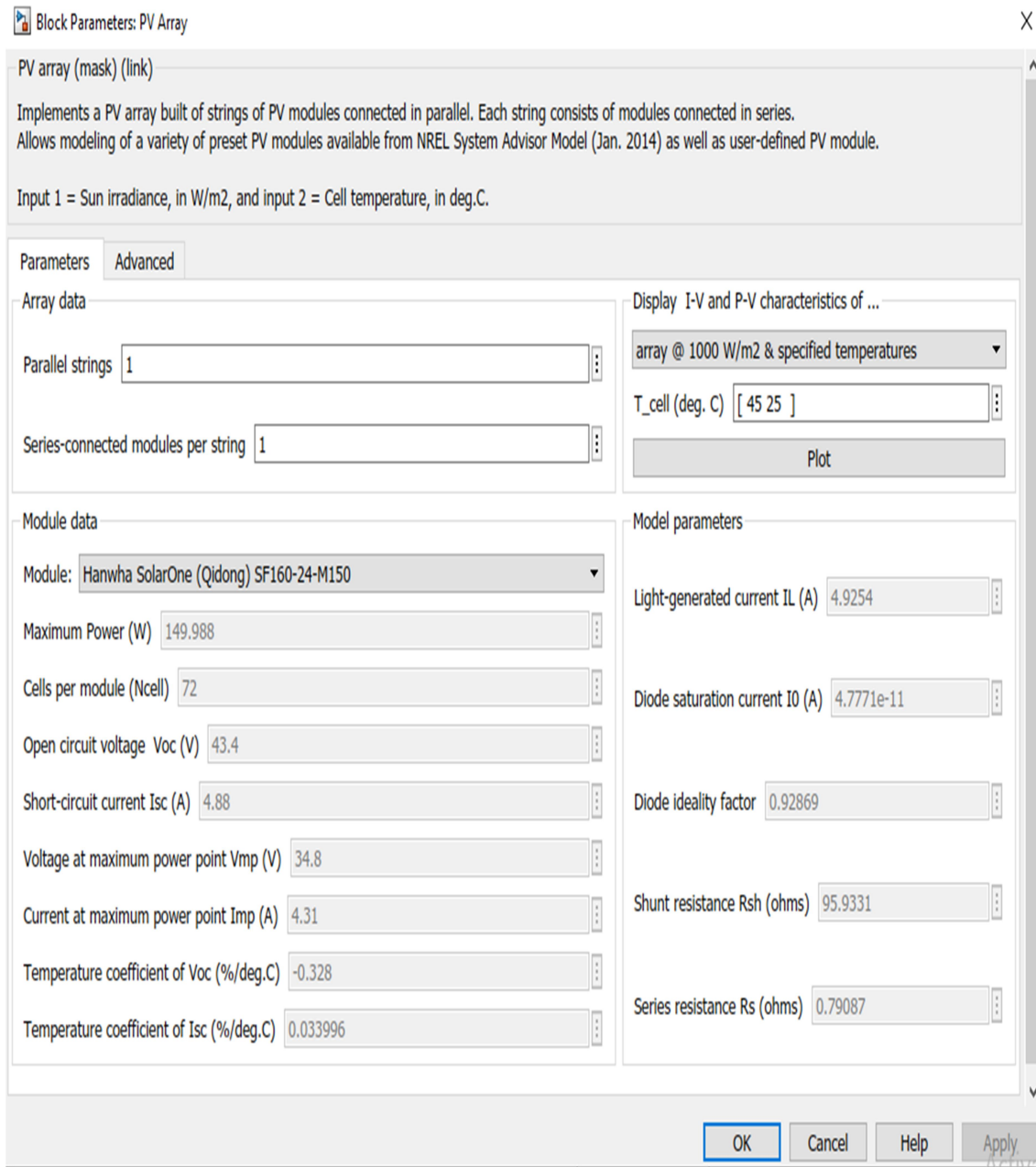


Fig 7.2: Parameter of PV array

From the fig .7.2 shows the PV array used in the system with various parameters in it, here the only 1 array is selected which generates a power of 150W. From the table 7.2 and 7.3 given below shows the various parameter of the PV array.

Design and Development of Series Resonant Converter for UPS Battery Charging
Application

Table 7.2: Module data

Module	Hanwha SolarOne (Qidong) sf160-24-M150
Maximum Power (W)	149.988W
Cells per module (Ncell)	72
Open circuit voltage Voc (V)	43.4V
Short circuit current Isc (A)	4.88A
Voltage at maximum power point Vmp (V)	34.8V
Current at maximum power point Imp (A)	4.31A
Temperature coefficient of Voc (%/deg.C)	-0.328 %/deg.C
Temperature coefficient of Isc (%/deg.C)	0.033996

Table 7.3: Model parameters.

Light-generated current IL (A)	4.9254
Diode saturation current I0 (A)	4.7771e-11A
Diode ideality factor	0.92869
Shunt resistance Rsh (ohms)	95.9331
Series resistance Rs (ohms)	0.79087

Design and Development of Series Resonant Converter for UPS Battery Charging Application

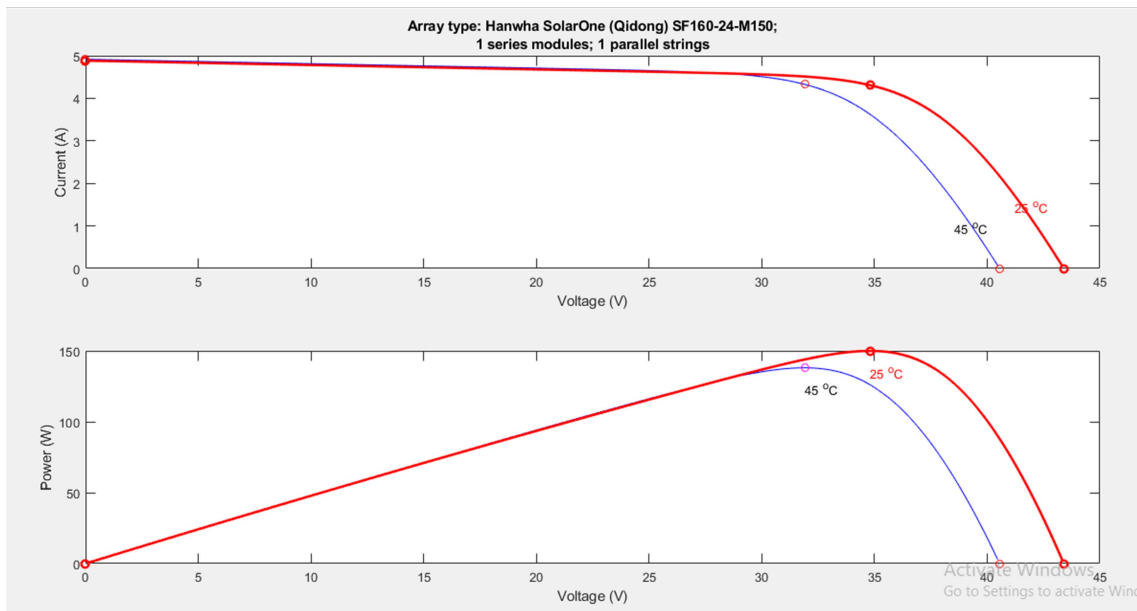


Fig 7.3: Plot for voltage, current and power of PV array

Fig 7.3, shows the plot of voltage, current and power of PV array for 1 series and 1 parallel module for 1000 W/m² at 45 degree temperature.

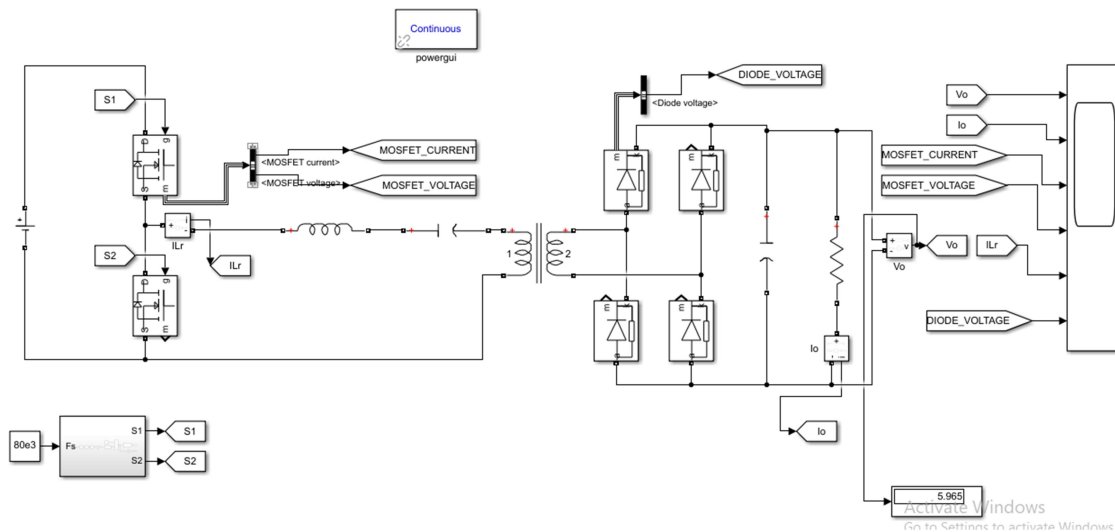


Fig 7.4: Matlab simulation model of LC resonant converter.

Fig. 7.4 depicts the Simulink model of the LC Resonant DC-DC Converter circuit. Where the supply is taken as dc source of 35V under open loop simulation. As the supply voltage

changes the output voltage also changes.

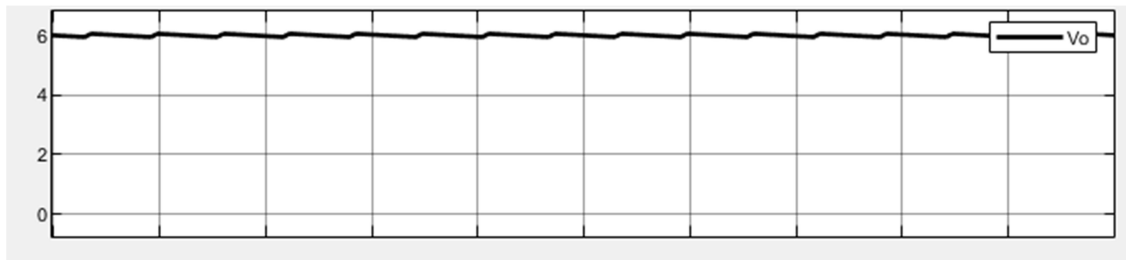


Fig 7.5: Output voltage of LC resonant converter.

Fig.7.5 depicts the output voltage which is 6.12 V. The high value 6.12 V and low value 6.09 V is measured. The gain of the converter is calculated by using equation for input voltage 35 V.

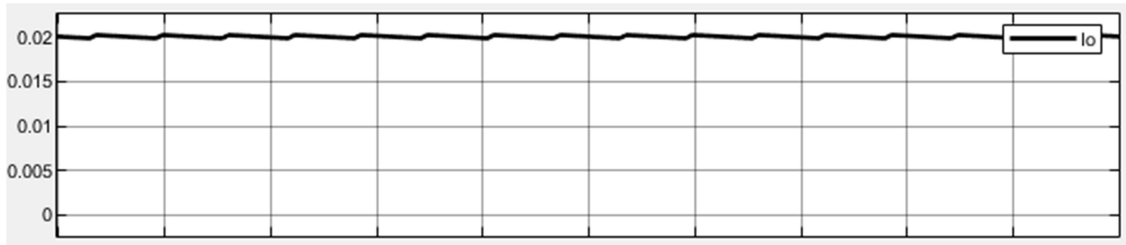


Fig 7.6: Output current of LC resonant converter.

The output current 0.021 A is shown in Fig. 7.6 which has ripple of 0.001 A. The high value 0.021 A and low value 0.02 A is measured from the simulation.

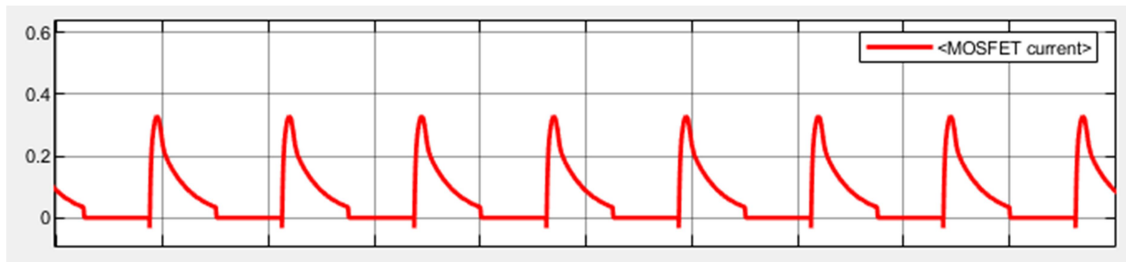


Fig 7.7: Mosfet current of LC resonant converter.

Fig. 7.7 shows the current flowing through the Mosfet with maximum current of 0.19A and a minimum current of -0.04 in the simulation

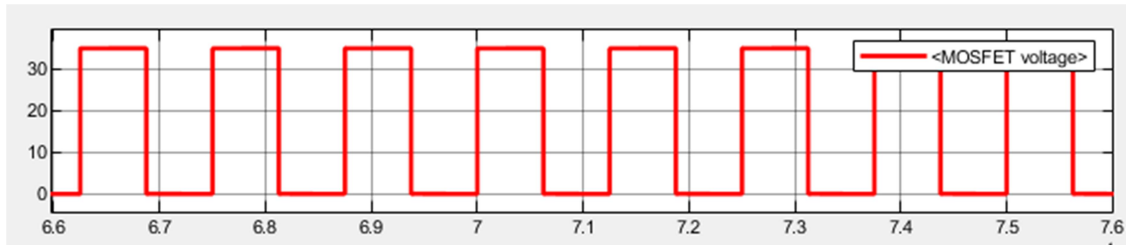


Fig 7.8: Mosfet voltage of LC resonant converter.

Fig. 7.8 shows the voltage across the mosfet with highest value of 35V and lowest value of 0V in the simulation.

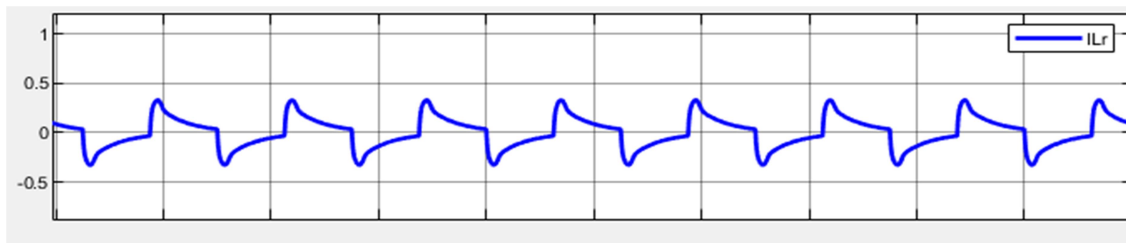


Fig 7.9: Inductor current of LC resonant converter.

Fig. 7.9 shows the flow of current across the induction with maximum current of 0.38A and minimum of -0.38A as done in the simulation

7.3. Simulation of PV System with LC Resonant Converter under Open Loop

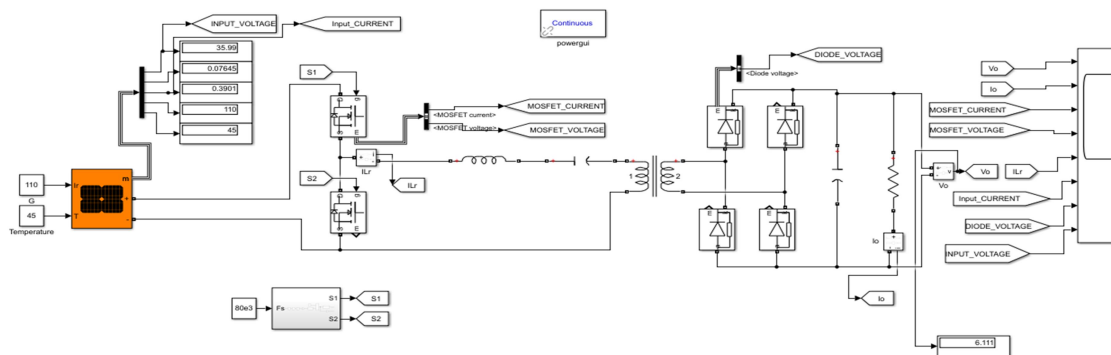


Fig 7.10: Matlab simulation for open loop LC resonant converter.

Fig. 7.10 shows Matlab simulation of combination of PV system and series resonant converter under open loop. Here the temperature is 45 degree and irradiance is 110 W/ m². The supply given to the resonant converter is 35.9V and 0.39A. The output of the resonant converter is measured as 6.11V and 0.020A.



Fig 7.11: Output voltage for open loop LC resonant converter.

Fig. 7.11 shows the output voltage of 6.11 under open loop simulation. The maximum output voltage obtained is 6.35V and the minimum is 6.08V

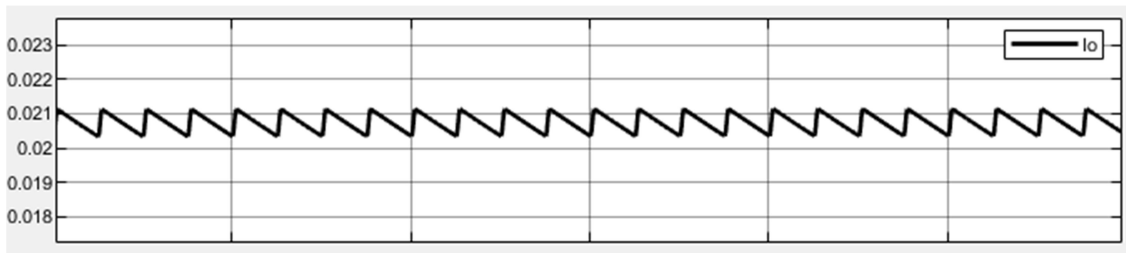


Fig 7.12: Output current for open loop LC resonant converter

Fig. 7.12 shows the output current for open loop which is 0.020A. The maximum current is 0.0212A and the minimum current is 0.0205A.

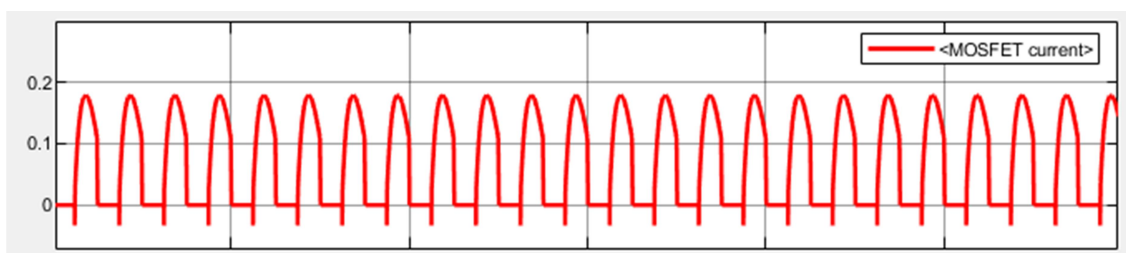


Fig 7.13: Mosfet current for open loop LC resonant converter

Fig. 7.13 shows the mosfet current for open loop simulation where the maximum current flow is 0.18A and the minimum current flow is -0.02A.

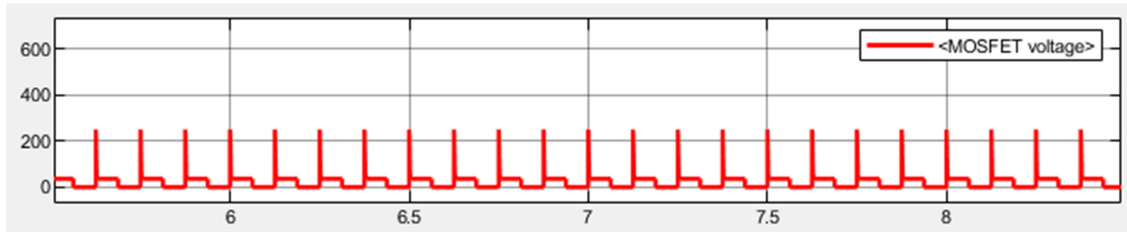


Fig 7.14: Mosfet voltage for open loop LC resonant converter.

Fig. 7.14 shows the mosfet voltage for open loop LC resonant converter with maximum voltage of 280V and minimum voltage of 0V.

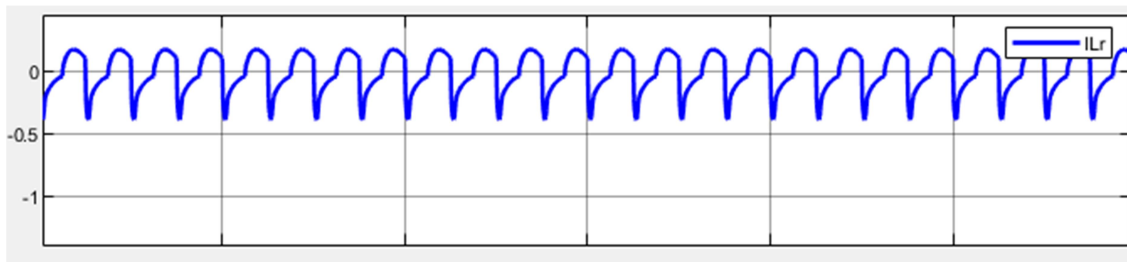


Fig 7.15: Inductor current for open loop LC resonant converter.

Fig. 7.15 shows the current flowing through the inductor under open loop system with maximum current of 0.3A and minimum of -0.4A.

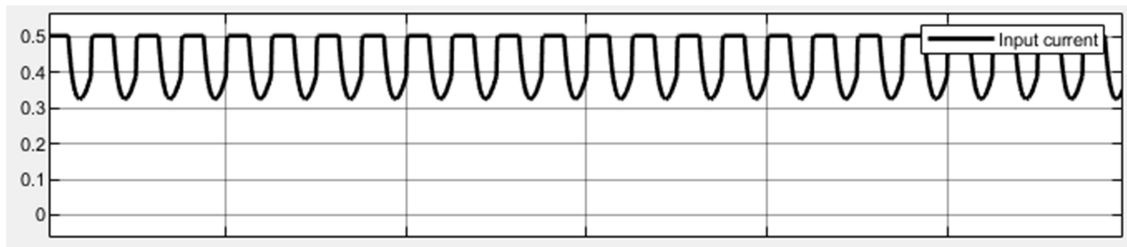


Fig 7.16: Input current for open loop LC resonant converter.

Fig. 7.16 shows the input current given to the LC resonant converter under open loop with maximum current of 0.5A and minimum current of 0.33A.

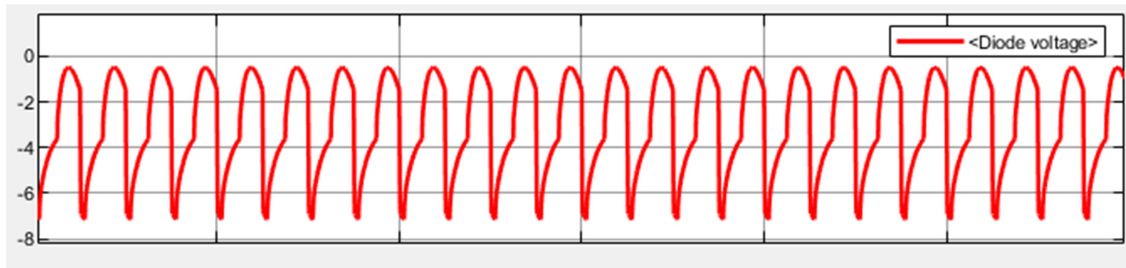


Fig 7.17: Diode voltage for open loop LC resonant converter.

Fig. 7.17 shows the voltage in the rectifier circuit with maximum voltage of -0.8V and minimum current of -7V under open loop system.

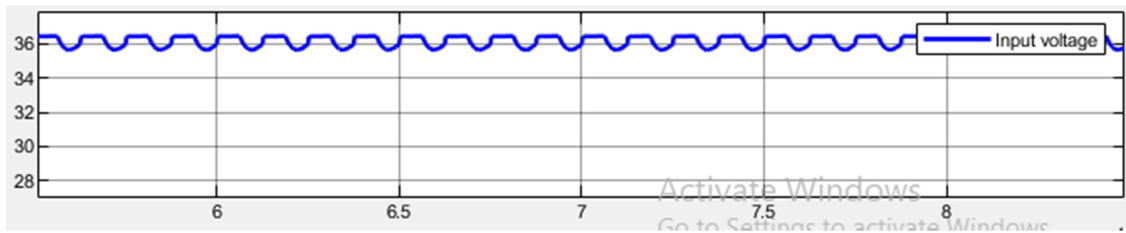


Fig 7.18: Input voltage for open loop LC resonant converter.

Fig. 7.18 shows the input voltage given to the LC resonant converter under open loop system with maximum voltage of 36.6V and minimum voltage of 35V.

7.4. Simulation of PV System with LC Resonant Converter for UPS Battery Charging under Open Loop

Fig 7.19 shows the Matlab simulation model of the PV system connected to the LC resonant converter which is connected to the battery charging for the UPS. Here the battery used is Lithium-Ion, the parameters of the battery is given in the table 7.4.

Design and Development of Series Resonant Converter for UPS Battery Charging Application

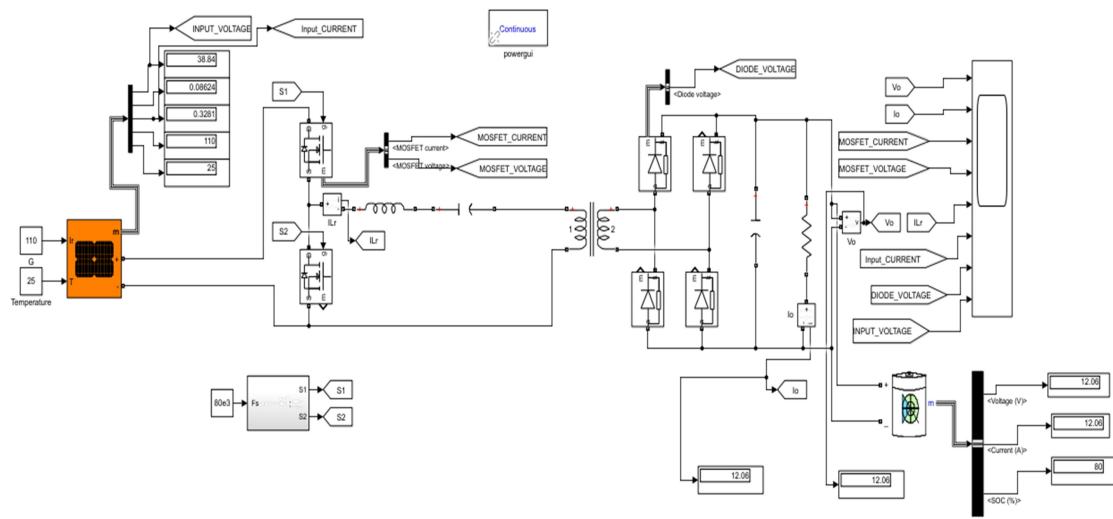


Fig 7.19: Matlab simulation for open loop LC resonant converter for battery charging application.

Table 7.4: Lithium-Ion battery parameters

Parameters	Ratings
Nominal voltage (V)	12V
Rated capacity (Ah)	12Ah
Initial state of charge (%)	80%
Battery response time (s)	1s
Maximum capacity (Ah)	12Ah
Cut off voltage (V)	9V
Fully charged voltage (V)	13.9678V
Nominal discharge current (A)	5.2174A
Internal resistance (Ohms)	0.01 Ohms
Capacity (Ah) at nominal voltage	10.8522Ah

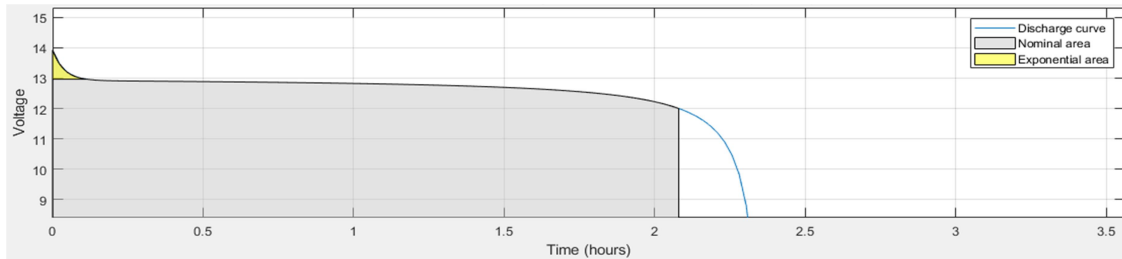


Fig 7.20: Nominal current discharge characteristics of the battery.

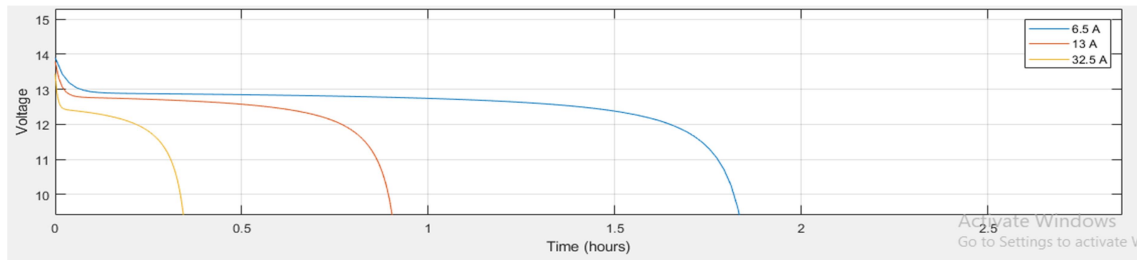


Fig 7.21: Voltage vs Time characteristics of Lithium-Ion battery.

The battery's nominal current discharging characteristics are shown in Fig. 7.20 at 0.43478C. (5.2174A). Lead - acid battery (4 to 6 percent each month) and NiMH batteries have self-discharge rates that are significantly higher than lithium-ion cells' 2 to 3 percent monthly rate (30 percent per month). Because of this, the Battery pack has a longer lifespan than other battery types. The discharge curve of a lithium-ion battery is also uniformly flat. It is well known that, particularly for high-power applications, a serious issue may develop at the conclusion of the discharge cycle if the battery's power output reduces rapidly. As shown in Figs. 7.20 and 7.21, the lithium-ion battery provides basically constant voltage (corresponding steady power) for roughly 80% of the discharge cycle.

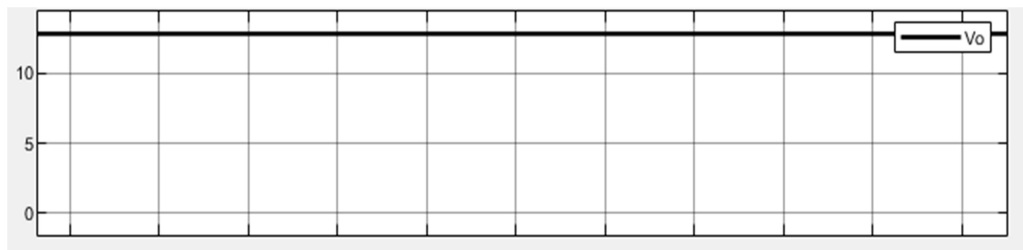


Fig 7.22: Output voltage of series resonant converter for battery charging under open loop.

Fig.7.22 shows the matlab simulated of output voltage of the series resonant converter for battery charging under open loop. Here the voltage is 12.8V

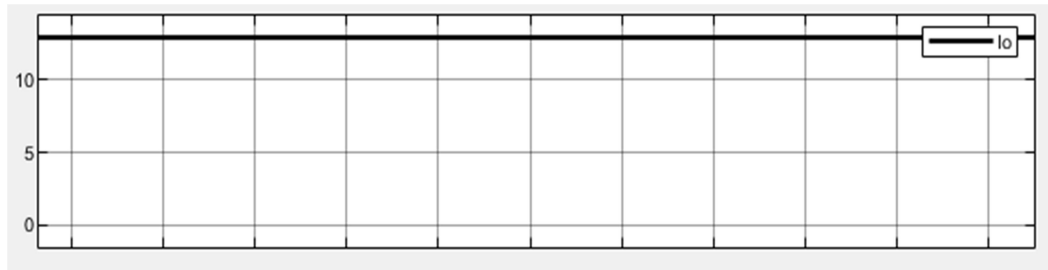


Fig 7.23: Output current of series resonant converter for battery charging under open loop

Fig.7.23 shows the matlab simulated of output current of the series resonant converter for battery charging under open loop. Here the current is 12.8A.

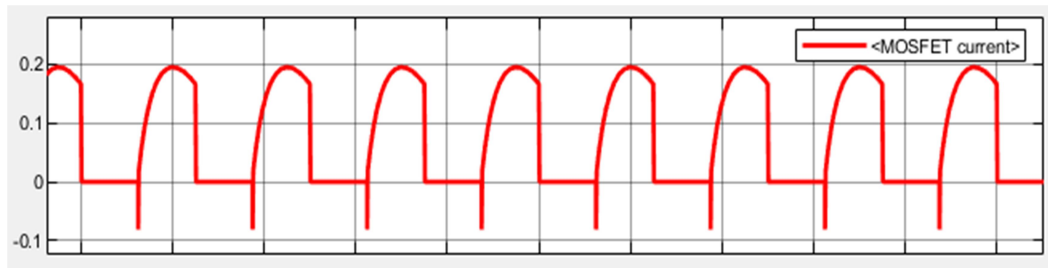


Fig 7.24: mosfet current of series resonant converter for battery charging under open loop

Fig.7.24 shows the matlab simulated of mosfet current of the series resonant converter for battery charging under open loop. Here the maximum current is 0.2Aand minimum current is -0.08A.

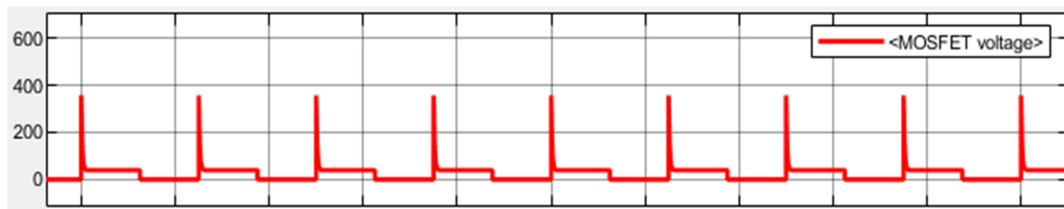


Fig 7.25: mosfet voltage of series resonant converter for battery charging under open loop

Fig.7.25 shows the matlab simulated of mosfet voltage of the series resonant converter for battery charging under open loop. Here the maximum voltage is 356V and minimum voltage is 0V.

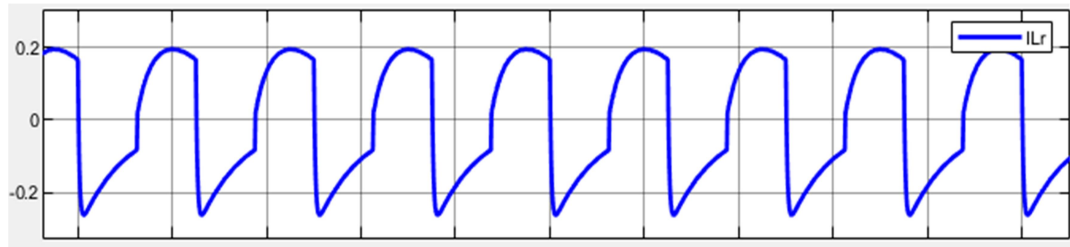


Fig 7.26: Inductor current of series resonant converter for battery charging under open loop

. Fig.7.26 shows the matlab simulated of Inductor current of the series resonant converter for battery charging under open loop. Here the maximum current is 0.2A and minimum current is -0.25A

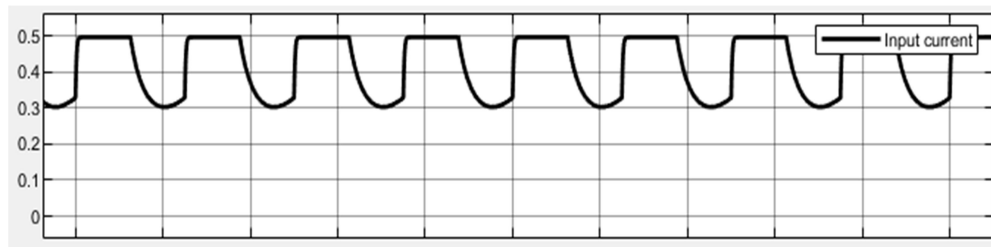


Fig 7.27: Input current of series resonant converter for battery charging under open loop

Fig.7.27 shows the matlab simulated of Input current of the series resonant converter for battery charging under open loop. Here the maximum current is 0.5A and minimum current is 0.3A

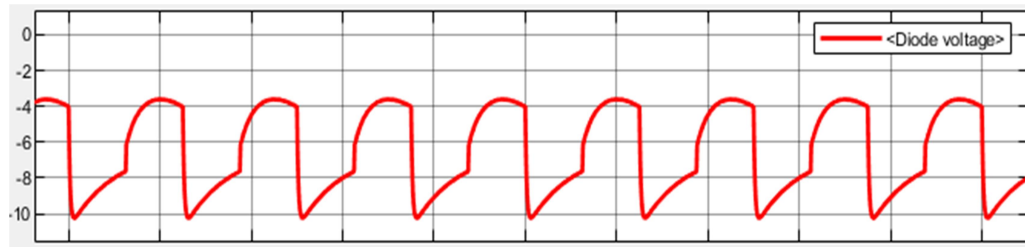


Fig 7.28: Diode voltage of series resonant converter for battery charging under open loop

Fig.7.28 shows the matlab simulated of Diode voltage of the series resonant converter for battery charging under open loop. Here the maximum voltage is -3.6V and minimum voltage is -10.23V.

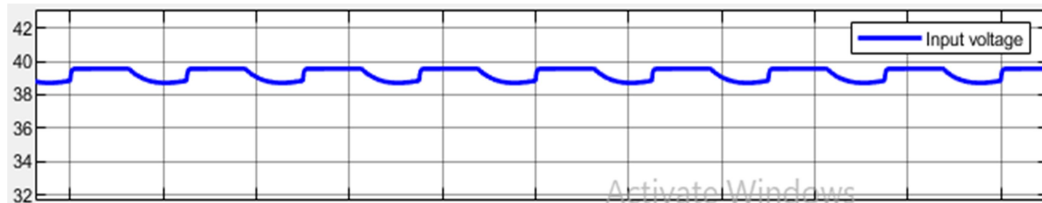


Fig 7.29: Input voltage of series resonant converter for battery charging under open loop

Fig.7.29 shows the matlab simulated of Input voltage of the series resonant converter for battery charging under open loop. Here the maximum voltage is 39.55V and minimum current is 38.7V.

7.5. Closed Loop Matlab Programming for Average Current Mode Control of Series Resonant Converter.

```
clc;
clear all;
close all;
%% Average Current Mode Controller Design for LC Resonant Converter

%% LC series resonant converter - Hard ware Specification
Ls = 12.73e-6;
Cs = 49.73e-9;
```

```
Cf = (5*330e-6 + 40e-06);
rd = 0.00725+0.008;
rc = 15e-3/6;
rs = 15e-3;
n = 2;
```

```
%% LC Operating Point
Duty = 0.5;
Vin = 40;
Po_desired = 150;
Vo = 12;
Io = Po_desired/Vo;
R = Vo/Io;
Re = (8*(n^2)/(pi^2))*(rd+R);
```

```
%% Sensor Circuit Parameters
% Current sensor parameters
Rfc = 10;
Cfc = 2e-6 ;
Gct = 1/50;
Gopamp = (1+(576/300));
Gpd = 20;
Gavg = 2/pi;
```

```
% Voltage sensor parameters
R9 = 1.50e3 ;
R8 = 5.02e3 ;
Cfv = 2000e-12;
```

```
%% ADC and PWM module gains
Gpwm = 1;
Kadc = 3.33 ;
```

```
%% Enter controller design parameters for desired controller
fc1 = 5540;
fcv = 1130;
TsC = 1/200000;
TsV = 1/50000;
```

```
Delay_Total = 3.558e-06;
T_zoh1 = TsV;
T_zoh2 = TsC;
```

```
% Inner loop controller parameters need to be adjusted for desired PM (See Plot-2 to adjust
PM of inner loop-gain)
z1shift = 0.6661;
z2shift = 0.3737;
```

```
p1shift = 0.06132;

% Outer loop controller parameter need to be adjusted for desired PM (see Plot-3 to adjust
PM of outer loop-gain)
Wv = 2500;

%% Finding switching frequency based on Gain-Frequency Curve
Vq = (Vin/2); % Half-bridge voltage

W0 = 1/sqrt(Ls*Cs) ;
f0 = W0/(2*pi);

Qfac = sqrt(Ls/Cs)/Re;
GainR = n*(Vo+(rd*Io))/Vq;

% Finding ratio of switching frequency to resonance frequency
Aa = (Qfac^2);
Bb = (2*(Qfac^2));
Cc = ((Qfac^2));
Dd = 1;
Fxp = [Aa 0 Bb 0 Cc 0 Dd];
Fxr = roots(Fxp);
Fxreal = real(Fxr);
Fx = max(Fxreal);
fs = Fx*f0;
Ws = 2*pi*fs;

%% Sampling time and Digital Delay Transfer Function
s=tf('s');

% 1st Order Pade's Approximation for delays
H_outDelay=(1-s*(Delay_Total/2))/(1+s*(Delay_Total/2));
% Zero order hold due to out loop lower sampling rate
exp_Ts_coeff = s*T_zoh1/2;
exp_Ts1 = (1-exp_Ts_coeff+exp_Ts_coeff^2-
exp_Ts_coeff^3)/(1+exp_Ts_coeff+exp_Ts_coeff^2+exp_Ts_coeff^3);

H_zoh1 = minreal((1 - exp_Ts1)/(s*T_zoh1));

exp_Ts_coeff = s*T_zoh2/2;
exp_Ts2 = (1-exp_Ts_coeff+exp_Ts_coeff^2-
exp_Ts_coeff^3)/(1+exp_Ts_coeff+exp_Ts_coeff^2+exp_Ts_coeff^3);

H_zoh2 = minreal((1 - exp_Ts2)/(s*T_zoh2));

%% Steady-State parameters; Derived in the application note
Ves = (2*Vin/pi);
```

```
X = [ rs+Re Ls*Ws 1 0 -Re 0 ;
      -Ls*Ws rs+Re 0 1 0 -Re ;
      1 0 0 -Cs*Ws 0 0 ;
      0 1 Cs*Ws 0 0 0 ;
      Re 0 0 0 -Re Ws ;
      0 Re 0 0 Ws -Re ] ;
```

```
U0 = [ Ves ; 0 ; 0 ; 0; 0 ; 0 ];
```

```
Y = linsolve(X,U0) ;
```

```
Is = Y(1); Ic = Y(2) ; Vs = Y(3) ; Vc = Y(4) ; Ims = Y(5) ; Imc = Y(6) ;
```

```
Ipc = Ic-Imc;
```

```
Ips = Is-Ims ;
```

```
Ipp = sqrt(Ips^2+Ipc^2);
```

```
Ir = sqrt(Is^2+Ic^2);
```

```
Im = sqrt(Ims^2+Imc^2);
```

```
Isp = n*Ipp ;
```

```
Vcf = 2*Isp*R/pi;
```

%% Small-Signal coefficients; Derived in the application note

```
rc1 = R*rc/(R+rc);
```

```
Hip = ((4*n*rc1*Vcf*Ipc^2)/(pi*rc*Ipp^3))+((8*(rd+rc1)*n^2)/(pi^2));
```

```
Hic = -(4*n*rc1*Vcf*Ips*Ipc)/(pi*rc*Ipp^3);
```

```
Hvcf = (4*n*rc1*Ips)/(pi*rc*Ipp);
```

```
Gip = -(4*n*rc1*Vcf*Ips*Ipc)/(pi*rc*Ipp^3);
```

```
Gic = ((4*n*rc1*Vcf*Ips^2)/(pi*rc*Ipp^3))+((8*(rd+rc1)*n^2)/(pi^2));
```

```
Gvcf = (4*n*rc1*Ipc)/(pi*rc*Ipp);
```

```
Kis = (2*n*Ips)/(pi*Ipp);
```

```
Kic = (2*n*Ipc)/(pi*Ipp);
```

```
Js= (2/pi)*Is/sqrt(Is^2+Ic^2);
```

```
Jc= (2/pi)*Ic/sqrt(Is^2+Ic^2);
```

%% LC EDF Model system matrices

```
A = [ -(Hip+rs)/Ls -(Ws+(Hic/Ls)) -1/Ls 0 (Hip/Ls) (Hic/Ls) -(Hvcf/Ls) ;
      (Ws-(Gip/Ls)) -((Gic+rs)/Ls) 0 -1/Ls (Gip/Ls) (Gic/Ls) -(Gvcf/Ls) ;
      1/Cs 0 0 -Ws 0 0 0 ;
      0 1/Cs Ws 0 0 0 0 ;
      (Hip) (Hic) 0 0 -(Hip) -(Ws+(Hic)) (Hvcf) ;
      (Gip) (Gic) 0 0 (Ws-(Gip)) -(Gic) (Gvcf) ;
      ((Kis*rc1)/(Cf*rc)) ((Kic*rc1)/(Cf*rc)) 0 0 -((Kis*rc1)/(Cf*rc)) -((Kic*rc1)/(Cf*rc))
      -rc1/(R*Cf*rc) ];
```

```
B = [ -Ic*W0 ;  
      Is*W0 ;  
      -Vc*W0 ;  
      Vs*W0 ;  
      -Imc*W0 ;  
      Ims*W0 ;  
      0 ];  
  
C= [ Kis*rc1 Kic*rc1 0 0 -Kis*rc1 -Kic*rc1 rc1/(rc) ;  
     Js Jc 0 0 0 0 0 ];  
  
D=[ 0 ;  
    0 ];  
  
%% EDF model transfer function  
sys = ss(A,B,C,D);  
EDF = tf(sys);  
  
Gvw = EDF(1);  
Giw = EDF(2);  
  
P = pole(Giw);  
[N,K] = zero(Giw);  
Giw = minreal(zpk(N,P,K));  
  
figure(1);  
P = bodeoptions;  
P.Grid = 'on';  
P.FreqUnits = 'Hz';  
P.PhaseWrapping = 'off' ;  
bode(Giw,P); hold on;  
  
%% Current sensor gain  
Gif = 1/(Rfc*Cfc*s+1);  
Gisense = Gif*Get*Gopamp*Gpd/Kadc;  
  
%% Current Loop Compensator design (2P2Z)  
% Chosen Gain Crossover frequency  
% Compensator one pole is to cancel the effect of Wesr.  
% place the compensator two zeros at complex pole location to cancel the effect of of  
% complex zeros  
% and get the proper shape of open-loop transfer function  
wc = 2*pi*fci ;  
  
%poles of plant and sensor gain
```

```
[Niw,Kiw] = zero(-Giw*Gisense);
Piw = pole(-Giw*Gisense);

Piw = Piw( Piw<=0 );
Niw = Niw( Niw<=0 );

Nreal = real(Niw);
Preal = real(Piw);

[Nmax,Index_N] = max(Nreal);
[Pmax,Index_P] = max(Preal);

% Compensator poles-zeros selection
Wesr = Nreal(Index_N);

Wz1 = Preal(Index_P)/z1shift;
Wz2 = Preal(Index_P)/z2shift;
Wp1 = Wesr/p1shift;

Gci = (s-Wz1)*(s-Wz2)/(s*(s-Wp1));

% Plant Gain calculation at Crossover frequency :
[Giw_fc Phiw_fc] = bode(-Giw*Gisense,wc);

%Compensator gain calculation at cross-over frequency
[Gci_fc Phci_fc] = bode(Gci,wc);

% At Crossover frequency K*Gc*Gp = 1
Kc = 1/(Giw_fc*Gci_fc);
% Overall compensator transfer function
Gci = Kc*Gci ;

% Discretization of compensator transfer function using tustin or bi-linear transformation
Gci_d = c2d(Gci,TsC,'tustin') ;

% Current-Loop-gain calculation
Giol = minreal(-Giw*Gisense*Gci) ;

figure(2);
P = bodeoptions;
P.Grid = 'on';
P.FreqUnits = 'Hz';
P.PhaseWrapping = 'off';
bode(Giol, P); hold on;
margin(Giol);

%% Closed-Loop Transfer function (Current Loop)
```

```
Gcl = (-Gci*Giw*H_outDelay*Gpwm)/(1-
(Gisense*Gci*H_outDelay*H_zoh2*Giw*Gpwm));
% Gcl = (-Gci*Giw*Gpwm)/(1-(Gisense*Gci*Giw*Gpwm));

%% feedback or sensor circuit gain
Gp_sensor = R9/(R9+R8);
Rfv = R8*R9/(R8+R9);
Gpfc = Gp_sensor/(Rfv*Cfv*s+1);
Gfv = Gpfc/Kadc ;

%% Voltage-to-Current Transfer function
Giv = -Gvw/-Giw ;

%% Current Loop Compensator design (PI)
w_cv = 2*pi*fcv;
Gvl = Gcl*Giv*Gfv;

Gcv =(s+Wv)/s ;

% Compensator gain calculation at cross-over frequency
[Gcv_fcv phic_fcv] = bode(Gcv,w_cv) ;

% Plant Gain calculation at Crossover frequency :
[Gvl_fcv phi_fcv] = bode(Gvl,w_cv);

% At Crossover frequency K*Gc*Gp*G_sensor = 1 :
Kc = 1/(Gvl_fcv*Gcv_fcv);

% Overall compensator transfer function
Gcv = Kc*Gcv ;

Gcv_d = c2d(Gcv,TsV,'tustin') ;
Gvs = Gcv*Gvl*H_zoh1*H_outDelay;

figure(3);
P = bodeoptions;
P.Grid = 'on';
P.FreqUnits = 'Hz';
P.PhaseWrapping = 'off' ;
bode(Gvs, P); hold on;
margin(Gvs);

%% Voltage to Frequency factor for simulink model
Vab = 40/2 ;
ws = 2*pi*fs ;
Xr = ws*Ls ;
Xm = ws ;
```

$XC = 1/(ws * Cs)$;
 $p = (Xr - XC + Xm)/Xm$;
 $fr = 200e3$;
 $frequencytovoltagefactor = (2*pi^2*fr^3*Cs)/Vab/p^2$;

Fig. 7.30 depicts the transfer function of the ACM. At low frequencies, I^2 control and ACM function as an ideal current source with the voltage loop open. It is demonstrated that I^2 ACM control boosts the phase margin and the current loop gain. As a result, I^2 control has less overshoot and quick tracking speed.

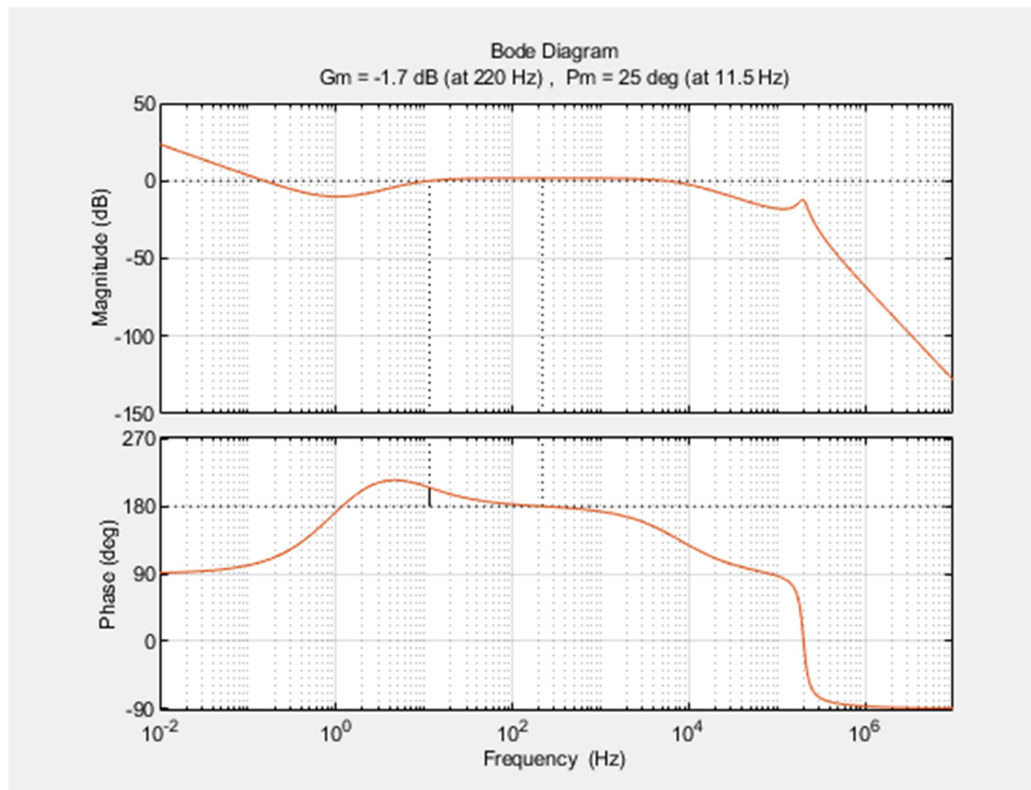


Fig 7.30: Bode plot of Current-Loop-gain for closed loop LC resonant converter

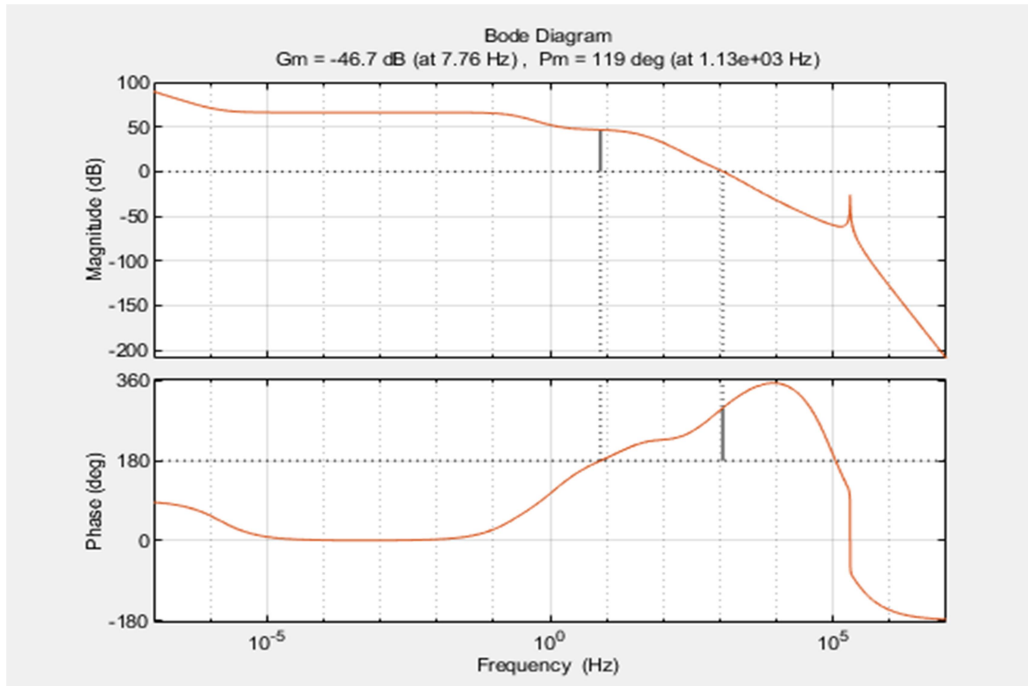


Fig 7.31: Bode plot of Outer loop-gain for closed loop LC resonant converter.

The closed - loop system LC resonant converter's outer loop gain bode plot is shown in Fig. 7.31. The shuttered audio susceptibility is the input-to-output power converter function for closed current loops as well as an open voltage loop. So because current loop for I^2 ACM management, PCM, and ACM have different frequency responses, the influence of the voltages loop compensators is ignored in order to emphasise the impact of the loops.

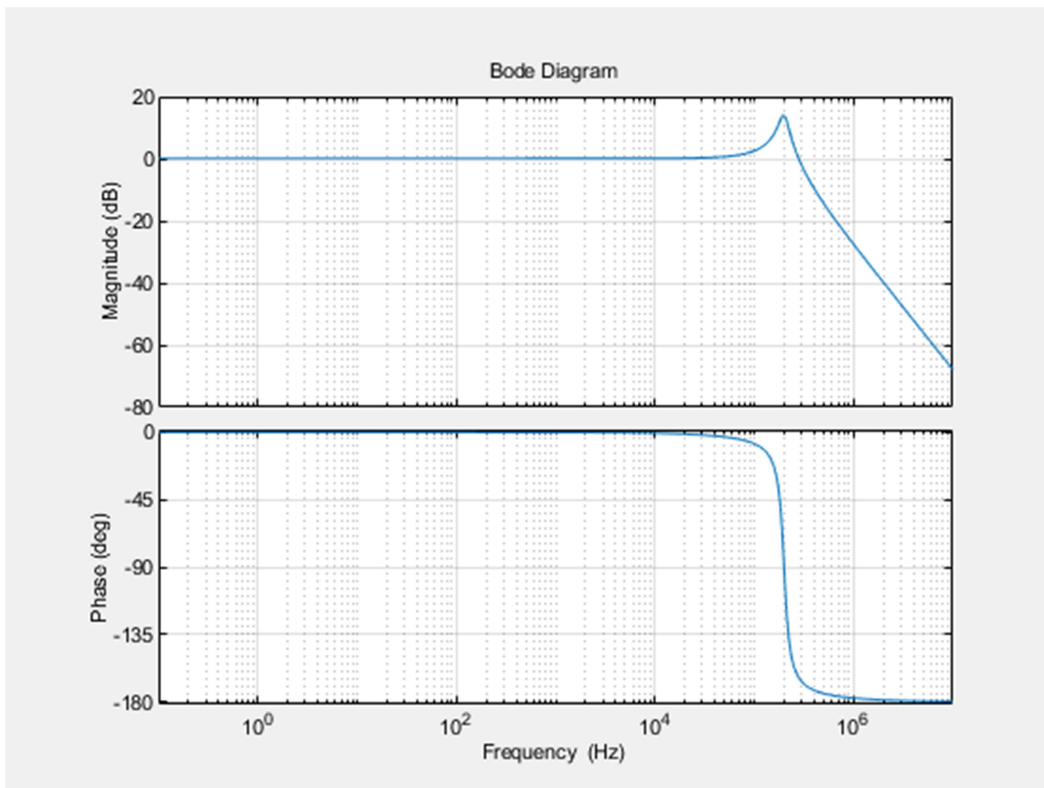


Fig 7.32: Bode plot for LC converter frequency to output voltage transfer function for closed loop

The control-to-output voltage transfer function with m_c as a variable is shown in Fig. 7.32. The system is unstable when $m_c = 0$ because a pair of right half-plane poles are indicated by an increase in magnitude peak and phase at half of the switching frequency. Even when the duty ratio is reduced to 0.4 for I^2 ACM control, the control loop still oscillates without slope compensation. The identical event occurs in Fig. 7.30 when $m_c = 1$. The RHP poles can be moved towards the left half plane via slope adjustment, which can also aid to reduce this peaking.

7.6. Conclusion

In this chapter, the simulation results of the series resonant converter under open loop and closed loop control with Average Current mode Control have been discussed. Initially the PV system was designed and simulated to various temperature and irradiance to get the desired voltage for the resonant converter then the PV system and series resonant was integrated to get the desired power for charging the UPS battery under open loop simulation. Later for the closed loop system MATLAB program was written for ACMC controller to get the desired simulation results.

CHAPTER – 8

CONCLUSION AND FUTURE SCOPE

8 CONCLUSION AND FUTURE SCOPE

The topic of the dissertation work was selected based on its serviceability. The structure of the converter and the control method was decided based on the research done related to this topic. The MATLAB Simulink platform was used to create and simulate the DC-DC UPS battery charger. A Half-Bridge LC resonant conversion is initially built and simulated under a range of frequencies, including those at, above, and below the resonance frequency. This LC resonant converter has been shown to work better when used close to the resonance frequency. PV system is used to provide supply to the LC resonant converter, it is designed to provide 35V, 40V and 45V under temperature of 45C, 25C and 15C. The analysis of LC resonant converter is done for Continuous and Discontinuous mode of operations. The supply of 35V, 40V and 45V is bucked to 12V which is used for battery charging.

The design of resonant tank is done for line regulation, load regulation, and efficiency. Detailed design and selection of Mosfet, Inductor, Capacitor, Transformer, Rectifier circuit, Filter circuit and Load design is done. The mathematical modeling for the resonant converter is carried out by First Harmonic Approximation (FHA) and Small signal modeling for series resonant converter. For a closed loop analysis the controller used here is Average Current Mode Controller (ACMC) which is a combination of voltage and current mode controller and it is found that ACMC has various advantages over them.

Resonant power converter development is primarily focused on achieving highly efficient, high-power density, small size, and cheap cost. The section on future research emphasizes the prospects for resonant converters within near future based on these goals. High reliability as well as high power density resonant converters with one and two stages are currently being researched. In order to reduce losses, it is also preferred that resonant

converter-based topology be small, inexpensive, and have low circulating current. The resonant converter's functioning needs to be steady in the face of parameter changes and outside disturbances. For resonant conversion tool EV charger to achieve these goals, effective and reliable control methods must be created. Effective bidirectional resonant converters must be created in order to increase system dependability and provide ancillary services such minimising harmonic distortion, voltage difference, harmonic correction, and reactive power support. These converters enable the system to operate in a number of operating modes, including V2G, V2H, and V2V, and they also provide the system access to the aforementioned auxiliary services. It is necessary to look at control strategies that may guarantee effective interchange of reactive and active power as well as auxiliary services to the system. Additionally, to minimize component cost and physical size, the best magnetic component design is required. As a result, the converter's performance is enhan

LIST OF PUBLICATIONS FROM THE DISSERTATION

WORK PHASE- II

- [1] Shubham Subhas Borkar and Guruswamy K P “A REVIEW ON COMPARISON STUDY OF DIFFERENT CONVERTER WITH VARIOUS CONTROL TECHNIQUES AND VARIOUS CONTROL TECHNIQUES AND VARIOUS MPPT TECHNIQUES”, International Journal of Innovative Research in Advanced Engineering (IJIRAE), Issue 02, Volume 9, pp. 43-51, February 2022.
- [2] Shubham Subhas Borkar and Guruswamy K P “A Comprehensive Review on Enhanced Series Resonant Converters”, International Journal for Modern trends in Science and Technology (IJMTST), Issue 08, Volume 08, PP. 14-21, August 2022.
- [3] Acceptance of paper “Shubham Subhas Borkar and Guruswamy K P, Performance Analysis of Half-Bridge LC Resonant Converter for UPS Battery Charging Application, 2023 International Conference on Recent Trends in Electronics and Communication (ICRTEC)

BIBLIOGRAPHY

- [1] Mohammad Hejri, Hossein Mokhtari, Mohammad Reza Azizian, Mehrdad Ghandhari, and Lennart Soder," On the Parameter Extraction of a Five-Parameter Double-Diode Model of Photovoltaic Cells and Modules", IEEE JOURNAL OF PHOTOVOLTAICS, VOL. 4, NO. 3, MAY 2014
 - [2] J. C. H. Phang, D. S. H. Chan, and J. R. Phillips, "Accurate analytical methods for the extraction of solar cell model parameters," Electron. Lett., vol. 20, no. 10, pp. 406–408, May 1984.
 - [3] D. S. H. Chan and J. C. H. Phang, "Analytical methods for the extraction of solar-cell single and double diode model parameters from I–V characteristics," IEEE Trans. Electron Devices, vol. 34, no. 2, pp. 286–293, Feb. 1987.
 - [4] J. A. Gow and C. D. Manning, "Development of a photovoltaic array model for use in power electronics simulation studies," IEE Proc., Electric Power Appl., vol. 146, no. 2, pp. 193–200, Mar. 1999.
 - [5] D. Sera, R. Teodorescu, and P. Rodriguez, "PV panel model based on datasheet values," in Proc. IEEE Int. Symp. Ind. Electron., 2007, pp. 2392–2396.
 - [6] Masri S., Mohamad, N. and Hariri M. H. M. (2012), "Design of DC-DC Buck Converter for Photovoltaic Application", 2012 International Conference on Power Engineering and Renewable Energy, (July), 1 5.
 - [7] T. Ajith Bosco Raj, R. Ramesh, J. R. Maglin, William Christopher, C. Gopinath, and C.Yaashuwanth "Solar PV system with SEPIC converter compared with parallel boost converter based MPPT", International Journal of Photo energy, Volume 2014, Article ID 385720, 12 pages.
 - [8] T. Ajith Bosco Raj, R. Ramesh, J. R. Maglin, William Christopher, C. Gopinath, and C. Yaashuwanth "Solar PV system with SEPIC converter compared with parallel boost converter based MPPT", International Journal of Photo energy, Volume 2014, Article ID 385720, 12 pages.
 - [9] Deepak, Pachauri R. K. and Chauhan Y. K. (2017), "Modeling and simulation analysis of PV fed Cuk, Sepic DC-DC converter" 1st IEEE International Conference, Intelligent Control and Energy Systems.
 - [10] S. Khireddine, M. Makhloufi, Y. A. Boutarafa," Tracking power photovoltaic with a fuzzy logic strategy" IEEE international conference on computer science, 2014, pp 42-49.
-

- [11] D. Rekioua , A.Y.Achour, T. Rekioua, "Tracking power photovoltaic system with sliding mode control strategy," IEEE international conference on computer science, 2014, 36 - 219 – 230, 201.
- [12] R. Mahalakshmi, A. Kumar, A. Kumar, " Design of Fuzzy logic based maximum power point tracking controller for solar array for cloudy weather conditions", IEEE power and energy systems: 2014, pp 1-4.
- [13] Hasan, K. N.; Haque, M. E.; Negnevitsky, M.; Muttaqi, K. M.: An improved maximum power point tracking technique for the photovoltaic module with current mode control, 2009, pp. 1-6.
- [14] Kiran B. R. and Ezhilarasi G. A. (2016), "Design of soft switched Buck-Boost Converter for PV applications", 12th IEEE International Conference Electronics, Energy, Environment, Communication, Computer, Control: (E3-C3), 1–5.
- [15] Liu X., and Lopes L.A.C.: "An improved perturbation and observation maximum power point tracking algorithm for PV arrays" IEEE Power lectronics Specialists Conference, 2004, pp2005-2010.
- [16] Hsieh, G. C.; Chen, H. L.; Chen, Y.; Tsai, C. M; Shyu, S. S.: Variable Frequency Controlled Incremental Conductance Derived MPPT Photovoltaic Stand-Along DC Bus System, 2008, pp. 1849-1854.
- [17] Safari and S. Mekhilef, "Simulation and hardware implementation of incremental conductance MPPT with direct control," IEEE Trans. Ind. Electron, pp. 1154–1161, Apr. 2011.
- [18] Casadei, D.; Grandi, C.; Rossi, C.: Single-Phase Single-stage Photovoltaic Generation System Based on a Ripple Correlation Control Maximum Power Point Tracking v. 21, n.2, pp. 562-568, 2006.
- [19] Y. Shen, H. Wang, Z. Shen, Y. Yang, and F. Blaabjerg, "A 1- MHz series resonant dc-dc converter with a dual-mode rectifier for pvmicroinverters," IEEE Trans. on Power Electron., vol. 34, no. 7, pp.6544-6564, Jul. 2019.
- [20] F. Musavi, M. Craciun, D. S. Gautam, W. Eberle, and W. G. Dunford, "An LLC resonant DC-DC converter for wide output voltage range battery charging applications," IEEE Trans. Power Electron., vol. 28, no. 12, pp. 5437-5445, Dec. 2013.

- [21] S. Zou, J. Lu, A. Mallik, and A. Khaligh, “Bi-directional CLLC converter with synchronous rectification for plug-in electric vehicles,” IEEE Trans. Ind. Appl., vol. 54, no. 2, pp. 998-1005, Mar.-Apr. 2017.
- [22] Fahad Alaql1 and IssaBatarseh “Review and Comparison of Resonant DC-DC Converters for Wide-Output Voltage Range Applications” in IEEE Transactions on Power Electronics, vol. 31, no. 3, pp. 2596–2608, 2020
- [23] H. Afshang and F. Tahami “ Voltage Regulation of DC-DC Series Resonant Converter Operating in Discontinuous Conduction Mode: The Hybrid Control Approach” IJE TRANSACTIONS B: Applications Vol. 32, No. 11, (November 2019) 1610-1619
- [24] Mehdi Mohammadi and Martin Ordonez “Fast Transient Response of Series Resonant Converters Using Average Geometric Control” IEEE Trans. on Power Electron., Vol. 30, no. 8, pp. 4560-4572, Aug. 2015.
- [25] Federico Martin Ibanez, Jose Martin Echeverria, Javier Vadillo, Luis Fontan CEIT and Manuel de Lardizabal “A step-up bidirectional series resonant DC/DC converter using a continuous current mode” in IEEE Transactions on Power Electronics, vol.14, no.1, pp.15,24, Jan 2019.
- [26] Swati Tandonand Akshay Kumar Rathore “ Novel Series LC Resonance-Pulse Based ZCS Current-Fed Full-Bridge DC-DC Converter: Analysis, Design and Experimental Results” in IEEE Transactions on Power Electronics, vol. 25, no. 3, pp. 686-698, March 2020.
- [27] Song Hu, Xiaodong Li and Ashoka K.S. Bhat “Operation of a Bidirectional Series Resonant Converter with Minimized Tank Current and Wide ZVS Range” in IEEE Trans. Power Electron., vol. 30, no. 12, pp. 6488-6494, Dec. 2018.
- [28] B. Zhao, Q. Song, W. Liu, G. Liu, and Y. Zhao, “Universal high-frequency-link characterization and practical fundamentaloptimal strategy for dual-active-bridge DC-DC converter under PWM plus phase-shift control,” IEEE Trans. Power Electron., vol. 30, no. 12, pp. 6488-6494, Dec. 2015.
- [29] Y. W. Cho, W. J. Cha, J. M. Kwon, and B. H. Kwon, “Highefficiency bidirectional DAB inverter using a novel hybrid modulation for stand-alone power generating system with low input voltage,” IEEE Trans. Power Electron, vol. 31, no. 6, pp. 4138-4147, Jun. 2016.

- [30] A. Tong, L. Hang, and S. Gao, "Modeling and analysis of dualactive-bridge isolated bidirectional DC/DC converter to minimize RMS current with whole operating range," *IEEE Trans. Power Electron.*, vol. 33, no. 6, pp. 5302-5316, Jun. 2017.
- [31] B. Zhao, Q. Yu, and W. Sun, "Extended-phase-shift control of isolated bidirectional DC–DC converter for power distribution in microgrid," *IEEE Trans. Power Electron.*, vol. 27, no. 11, pp. 4667-4680, Nov. 2012.
- [32] Sheetal Deshmukh (Gore)Atif IqbalShirazul IslamIrfan KhanMousa MarzbandSyed RahmanAbdullah M.A.B. Al-Wahedi," Review on classification of resonant converters for electric vehicle application", Energy reports, Volume 8, November 2022, pages 1091-1113.
- [33] Simon Ang. and Alejandro olive," Power Switching Converters", second edition 2005.
- [34] Hong Huang," Designing an LLC Resonant Half-Bridge Power Converter", 2010 Texas Instruments Power Supply Design Seminar SEM1900, Topic 3, pp: 1 – 27.
- [35] R. D. Middlebrook and S. Cuk, "A general unified approach to modelling switching converter power stages," in *IEEE Power Electronics Specialists Con6 Rec.*, 1976, pp. 18-31.
- [36] G. W. Wester and R. D. Middlebrook, "Low frequency characterization of switched dc-dc converters," in *Third IEEE Power Processing and Electronics Specialists Conference Rec.*, Atlantic City, NJ, May 1972.
- [37] R. J. King and T. A. Stuart, "Small-signal model for the series resonant converter," *IEEE Trans. Aerosp. Electron. Syst.*, vol. AES-21, no. 3, pp. 301-319, May 1985.
- [38] A. F. Hernandez, "Dynamic analysis of the parallel resonant converter," Master of Science thesis, University of Colorado, Boulder, 1988.
- [39] L. H. Dixon, "Average current-mode control of switching power supplies," Unitrode (Texas Instruments) Power Supply Design Seminar Manual, 1990.
- [40] P. Cooke, "Modeling average current mode control," Conference Proc. of IEEE APEC 2000, Vol. 1, pp. 256-262.

M.Tech report new

ORIGINALITY REPORT



PRIMARY SOURCES

- | | | |
|---|---|-----|
| 1 | A.F. Witulski, A.F. Hernandez, R.W. Erickson.
"Small signal equivalent circuit modeling of resonant converters", IEEE Transactions on Power Electronics, 1991
Publication | 4% |
| 2 | bbs.dianyuan.com
Internet Source | 4% |
| 3 | etd.auburn.edu
Internet Source | 1 % |
| 4 | archive.org
Internet Source | 1 % |
| 5 | He, Siyu, R Nelms, and John Hung. "Small-Signal Modeling of I^2 Average Current Mode Control", IEEE Transactions on Power Electronics, 2015.
Publication | 1 % |
| 6 | Jinhaeng Jang, Pidaparthy Syam Kumar, Dongyun Kim, Byungcho Choi. "Average current-mode control for LLC series resonant dc-to-dc converters", Proceedings of The 7th | 1 % |

International Power Electronics and Motion Control Conference, 2012

Publication

7 Submitted to University of Technology,
Sydney 1 %

8 Ruqi Li, T. O'Brien, J. Lee, J. Beecroft. "A unified small signal analysis of DC-DC converters with Average Current Mode Control", 2009 IEEE Energy Conversion Congress and Exposition, 2009 1 %

9 Mohammad Hejri, Hossein Mokhtari, Mohammad Reza Azizian, Mehrdad Ghandhari, Lennart Soder. "On the Parameter Extraction of a Five-Parameter Double-Diode Model of Photovoltaic Cells and Modules", IEEE Journal of Photovoltaics, 2014 <1 %

10 nrl.northumbria.ac.uk <1 %
Internet Source

11 corescholar.libraries.wright.edu <1 %
Internet Source

12 Submitted to Curtin University of Technology <1 %
Student Paper

13 dokumen.pub <1 %
Internet Source

- 14 vtechworks.lib.vt.edu <1 %
Internet Source
-
- 15 Byungcho Choi. "Pulsewidth Modulated DC - to - DC Power Conversion", Wiley, 2021 <1 %
Publication
-
- 16 Ivo Barbi, Fabiana Pöttker. "Soft Commutation Isolated DC-DC Converters", Springer Science and Business Media LLC, 2019 <1 %
Publication
-
- 17 journal.uad.ac.id <1 %
Internet Source
-
- 18 Submitted to The University of the South Pacific <1 %
Student Paper
-
- 19 Submitted to Wawasan Open University <1 %
Student Paper
-
- 20 Submitted to College of Engineering, Pune <1 %
Student Paper
-
- 21 T.H. Sloane. "Computer-based design of optimal efficiency series-resonant converters above resonance", Proceedings Fourth Annual IEEE Applied Power Electronics Conference and Exposition, 1989 <1 %
Publication
-
- 22 Submitted to University of Massachusetts - Amherst <1 %
Student Paper

-
- 23 Y. Chéron. "Soft Commutation", Springer Science and Business Media LLC, 1992 Publication <1 %
-
- 24 Robert W. Erickson, Dragan Maksimović. "Fundamentals of Power Electronics", Springer Science and Business Media LLC, 2020 Publication <1 %
-
- 25 Byungcho Choi. "Pulsewidth Modulated Dc-to-Dc Power Conversion", Wiley, 2013 Publication <1 %
-
- 26 Submitted to Visvesvaraya Technological University, Belagavi <1 % Student Paper
-
- 27 hdl.handle.net <1 % Internet Source
-
- 28 studylib.net <1 % Internet Source
-
- 29 Submitted to Coventry University <1 % Student Paper
-
- 30 research.library.mun.ca <1 % Internet Source
-
- 31 Arnold Fredderics, K.Vinoth Kumar, Jeya Selvan Renius, Raja Guru. "The FHA Analysis of Dual-Bridge LLC Type Resonant Converter", <1 %

International Journal of Power Electronics and Drive Systems (IJPEDS), 2014

Publication

-
- 32 Submitted to Indian Institute of Technology <1 %
Student Paper
-
- 33 Submitted to University of Glamorgan <1 %
Student Paper
-
- 34 Witulski, Arthur F., and Robert W. Erickson.
"Small signal ac equivalent circuit modelling of
the series resonant converter", 1987 IEEE
Power Electronics Specialists Conference,
1987.
Publication
-
- 35 www.coursehero.com <1 %
Internet Source
-
- 36 Hai-Jiang Jiang, G. Maggetto, P. Lataire.
"Steady-state analysis of the series resonant
DC-DC converter in conjunction with loosely
coupled transformer-above resonance
operation", IEEE Transactions on Power
Electronics, 1999
Publication
-
- 37 helliesenlumber.com <1 %
Internet Source
-
- 38 Ouadia Elmaguiri, Abdelmajid Farchi, Abdellah
Boulal, Aziz Akhiate. "Nonlinear
interconnected high gain observer for series-

parallel resonant DC/DC converter",
International Journal of Modelling,
Identification and Control, 2019

Publication

39	jpels.org Internet Source	<1 %
40	www.mdpi.com Internet Source	<1 %
41	idoc.pub Internet Source	<1 %
42	Submitted to University of Greenwich Student Paper	<1 %
43	Zhong Chen. "Analysis and design of three-phase rectifier with near-sinusoidal input currents", 2009 IEEE 6th International Power Electronics and Motion Control Conference, 05/2009 Publication	<1 %
44	core.ac.uk Internet Source	<1 %
45	repositorio.ufsm.br Internet Source	<1 %
46	Shahzad, M. Imran, Shahid Iqbal, and Soib Taib. "LLC series resonant converter with PID controller for battery charging application",	<1 %

2014 IEEE Conference on Energy Conversion (CENCON), 2014.

Publication

-
- 47 Su-Jin Jang. "", IEEE Transactions on Energy Conversion, 6/2007 <1 %
Publication
-
- 48 pels.edv.uniovi.es <1 %
Internet Source
-
- 49 cora.ucc.ie <1 %
Internet Source
-
- 50 ir.lib.ksu.edu.tw <1 %
Internet Source
-
- 51 open.library.ubc.ca <1 %
Internet Source
-
- 52 worldwidescience.org <1 %
Internet Source
-
- 53 Swati Tandon, Akshay Kumar Rathore. " Novel Series Resonance-Pulse-Based ZCS Current-Fed Full-Bridge DC–DC Converter: Analysis, Design, and Experimental Results ", IEEE Transactions on Power Electronics, 2021 <1 %
Publication
-
- 54 Submitted to University of Sheffield <1 %
Student Paper
-
- 55 www.researchgate.net <1 %
Internet Source
-

56

Attivissimo, Filippo, Attilio Di Nisio, Mario Savino, and Maurizio Spadavecchia.

<1 %

"Uncertainty Analysis in Photovoltaic Cell Parameter Estimation", IEEE Transactions on Instrumentation and Measurement, 2012.

Publication

57

Submitted to Jawaharlal Nehru Technological University

<1 %

Student Paper

58

Mingxiao Li, Ziwei Ouyang, Michael A.E. Andersen. "A Hybrid Multitrack-Sigma Converter with Integrated Transformer for Wide Input Voltage Regulation", 2020 IEEE Applied Power Electronics Conference and Exposition (APEC), 2020

<1 %

Publication

59

Navid Shafiei, Martin Ordonez, Marian Craciun, Chris Botting, Murray Edington.

<1 %

"Burst Mode Elimination in High-Power LLC Resonant Battery Charger for Electric Vehicles", IEEE Transactions on Power Electronics, 2016

Publication

60

Song Hu, Xiaodong Li, Ashoka K.S. Bhat. "Operation of a bidirectional series resonant converter with minimized tank current and wide ZVS range", IEEE Transactions on Power Electronics, 2018

<1 %

- 61 Submitted to Associate K.U.Leuven <1 %
Student Paper
-
- 62 "Pulse - Width Modulated DC-DC Power Converters", Wiley, 2013 <1 %
Publication
-
- 63 Byungcho Choi, Wonseok Lim, Seungwon Choi, Jian Sun. "Comparative Performance Evaluation of Current-Mode Control Schemes Adapted to Asymmetrically Driven Bridge-Type Pulsewidth Modulated DC-to-DC Converters", IEEE Transactions on Industrial Electronics, 2008 <1 %
Publication
-
- 64 Robert W. Erickson. "Fundamentals of Power Electronics", Springer Nature, 1997 <1 %
Publication
-
- 65 P. Cooke. "Modeling average current mode control [of power convertors]", APEC 2000 Fifteenth Annual IEEE Applied Power Electronics Conference and Exposition (Cat No 00CH37058) APEC-00, 2000 <1 %
Publication
-
- 66 Submitted to Wright State University <1 %
Student Paper
-
- 67 pt.scribd.com <1 %
Internet Source

- 68 B.S. Nathan, V. Ramanarayanan. "Analysis, simulation and design of series resonant converter for high voltage applications", Proceedings of IEEE International Conference on Industrial Technology 2000 (IEEE Cat. No.00TH8482), 2000 <1 %
Publication
-
- 69 Chang Hee Park, Sung Ho Cho, Jinhaeng Jang, Syam Kumar Pidaparthi, Taeyoung Ahn, Byungcho Choi. "Average Current Mode Control for LLC Series Resonant DC-to-DC Converters", Journal of Power Electronics, 2014 <1 %
Publication
-
- 70 Di Piazza, Maria Carmela, Massimiliano Luna, and Gianpaolo Vitale. "Dynamic PV Model Parameter Identification by Least-Squares Regression", IEEE Journal of Photovoltaics, 2013. <1 %
Publication
-
- 71 Jung, J., H. Kim, M. Ryu, and J. Baek. "Design Methodology of Bidirectional CLLC Resonant Converter for High Frequency Isolation of DC Distribution Systems", IEEE Transactions on Power Electronics, 2012. <1 %
Publication
-
- 72 Keliang Yuan, Flavia Grassi, Giordano Spadacini, Sergio A. Pignari. "Reproducing <1 %

Field-to-Wire Coupling Effects in Twisted-Wire Pairs by Crosstalk", IEEE Transactions on Electromagnetic Compatibility, 2018

Publication

-
- 73 Mehdi Abbasi, Reza Emamalipour, Kajanan Kanathipan, Muhammad Ali Masood Cheema, John Lam. " A Step-Up Reconfigurable Multimode Converter Module With Extended High-Efficiency Range for Wide Voltage Gain Application in Medium Voltage DC Grid Systems ", IEEE Transactions on Power Electronics, 2022 <1 %
- Publication
-
- 74 Paramjit Saha, Saurabh Kumar, Sisir Kr. Nayak, Himanshu Sekhar Sahu. "Parameter estimation of double diode photo-voltaic module", 2015 1st Conference on Power, Dielectric and Energy Management at NERIST (ICPDEN), 2015 <1 %
- Publication
-
- 75 ijrer.ijrer.org <1 %
- Internet Source
-
- 76 ira.lib.polyu.edu.hk <1 %
- Internet Source
-
- 77 C. Hattrup, H.W. van der Broeck, M. Ossmann. "Fast estimation techniques for digital control of resonant converters", IEEE Transactions on Power Electronics, 2003 <1 %

- 78 Claudio Adragna. "LLC Resonant Converters: An Overview of Modeling, Control and Design Methods and Challenges", Foundations and Trends® in Electric Energy Systems, 2022 <1 %
- Publication
-
- 79 Hyuntae Choi, Wei Zhao, M. Ciobotaru, V. G. Agelidis. "Large-scale PV system based on the multiphase isolated DC/DC converter", 2012 3rd IEEE International Symposium on Power Electronics for Distributed Generation Systems (PEDG), 2012 <1 %
- Publication
-
- 80 L. Fiorella, C. Di Miceli, T. Raimondi, C. Cutrona. "Analysis of a series resonant converter", Conference Proceedings., Eleventh International Telecommunications Energy Conference, 1989 <1 %
- Publication
-
- 81 M.G. Kim, D.S. Lee, M.J. Youn. "A new state feedback control of resonant converters", IEEE Transactions on Industrial Electronics, 1991 <1 %
- Publication
-
- 82 MILAN M. JOVANOVIĆ. "Invited paper. Resonant, quasi-resonant, multi-resonant and soft-switching techniques—merits and <1 %

limitations", International Journal of Electronics, 1994

Publication

- 83 Mehdi Mohammadi, Franco Degioanni, Mohammad Mahdavi, Martin Ordóñez. "Small-Signal Modeling of Converters Using Homopolarity Cycle ", IEEE Transactions on Power Electronics, 2020 <1 %
- Publication
-
- 84 Mehdi Mohammadi, Martin Ordóñez. "Extreme start-up response of LLC converters using average geometric control", 2016 IEEE Energy Conversion Congress and Exposition (ECCE), 2016 <1 %
- Publication
-
- 85 P.C. Sen. "High switching frequency power converters", Proceedings 1995 Canadian Conference on Electrical and Computer Engineering CCECE-95, 1995 <1 %
- Publication
-
- 86 Sarnago, Héctor, Arturo Mediano, and Óscar Lucía. "High Efficiency AC-AC Power Electronic Converter Applied to Domestic Induction Heating", IEEE Transactions on Power Electronics, 2012. <1 %
- Publication
-
- 87 eprints.nottingham.ac.uk <1 %
- Internet Source

88	gyan.iitg.ernet.in Internet Source	<1 %
89	ir.lib.uwo.ca Internet Source	<1 %
90	mdpi-res.com Internet Source	<1 %
91	theses.lib.polyu.edu.hk Internet Source	<1 %
92	vdocuments.mx Internet Source	<1 %
93	www.cuchd.in Internet Source	<1 %
94	www.ijarse.com Internet Source	<1 %
95	www.koreascience.or.kr Internet Source	<1 %
96	"Digital Technologies and Applications", Springer Science and Business Media LLC, 2022 Publication	<1 %
97	"Modeling, Simulation and Optimization", Springer Science and Business Media LLC, 2021 Publication	<1 %

- 98 "Smart Energy and Advancement in Power Technologies", Springer Science and Business Media LLC, 2023 **<1 %**
Publication
-
- 99 A.M. Sharaf. "Optimal trajectory control of series resonant converter using modified capacitor voltage control technique", PESC 91 Record 22nd Annual IEEE Power Electronics Specialists Conference, 1991 **<1 %**
Publication
-
- 100 H. Abe, H. Sakamoto, K. Harada. "A noncontact charger using a resonant converter with parallel capacitor of the secondary coil", IEEE Transactions on Industry Applications, 2000 **<1 %**
Publication
-
- 101 I. Batarseh. "Modeling and PSPICE simulation of a power resonant converter", Conference Record Southcon SOUTHC-94, 1994 **<1 %**
Publication
-
- 102 M. Nakaoka. "Instantaneous space voltage vector controlled three-phase ZVS-PWM active converter with new auxiliary transformer assisted resonant DC link", Proceedings of Intelec 96 - International Telecommunications Energy Conference INTLEC-96, 1996 **<1 %**
Publication

- 103 Ngoc Dat Dao, Dong Choon Lee, Quoc Dzung Phan. "High-Efficiency SiC-Based Isolated Three-Port DC/DC Converters for Hybrid Charging Stations", IEEE Transactions on Power Electronics, 2020 <1 %
- Publication
-
- 104 Praveen K. Jain. "Resonant Power Conversion: Insights From a Lifetime of Experience", IEEE Journal of Emerging and Selected Topics in Power Electronics, 2021 <1 %
- Publication
-
- 105 Siyu He, John Y. Hung, R. M. Nelms. "Small-signal modeling of I^2 average current mode control", 2015 IEEE Applied Power Electronics Conference and Exposition (APEC), 2015 <1 %
- Publication
-
- 106 Sujoy Deb, A. Joshi, S. R. Doradla. "A novel frequency domain model for a parallel resonant converter", 1987 IEEE Power Electronics Specialists Conference, 1987 <1 %
- Publication
-
- 107 Swagatika Mishra, Lalit Kumar Sahu, Akhilesh Kumar Tiwari. "Modelling of Three port DC/DC converter Topology for Electric Vehicle charging system", 2021 IEEE 2nd International Conference on Smart Technologies for Power, Energy and Control (STPEC), 2021 <1 %
- Publication
-

- 108 Thomas LaBella, Wensong Yu, Jih-Sheng Lai, Matthew Senesky, David Anderson. "A Bidirectional-Switch-Based Wide-Input Range High-Efficiency Isolated Resonant Converter for Photovoltaic Applications", IEEE Transactions on Power Electronics, 2014
Publication <1 %
- 109 Yi Zhang, Donglai Zhang, Jie Li, Hongyu Zhu. "Bidirectional LCLL Resonant Converter With Wide Output Voltage Range", IEEE Transactions on Power Electronics, 2020
Publication <1 %
- 110 Yingyi, , Fred C., and Paolo. "Analysis and Design of Average Current Mode Control Using a Describing-Function-Based Equivalent Circuit Model", IEEE Transactions on Power Electronics, 2013.
Publication <1 %
- 111 Yue Guan, Lei Li, Jinchuan Zhang. "Novel multi-level inverters with flyback high frequency link", IET Power Electronics, 2020
Publication <1 %
- 112 ebin.pub
Internet Source <1 %
- 113 eprints.utas.edu.au
Internet Source <1 %
- etheses.whiterose.ac.uk

- 114 Internet Source <1 %
-
- 115 [findresearcher.sdu.dk](#) <1 %
Internet Source
-
- 116 [kth.diva-portal.org](#) <1 %
Internet Source
-
- 117 [pureadmin.qub.ac.uk](#) <1 %
Internet Source
-
- 118 [scholar.colorado.edu](#) <1 %
Internet Source
-
- 119 [studyres.com](#) <1 %
Internet Source
-
- 120 [www.iasj.net](#) <1 %
Internet Source
-
- 121 [www.ti.com](#) <1 %
Internet Source
-
- 122 A.K.S. Bhat. "A generalized steady-state analysis of resonant converters using two-port model and Fourier-series approach", IEEE Transactions on Power Electronics, 1998 <1 %
Publication
-
- 123 B.K.H. Wong, H. Shu-Hung Chung. "A systematic graphing technique for small-signal low-frequency characterization of PWM <1 %

DC/DC converters", IEEE Transactions on
Industrial Electronics, 2000

Publication

-
- 124 J.A. Ferreira. "A new, partial series resonant converter for efficient DC to DC conversion", Conference Record of the Power Conversion Conference - Yokohama 1993, 1993 <1 %
- Publication
-
- 125 Jang, Jinhaeng, Syam Pidaparthi, and Byungcho Choi. "Current Mode Control for LLC Series Resonant DC-to-DC Converters", Energies, 2015. <1 %
- Publication
-
- 126 Koohi-Kamali, Sam, N.A. Rahim, H. Mokhlis, and V.V. Tyagi. "Photovoltaic electricity generator dynamic modeling methods for smart grid applications: A review", Renewable and Sustainable Energy Reviews, 2016. <1 %
- Publication
-
- 127 Luca Corradini, Dragan Maksimović, Paolo Mattavelli, Regan Zane. "Digital Control", Wiley, 2015 <1 %
- Publication
-
- 128 Mohamed A. Awadallah, Bala Venkatesh. "Optimisation-based parameter estimation of photovoltaic modules", International Journal of Industrial Electronics and Drives, 2018 <1 %
- Publication

- 129 O.P. Mandhana. "Computer aided analysis and design of load commutated resonant converters", PESC Record 27th Annual IEEE Power Electronics Specialists Conference PESC-96, 1996 <1 %
Publication
-
- 130 Parminder Kaur Saini, Amanpreet Singh, J. S. Sohal. "Proactive Prevention Key Solution for Wormhole Attack in IEEE 802.11 Networks Using AODV", Wireless Personal Communications, 2022 <1 %
Publication
-
- 131 Prajeet Shukla, Vishal Verma. "Pulse splitting cum width control for transient handling of LLC Resonant Converter", 2022 IEEE Global Conference on Computing, Power and Communication Technologies (GlobConPT), 2022 <1 %
Publication
-
- 132 Sheetal Deshmukh (Gore), Atif Iqbal, Shirazul Islam, Irfan Khan, Mousa Marzband, Syed Rahman, Abdullah M.A.B. Al-Wahedi. "Review on classification of resonant converters for electric vehicle application", Energy Reports, 2022 <1 %
Publication
-
- 133 V. Agarwal, A.K.S. Bhat. "Small signal analysis of the LCC-type parallel resonant converter" <1 %

using discrete time domain modeling", IEEE Transactions on Industrial Electronics, 1995

Publication

-
- 134 A.F. Hernandez, R.W. Erickson, S. Lofton, P. Anderson. "A large signal computer model for the series resonant converter", PESC '91 Record 22nd Annual IEEE Power Electronics Specialists Conference, 1991 <1 %
- Publication
-
- 135 Abdessamad Boussafa, Mohammed Ferfra, Yahia El Ouazzani, Reda Rabeh, Khalid Chennoufi. "Extraction Of Electrical Parameters for Two-Diode Photovoltaic Model Using Combined Analytical and Genetic Algorithm", 2022 4th Global Power, Energy and Communication Conference (GPECOM), 2022 <1 %
- Publication
-
- 136 Alex Lidow, Michael de Rooij, Johan Strydom, David Reusch, John Glaser. "GaN Transistors for Efficient Power Conversion", Wiley, 2019 <1 %
- Publication
-
- 137 Fengjiang Wu, Shuai Fan, Xiaoguang Li, Suhua Luo. "Bidirectional Buck-Boost Current-Fed Isolated DC-DC Converter and Its Modulation", IEEE Transactions on Power Electronics, 2020 <1 %
- Publication
-

138

Jang, Yungtaek, Milan M. Jovanovic, Juan M. Ruiz, and Gang Liu. "Series-resonant converter with reduced-frequency-range control", 2015 IEEE Applied Power Electronics Conference and Exposition (APEC), 2015.

<1 %

Publication

Exclude quotes On

Exclude bibliography On

Exclude matches Off